IDEAL CYCLE ANALYSIS OF A REGENERATIVE PULSE DETONATION ENGINE FOR POWER PRODUCTION

by

RAFAELA BELLINI

Presented to the Faculty of the Graduate School of
The University of Texas at Arlington in Partial Fulfillment
of the Requirements
for the Degree of

DOCTOR OF PHILOSOPHY

THE UNIVERSITY OF TEXAS AT ARLINGTON

December 2010

ACKNOWLEDGEMENTS

I would like to express my deepest gratitude to my advisor, Dr. Frank Lu, for his guidance, encouragement and support in my research work as well as all the help that he provided me in preparing this manuscript. I am sincerely thankful for his council that helped me get where I am today. I would also like to thank Dr. Don Wilson for his suggestions and the support extended towards my work. I am also thankful to the rest of my committee members, including Dr. Luca Massa, Dr. Luca Maddalena and Dr. Dereje Agonafer for all their help and support.

I would like to thank my colleagues Ronnachai Vutthivithayarak and Sushma Rao for their help in my research work. I am very grateful to all the administrative staff at the Mechanical and Aerospace Engineering Department, including Debi Barton, Louella Carpenter, Janet Gober, Lanie Gordon, Kathy Priester, and Sally Thompson, as well as former staff members, Barbara Sanderson and Donna Woodhead for all the timely help with administrative tasks. I am also grateful to the late Connie Niece for all her help. She will always be remembered for her friendly words and for her help with travel arrangements.

I am very grateful to Dr. Carter Tiernan for letting me serve as mechanical engineering project mentor for the annual Engineering and Computer Science Summer Camp. I would also like to thank my fellow engineering summer camp crew for all the wonderful memories.

I would like to thank Satu Birch, Jay P. Horn and Catalina Rosquero, of the Office of International Education, for all their invaluable help. I would like to thank my friends,

colleagues and students from the Campus Recreation Department for all the great times and good memories.

I am very grateful to my husband, Philip Panicker, for all his love, assistance and support in my research work and encouraging me through the tough times during my course. I am extremely indebted to my mother Ana Maria, my father Ione Valmir and my sister Stefania, for all their love, prayers, encouragement, spiritual and financial support during my course of study.

I would also like to thank my husband's parents, brother, sister and her husband for their love, prayers and support. I am grateful to the Kuruvilla family and their relatives for their love and support. I am thankful to my friends, Jolanta Matusewicz and Amith Kalaghatagi, for all the good times and wonderful memories.

I am very grateful to my church family at Christ Family Church Arlington for their prayers, support and love. I would also like to thank all my other friends, who have become a part of my life and I cannot name, for all the love and support they have given me.

Above all, I am indebted to my Lord and Savior, Jesus Christ, who has blessed my life abundantly and given my life meaning and purpose.

"Therefore I take pleasure in infirmities, in reproaches, in necessities, in persecutions, in distresses for Christ's sake: for when I am weak, then am I strong."

2 Corinthians 12:10, KJV

"Praise ye the Lord. Blessed is the man that feareth the Lord, that delighteth greatly in his commandments."

Psalms 112:1, KJV

November 24, 2010

ABSTRACT

IDEAL CYCLE ANALYSIS OF A REGENERATIVE PULSE DETONATION ENGINE FOR POWER PRODUCTION

RAFAELA BELLINI, Ph.D.

The University of Texas at Arlington, 2010

Supervising Professor: Frank K. Lu

Over the last few decades, considerable research has been focused on pulse detonation engines (PDEs) as a promising replacement for existing propulsion systems with potential applications in aircraft ranging from the subsonic to the lower hypersonic regimes. On the other hand, very little attention has been given to applying detonation for electric power production. One method for assessing the performance of a PDE is through thermodynamic cycle analysis. Earlier works have adopted a thermodynamic cycle for the PDE that was based on the assumption that the detonation process could be approximated by a constant volume process, called the Humphrey cycle. The Fickett-Jacob cycle, which uses the one–dimensional Chapman–Jouguet (CJ) theory of detonation, has also been used to model the PDE cycle. However, an ideal PDE cycle must include a detonation based compression and heat release processes with a finite chemical reaction rate that is accounted for in the Zeldovich – von Neumann – Döring model of detonation where the shock is considered a discontinuous jump and is followed by a finite exothermic reaction zone.

This work presents a thermodynamic cycle analysis for an ideal PDE cycle for power production. A code has been written that takes only one input value, namely the heat of reaction of a fuel-oxidizer mixture, based on which the program computes all the points on the ZND cycle (both p–v and T–s plots), including the von Neumann spike and the CJ point along with all the non-dimensionalized state properties at each point. In addition, the program computes the points on the Humphrey and Brayton cycles for the same input value. Thus, the thermal efficiencies of the various cycles can be calculated and compared. The heat release of combustion is presented in a generic form to make the program usable with a wide variety of fuels and oxidizers and also allows for its use in a system for the real time monitoring and control of a PDE in which the heat of reaction can be obtained as a function of fuel-oxidizer ratio. The Humphrey and ZND cycles are studied in comparison with the Brayton cycle for different fuel-air mixtures such as methane, propane and hydrogen. The validity and limitations of the ZND and Humphrey cycles related to the detonation process are discussed and the criteria for the selection of the best model for the PDE cycle are explained. It is seen that the ZND cycle is a more appropriate representation of the PDE cycle.

Next, the thermal and electrical power generation efficiencies for the PDE are compared with those of the deflagration based Brayton cycle. While the Brayton cycle shows an efficiency of 0 at a compressor pressure ratio of 1, the thermal efficiency for the ZND cycle starts out at 42% for hydrogen–air and then climbs to a peak of 66% at a compression ratio of 7 before falling slowly for higher compression ratios. The Brayton cycle efficiency rises above the PDEs for compression ratios above 23. This finding supports the theoretical advantage of PDEs over the gas turbines because PDEs only require a fan or only a few compressor stages, thereby eliminating the need for heavy compressor machinery, making the PDEs less complex and therefore more cost effective than other engines.

Lastly, a regeneration study is presented to analyze how the use of exhaust gases can improve the performance of the system. The thermal efficiencies for the regenerative ZND cycle are compared with the efficiencies for the non–regenerative cycle. For a hydrogen–air mixture the thermal efficiency increases from 52%, for a cycle without regeneration, to 78%, for the regenerative cycle. The efficiency is compared with the Carnot efficiency of 84% which is the maximum possible theoretical efficiency of the cycle. When compared to the Brayton cycle thermal efficiencies, the regenerative cycle shows efficiencies that are always higher for the pressure ratio studied of $5 \leq \pi_c \leq 25$, where π_c the compressor pressure ratio of the cycle. This observation strengthens the idea of using regeneration on PDEs.

TABLE OF CONTENTS

LIST OF FIGURES

LIST OF TABLES

NOMENCLATURE

a	speed of sound
CJ	Chapman–Jouguet
c_p	specific heat at constant pressure
c_v	specific heat at constant volume
D_{CJ}	CJ detonation speed
f	equivalence ratio
f_{max}	maximum frequency of a PDE cycle
h	specific enthalpy
h_P	specific enthalpy of formation of products
h_R	specific enthalpy of formation of reactants
M_{CJ}	CJ Mach number
k_i	parameter for average model
K_i	parameter for average model
p	pressure
p_{fill}	pressure at $t = t_{fill}$
$p_{plateau}$	pressure at $t = t_{plateau}$
q	heat transfer
q_{add}	heat added to the system
q_{rej}	heat rejected to the surroundings
R	universal gas constant
s	specific entropy
T	temperature

t	time
t_{CJ}	time for detonation wave to reach the CJ position
t_{fill}	time to fill the tube with the fuel–air mixture
$t_{plateau}$	time for detonation wave to take place
$t_{exhaust}$	time for the mixture to exit the tube
T_{cycle}	period of a PDE cycle
v	specific volume
W_{out}	shaft work output
ZND	Zeldovich–von Neumann–Döring
α	nondimensional heat release
η_{th}	thermal efficiency
η_{MEC}	mechanical to electrical conversion efficiency
η_{shaft}	shaft efficiency
η_{gen}	generator efficiency
ρ	density
π_c	compressor pressure ratio
γ	ratio of specific heats
$\gamma_{products}$	ratio of specific heats of products
$\gamma_{reactants}$	ratio of specific heats of reactants

CHAPTER 1

INTRODUCTION

Deflagration is a subsonic combustion process where the flame propagates at a few meters per second [2], producing small decreases in pressure. Deflagration is the means of chemical energy addition for conventional internal combustion engines, gas turbine engines and rockets. A paradigm shift in propulsion from deflagration can be achieved by utilizing detonations to develop thrust. A detonation, unlike deflagration, produces a supersonic combustion wave that propagates at a few thousands of meters per second relative to an unburned reactant–air mixture [2, 3, 4]. A detonation wave compresses the fluid, increasing its pressure and density, in addition to increasing its temperature, thereby triggering chemical reactions. The energy from the chemical reactions support the traveling shock wave in turn and a balance is attained to form a self-sustaining detonation wave. The above description of a detonation wave, however, is grossly simplified. Detonation waves are actually complex, oscillatory phenomena with three-dimensional time-dependent cellular structures [3, 4].

1.1 Literature Review

1.1.1 Overview of Early Studies in Detonations

The phenomenon of detonation was first recognized simultaneously by Berthelot and Vielle [5, 6] and by Mallard and Chatelier [7] in the early 1880s. Berthelot and Vielle, when studying coal explosions, ascertained the existence of a detonation wave in explosive gaseous mixtures. On the other hand, Mallard and Chatelier [7] made the same discovery during studies of flame propagation. Mallard and Chatelier [8] demonstrated

that deflagration can transition into a detonation wave in gaseous explosives. They stated that a detonation propagates as an adiabatic compression wave and its propagation velocity can be related to the speed of sound of the combustion products. They found that the detonation wave velocity is independent of the ignition source (explosive or non-explosive [9]) and tube diameter and is primarily a function of the explosive mixture composition.

Not long later, Chapman [10] established the classical Chapman-Jouguet (CJ) theory for the propagation of a steady plane detonation wave in a gaseous mixture, based on the one-dimensional Rankine–Hugoniot theory [11, 12]. Chapman showed that the lowest value of the velocity with respect to the burned gas is equal to the velocity of sound in this gas and that the detonation wave, relative to the laboratory frame, is supersonic. In 1905, Jouguet [13] showed that if one assumes that if the velocity of the products behind the wave front with respect to the detonation wave front is equal to the local speed of sound, the main properties of a detonation wave propagating at constant velocity can be quantified.

In the CJ model, the detonation wave is closely coupled to a thin flame front or combustion region [2]. The conservation conditions require that the final state lie on both the reactive Hugoniot curve and a Rayleigh line as shown in Fig. 1.1. The figure shows five possible regimes along the reactive Hugoniot. Regions I and II are for a strong and a weak detonation respectively, regions IV and V are for a weak and a strong deflagration respectively, while region III, between points W_1 and F, is not physically possible. For detonation wave propagation velocities lower than the CJ velocity, the Rayleigh line and the Hugoniot curve do not intersect, so there is no solution that satisfies the conservation conditions. There are two particular values of flame velocity that makes the Rayleigh line tangent to the Hugoniot curve. These tangent points are called the upper and lower CJ points, U and L, respectively in Fig. 1.1. The upper CJ point represents

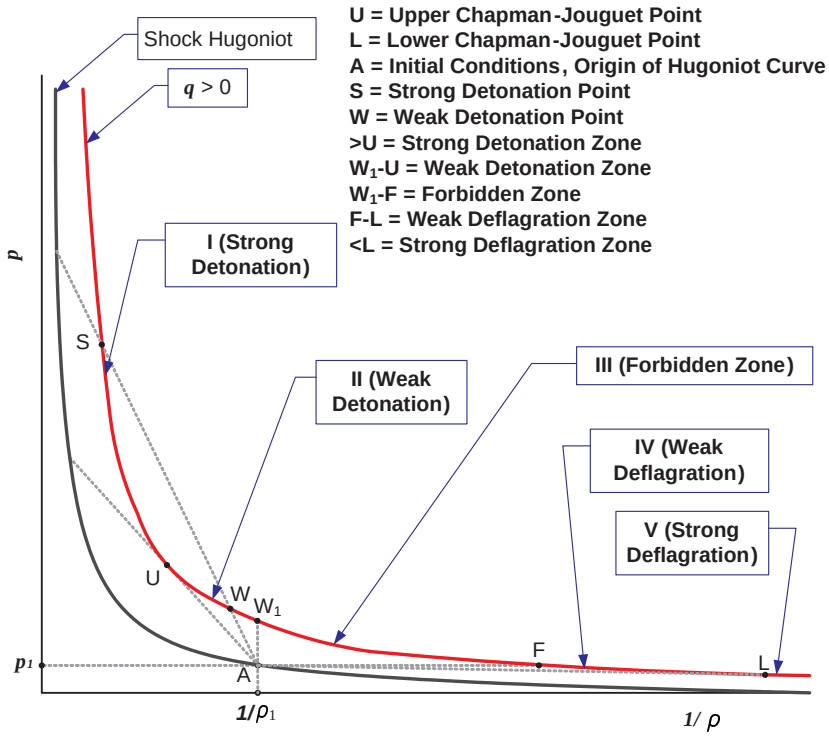

Figure 1.1. Various combustion regimes accessible from an initial state ($p = 1$, $\rho = 1$): inert Hugoniot shown as a black line, Hugoniot with heat addition shown as a red line.

the stable end state for a self-sustaining detonation wave, and the corresponding flame velocity is the CJ detonation velocity V_d. The upper CJ point separates the strong and weak detonation regimes. It can be shown from the tangency condition that, at the CJ point, the detonation velocity relative to the reaction products is equal to the local speed of sound in the reaction products [3, 4]. Similarly, the lower CJ point separates the strong and weak deflagration regions and the corresponding velocity is the CJ deflagration velocity.

The first observation that detonation waves are more complex than described by the CJ theory came in 1927, with the discovery of the spin phenomenon in detonation waves propagating in tubes [14]. Photographs of certain detonation mixtures showed an undulating front with striations behind it. The undulations are most likely due to a

region of higher than average temperature and luminosity which rotates around the axis of the tube as the detonation advances. This discovery initiated numerous studies of the detonation wave structure.

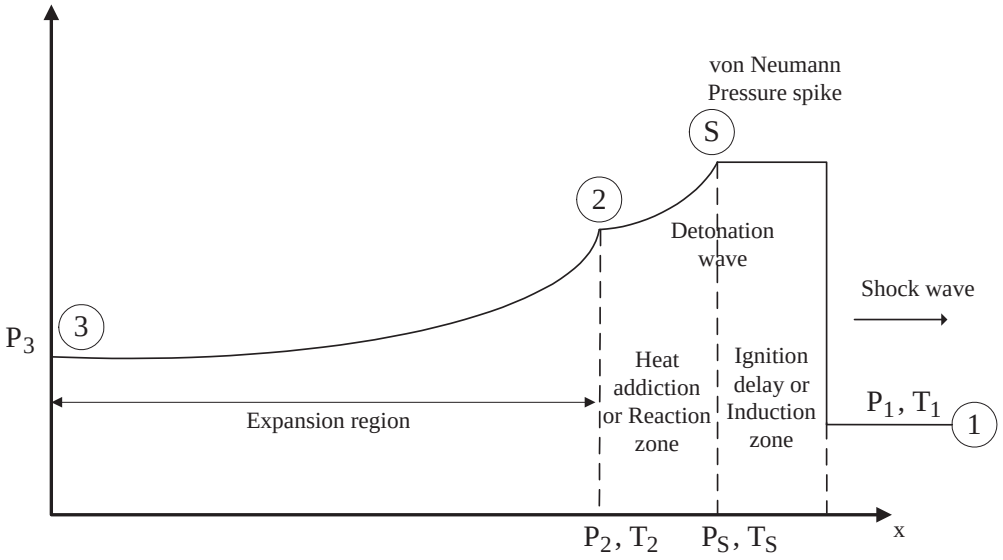

Figure 1.2. Detonation pressure profile for one-dimensional detonation.

In the early 1940s, Zeldovich [15, 16], von Neumann [17] and Döring [18] each independently formulated similar models for the one-dimensional structure of a detonation wave by taking into account the finite-rate chemistry. The detonation wave in the ZND model comprises of a lead shock followed by the reaction front. The shock wave compresses a gas from its initial state along the Rayleigh line to a high-pressure state on the Hugoniot curve called the von Neumann spike as indicated in Fig. 1.2. The reaction zone is divided into two regions, namely, an induction zone and a heat addition zone. In the induction zone, the reaction is delayed due to the finite time required to initiate chemical reactions. Once the reaction is initiated, energy is released into the flow so that the temperature is further increased. Taylor rarefaction waves are generated behind this

point. Thus, the pressure and temperature in this region are decreased to match the left wall boundary conditions. The ZND model is physically well-based and is a helpful idealization of a real detonation wave. However, it was clearly demonstrated later, both experimentally and theoretically, that a detonation is essentially three-dimensional and steady-state only on average.

1.1.2 Pulse Detonation Devices

A detonation cycle can be represented in Fig. 1.1 by the path $AUFA$, where $A \rightarrow U$ is the detonation path, $U \rightarrow F$ is the expansion of the burned gas and $F \rightarrow A$ is isobaric return to the initial state [19, 20]. For analytical simplicity, the detonation cycle can be approximated for example as a constant volume process AW_1FA, known as the Humphrey cycle [21, 22, 23, 24, 25, 26] or, alternatively, as a Fickett–Jacobs cycle [27] and ZND cycle. Regardless of whether the detonation cycle or its surrogate cycles are considered, all of these cycles produce work without the need to pre-compress the working fluid. This is unlike deflagration-based cycles such as the Otto, Diesel and Brayton cycles.

The detonation cycle forms the basis of pulsed detonation engines, similar to the Otto gas cycle being the basis of internal combustion engines. A pulse detonation device operates intermittently with each cycle comprising of several interdependent processes. These processes are illustrated by the basic scheme shown in Fig. 1.3. A tube, initially at quiescent conditions (1), is filled with propellants (2). The propellants could be either a fuel–air or a fuel–oxygen mixture. The propellants are shown in (2) as being fed from an end wall and propagating to the right at a relatively slow speed. At some instant during this fill process (3), combustion is triggered. Usually, due to the low initiation energy of the igniter, a run-up distance is required to transition to detonation. The detonation wave propagates into the tube (4). Ideally, the propellants are consumed at the end of the tube (5). The tube is purged in (6) by a reflected expansion that draws in the ambient gas

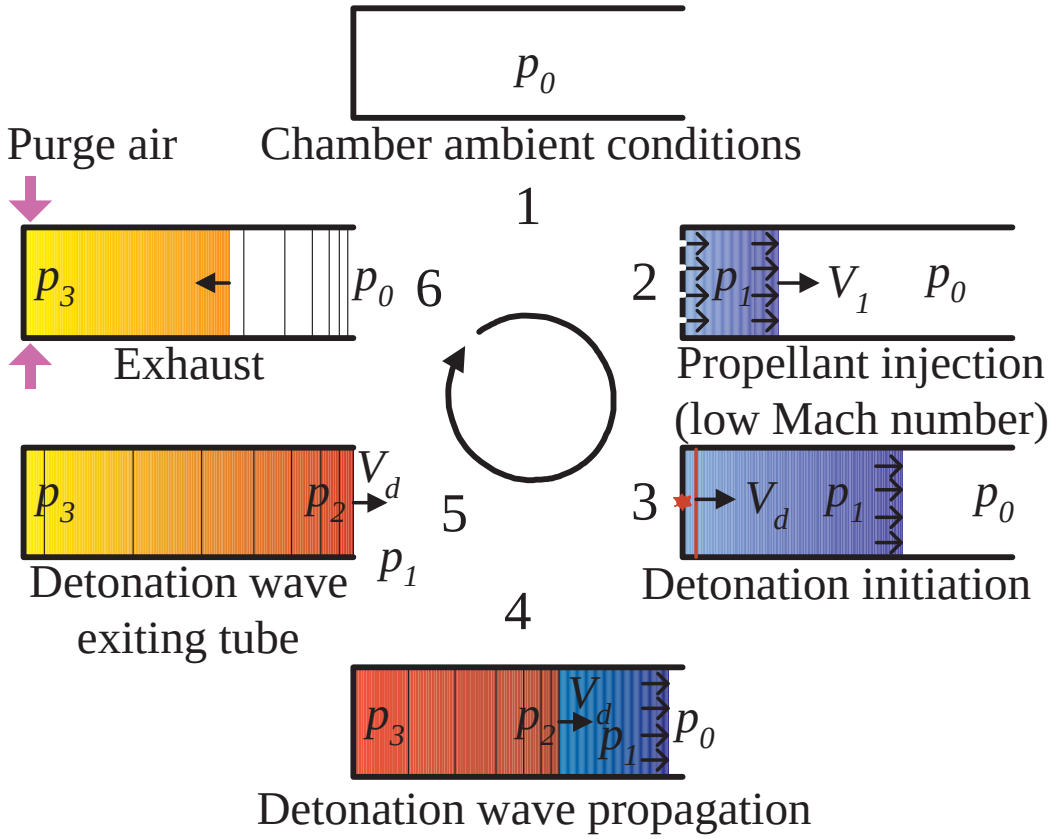

Figure 1.3. Basic pulse detonation scheme.

and returns the tube to its initial state (1) thereafter. In some implementations, a purge cycle is included to scavenge the tube off hot, burnt products prior to the injection of propellants for the next cycle. Theoretical analyses have shown that pulsed detonation devices have improved efficiency compared to existing deflagration-type systems, such as those based on the Brayton cycle [21, 22, 23, 24, 25, 28, 29, 30]. This is because, in principle, detonations are an extremely efficient means of combusting a fuel–oxidizer mixture and releasing its chemical energy content for work. Other than the improved thermodynamic efficiency of pulsed detonation systems versus deflagrative systems, the

former also possesses other advantages, such as wide operating range, scalability, reduced moving parts and operational simplicity, to name a few [20, 31, 32].

Research in pulse detonation has embraced the development of basic theory, design concepts, and detonation initiation and enhancement involving experimental and numerical simulations, amongst others. It is pertinent to point out that most of the emphasis to date has been in utilizing pulse detonation for airbreathing or rocket propulsion systems. Other than studying the core detonation process for propulsion, some work has also been performed to integrate pulse detonation into a propulsion system, such as modifying existing turbomachinery-based systems [33, 34, 35, 36, 37] or proposals for revolutionary systems in applications ranging from low-speed unmanned vehicles to missiles to space access vehicles [38, 39, 40, 41, 42, 43, 44, 45, 46, 47].

Practically all of the efforts on developing pulse detonation devices to date have been channeled toward propulsion [48] and the above-cited works, although some potential industrial applications have been reported [49, 50, 51]. It appears that pulse detonation may be the basis of electric power production systems. Many of the advantages pertinent to propulsion applications also are valid for power production applications, for example, high efficiency, reduced moving parts and scalability. Interestingly, the first reports of power applications were centered on exotic concepts coupling a magnetohydrodynamic generator to a pulse detonation engine for high-speed airbreathing flight or deep space applications [52, 53]. Nonetheless, it appears feasible to apply a more conventional approach whereby the available work from pulse detonation can be converted to electricity via a turbine–generator combination. Frankey et al. [36] and Hoke et al. [37] have performed preliminary studies on conventional power extraction. In particular, Hoke et al. showed that a turbine can survive long-duration, high shock loading from detonation waves.

1.1.3 Cycle Analysis

Attempts have been made to model pulse detonation propulsion systems with emphasis on obtaining performance estimates, such as thrust and impulse [54, 55, **?**, 56]. The modeling can be performed at different levels of detail [57], including interaction of the filling process with the detonation. However, the complexities involved in modeling the unsteady, pulsed detonation processes have thus far restricted most studies to using simple models [58, 59].

Other than numerical modeling, thermodynamic cycle analysis has been applied to assess the performance of pulse detonation devices [60, 61, 62, 63, 64, 65]. The techniques used typically avoid numerical modeling, thereby yielding algebraic relationships through simplifying assumptions. The above-cited works use first law, namely, energy concepts, to analyze the efficiency of propulsion systems, to study the interaction of processes such as filling with the detonation process [66] or to study the performance of the detonation process itself.

Hutchins and Metghalchi [67] present an energy and exergy analysis of a pulse detonation engine. They showed that detonation can be modeled as a Humphrey cycle. For different fuels such as methane and JP-10, Hutchins and Metghalchi showed that for the same pressure ratio, pulse detonation engines have better efficiency than gas turbines, especially at low pressure ratios.

Similar to the Otto and Diesel cycles that are used to understand the performance of intermittent combustion engines, the performance of PDEs can be estimated through a thermodynamic cycle analysis despite their unsteady behavior. Such a performance estimate based on ideal thermodynamic cycle analysis can be extended to "real" cycles, as is the acceptable practice in analyzing various types of thermodynamic systems [68]. In other words, using such a conceptual thermodynamic cycle provides a simple framework

for handling detonations in a purely thermodynamic fashion, avoiding the complexity of unsteady gas dynamics of realistic pulse detonation [69, 63].

1.2 Motivation and Scope of Present Research

The cycle analysis of PDEs is a great analytical tool to estimate the performance of such engines without the necessity of heavy computational fluid dynamics or expensive experimental equipment. Performing this analysis in such a way that the energy released in the chemical reaction is in a generalized form, i.e. independent of the fuel-oxidizer mixture, creates the possibility of applying the analysis for different purposes, such as propulsion or power production. Moreover, a comparison of the performance of different fuel-oxidizer mixtures can be made prior to engaging in experimental work. Finally, the addition of regeneration intends to deal with the utilization of the high temperature exhaust gases for useful work that, so far, has been ignored in previous analyses.

This work has as a goal the development of a generalized cycle analysis of an ideal PDE and to study the utilization of regeneration to improve the overall cycle performance and to harvest more useful work from the higher temperatures of the working fluid mixture achieved by the detonation process.

The objectives can be specified as to:

1. develop generilized thermodynamic relations that can be applied to a cycle analysis, that will be dependent on the initial condition, fuel-oxidizer mixture and heat addition;
2. perform a study of different fuel-oxidizer mixtures and compare the results to determine the most efficient and appropriate fuel-oxidizer mixture to be used. The analysis includes $p - v$ and $T - s$ diagrams and thermal efficiency;
3. use fuel-oxidizer mixtures that can be of interest for power production such as methane-air, propane-air and hydrogen-air;

4. for those specific fuel-oxidizer mixtures, an analytical approach will used in order to identify the CJ and ZND points in an ideal PDE cycle;
5. the approximations adopted for the detonation process are represented through the use of the Humphrey and ZND cycles;
6. The cycle analysis results for detonation are compared with the Brayton cycle which is the constant pressure cycle adopted to approximate the deflagration process;
7. introduce the concept of regeneration into the PDE cycle to utilize the high temperatures achieved by the mixture after the detonation process to improve the cycle efficiency;

Many theoretical concepts and models are considered for this work. An understanding and application of CJ and ZND model, especially the calculation of the CJ and ZND points; Rankine–Hugoniot relations, Rayleigh line; the states of an ideal PDE cycle, cycle efficiency and the concept of regeneration are necessary for the accomplishment of the objectives previously mentioned.

Chapter 2 introduced the detonation theory, its models and approximations. It explains how the PDE cycle can be represented thermodynamically. Chapter 3 discusses the thermodynamic analysis. The difference between the cycle and its approximations is presented It also shows how the thermodynamic states can be obtained. Chapter 4 discusses the use of regeneration and cogenerations in this study and how that can affect the performance of a PDE for power production. The following chapter presents the results for a cycle analysis and for the concerns about using regeneration in the system. The last chapter concludes this study, making points from the results that needed to be highlighted. It also introduces the possible improvements that can be made on this study and some suggestions for new approaches.

CHAPTER 2

DETONATION THEORY

2.1 Detonation vs. Deflagration

As previously mentioned, deflagration is a subsonic combustion process in which a flame front passes through the reactant mixture with flame speeds from less than a few meters per second to a few hundred meters per second, releasing the heat of reaction at a slow pace. On the other hand, detonation produces a supersonic combustion wave that propagates at a few thousands of meters per second relative to an unburned reactant–air mixture. The detonation wave is a shock wave driven by the energy released in the reaction zones right behind it. The reaction zone is known to be much thicker than the shock wave. The reaction zone and the shock wave are tightly coupled in a detonation wave and both propagate through the mixture at supersonic speeds.

When comparing the flow and thermodynamic properties for shock and reaction processes, one can notice that detonation is able to produce higher pressures, temperatures and densities at much higher speeds than deflagration. The benefit of this consequence for many applications, including not only propulsion but also power production, is evident.

In the previous chapter the beginning of detonation studies was discussed. Also mentioned is that there are presently two well-known theories that are used to model detonation waves, namely the Chapman–Jouguet (C-J) theory and the Zeldovich–von Neumann–Döring (ZND) theory. In the following section, a description of these models will be presented.

2.2 CJ Theory

The simplest theory adopted to describe the detonation wave is the Chapman–Jouguet theory [10, 13]. In this theory, the chemistry reaction rate is considered infinite, meaning the reaction is completed instantaneously. Additionally, the reaction zone and the shock are coupled and accounted for as a single jump discontinuity.

The detonation wave has a constant velocity, u_D, from the moment of initiation. The flow final state, right behind the reactive shock, satisfies the following one-dimensional flow conservation relation where (1) and (2) indicate the upstream and downstream states. In Eqs. (2.1–2.3) ρ, u, p and h are the density, velocity, pressure and enthalpy respectively, of the flow. The velocities u are measure with respect to the detonation wave. When Eqs. (2.1,2.3) are combined and u_2 is eliminated, a line in the p-v diagram can be defined. This is called the Rayleigh line and

$$\rho_1 u_1 = \rho_2 u_2 \tag{2.1}$$

$$p_1 + \rho_1 u_1^2 = p_2 + \rho_2 u_2^2 \tag{2.2}$$

$$h_1 + \frac{1}{2}u_1^2 = h_2 + \frac{1}{2}u_2^2 \tag{2.3}$$

$$\frac{u_1^2}{v_1^2} = \frac{u_D^2}{v_1^2} = \frac{p_2 - p_1}{v_1 - v_2} \tag{2.4}$$

Combining the conservation relations and the Rayleigh line equation, in such a way that the detonation speed u_D is eliminated, results in the relation for the Hugoniot curve in the p–v diagram.

$$h_2 - h_1 = \frac{1}{2}\left(p_2 - p_1\right)\left(v_1 + v_2\right) \tag{2.5}$$

The enthalpy can be expressed as

$$h_1 = c_{p1} T_1 + h_1^o \tag{2.6}$$

$$h_2 = c_{p2} T_2 + h_2^o \tag{2.7}$$

and where h^o is the enthalpy of formation at standard state, 298.15 K and 1 atm and c_p is the specific heat capacity at constant pressure. For a polytropic gas (ideal gas with constant heat capacity), the heat of combustion (heat release) is given by

$$q \equiv h_1^o - h_2^o \tag{2.8}$$

Combining Eqs. (2.4) and (2.5) yields the Rankine–Hugoniot relation.

$$\left(\frac{p}{p_0} + \mu^2\right)\left(\frac{v}{v_0} - \mu^2\right) = 1 - \mu^4 + 2\mu^2 \frac{q}{p_0 v_0} \tag{2.9}$$

where,

$$\mu^2 = \frac{(\gamma - 1)}{(\gamma + 1)} \tag{2.10}$$

It describes the detonation state, represented by (p, v), for a given detonation velocity as the intersection of both the Rayleigh and the Hugoniot curves.

Equation (2.9 is the equation for a rectangular hyperbola in the p–v plane, centered at the point $v = \mu^2$ and $p = -\mu^2$, where the distance between the center and the curve is a linear function of the heat release q. For the above equation, γ is the ratio of specific heats, and the gas is assumed to have constant specific heat.

From the equation described here, the final states of the flow are given as:

$$\frac{p_2}{p_1} = \frac{1+\gamma M_1^2}{1+\gamma} \tag{2.11}$$

$$\frac{\rho_2}{\rho_1} = \frac{(1+\gamma)\, M_1^2}{1+\gamma M_1^2} \tag{2.12}$$

$$\frac{T_2}{T_1} = \frac{\left(1+\gamma M_1^2\right)^2}{M_1^2\,(1+\gamma)^2} \tag{2.13}$$

where M, in the above equations, is the Mach number. From

$$M_1 = \sqrt{2\,(\gamma+1)\left(\frac{q}{\dot{m} c_p T_1}\right)} \tag{2.14}$$

it is seen that pre-heating the reactants reduces the detonation Mach number (though not the velocity), whereas, increasing the initial pressure increases the detonation velocity.

The Rankine–Hugoniot curve is the domain where all possible solutions for any flow going through a shock or combustion wave can be found. Figure 1.1 represents the Rankine–Hugoniot (R–H) curve and Rayleigh line on a p vs. $1/\rho = v$ space for a given value of heat release q. The characterization and validity of the different conditions of the flow were discussed in the Introduction.

The Rayleigh line equation can be used to plot constant velocity lines on the same chart, originating on the shock R–H curve at a point A, denoting the initial pressure and density, as seen in Fig. (1.1). The intersection of a Rayleigh line and the R–H curve of the particular value of q is the steady state solution of the final state of a detonation or deflagration wave. Based on the flow velocity, the R–H curve can thus be divided into five regions, each yielding a different solution of the final state, as shown in Fig. (1.1). At a certain minimum velocity, the Rayleigh line touches the R–H curve tangentially at the point U, called the upper Chapman–Jouguet (C–J) point. This is the minimum velocity solution for detonation of the particular mixture, at which the burnt products

are traveling at Mach 1 with respect to the detonation wave. For higher velocities, the Rayleigh line cuts the R–H curve at two locations, denoted by W and S; W is the weak solution for detonation, at which point the velocity of the burnt products is supersonic ($M_3 > 1$) with respect to the detonation wave. As a result, a growing region of constant state is created between the reaction zone of the detonation wave and the head of the rarefaction wave. The region between U and W1 (Region II in Fig. (1.1)) yields the weak detonation solution. The point S is called the strong point, representing a pressure higher than C–J pressure. The velocity of the burnt products in this solution is subsonic with respect to the detonation wave. As a result, the rarefaction wave may overtake the detonation wave and weaken it to a C–J detonation. Therefore, the strong, or over-driven, detonation is unstable. The portion of the R–H curve above U, called Region I in Fig. (1.1), is called the strong detonation region, in which the final state of the flow is always a strong detonation. In region III of the R–H curve, the slope of the Rayleigh line is positive and the wave velocity u_D is imaginary. Therefore, region III has no solutions and offers no state that is physically possible.

2.3 ZND Theory

The basics and origins of this one-dimensional theory were described in Chapter 1. Although, the ZND theory also predicts the same final state for the detonation process as the C–J theory, the former is able to predict the von Neumann spike.

Figure (2.1) shows all the possible solution for a flow going from the initial state A to the upper CJ point U. Solution a requires a large amount of energy deposition to the flow to induce direct detonation initiation. Solution b requires a very fast chemical kinetics, while solution c requires slow chemical kinetics. The most feasible solution is then solution d, starting with an adiabatic compression along the shock Hugoniot curve,

until it reaches the von Neumann spike, and finally the solution diverts sharply downward along the Rayleigh line to complete the course at point U.

The von Neumann spike presents an increase in pressure that is about 30 to 100 times higher than the initial pressure, lasting for a very small fraction of time [2].

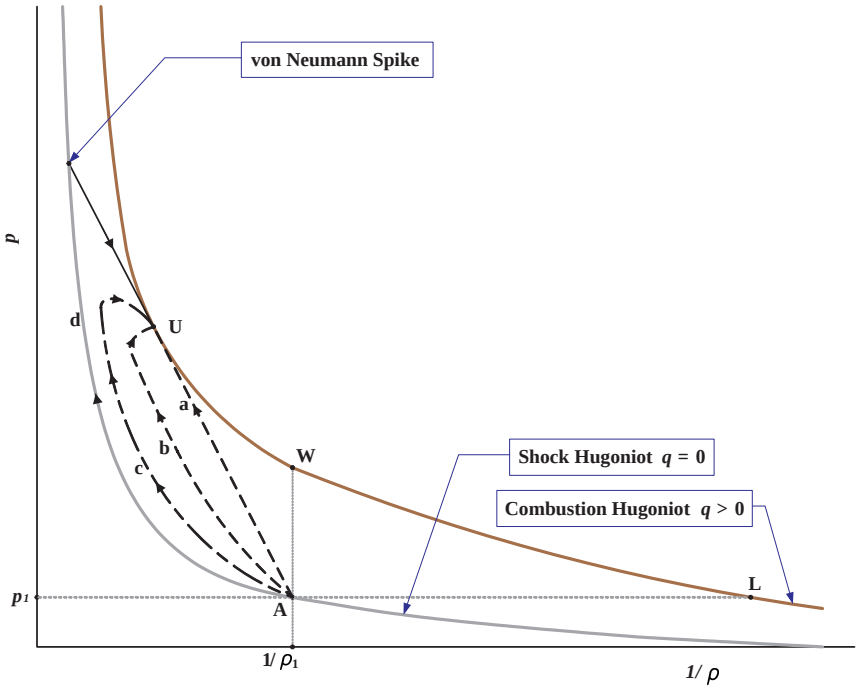

Figure 2.1. Rankine–Hugoniot curve showing the possible solutions that take the flow from initial state to the C–J point.

CHAPTER 3

CYCLE ANALYSIS

Thermodynamic analysis of PDEs usually makes use of one-dimensional models, based on the Chapman- Jouguet (CJ) and the Zeldovich-von Neumann- Doring (ZND) theories, although increasingly sophisticated techniques partly involving numerical modeling have also been developed lately.

Traditional gas cycles, such as the Otto, Diesel, and Brayton cycles, are based on the deflagrative mode of combustion for adding energy to the working fluid. A paradigm shift from deflagration-based cycles can be achieved by using detonations to develop thrust or power. A detonation wave travels at a few thousand meters per second compressing the quiescent upstream reactive mixture to trigger chemical reactions.

In this chapter the theories and equations that can be applied to the thermodynamic cycle analysis of a detonation and deflagration cycle are introduced and explained. The cycles adopted for this analysis are the Humphrey, ZND and Brayton cycles.

It will be shown that the more complex ZND cycle is preferable for PDE cycle analysis. The ZND cycle is practically different from the PDE cycle since the ZND cycle does not take into account the frequency of the PDEs. The ZND cycle is a representation of one detonation cycle.

To achieve these goals, the cycles, state properties and efficiencies have to be defined. The assumptions made will be laid out clearly in this section. The regeneration study will also be performed using the methodology and assumptions stated here.

3.1 Cycle Modeling

Cycle analysis is an excellent tool to compute the performance and to analyze the detonation process model. As stated above, the analysis will utilize two different models for the detonation process and will compare them with a model for a deflagration mode of combustion. Their performance will be presented and compared and the best model for the detonation process, according to the analysis made, will be selected.

Since the gas turbine engine is most commonly used as the prime-mover in medium to large scale power generators, the Brayton cycle is modeled here for comparison with the PDE cycles. As described earlier, the combustion process in the Brayton cycle is modeled as a constant pressure process as seen and described in detail in Figs. (3.8) and (3.9).

To model the detonation process, the aforementioned two cycles are shown. The first one is represented by the Humphrey cycle, show in Figs. (3.6) and (3.7). This cycle is a simple model for the detonation process. The detonation is modeled as a constant volume combustion process.

The fundamental advantage of the Humphrey cycle over the Brayton cycle is that the heat release is accompanied by an increase in pressure due to volumetric confinement. This allows Humphrey cycle engines to develop power more efficiently than a Brayton cycle engine with the same inlet state at the combustor.

The ZND cycle, which describes the detonation process in more detail, follows the ZND theory. According to that theory the detonation process can be described by two different specific parts described later in the chapter.

3.2 Mixture

For the present analysis, various fuel–air mixtures are examined as will be discussed later. However, independent of the fuel, the mixture is assumed to be fully mixed, in complete thermodynamic equilibrium, with no change in chemical composition and to have a constant specific heat ratio throughout the cycle, this approach is called the one-gamma model.

Table 3.1 shows the specific heat ratio for a methane–air mixture that goes through a detonation process. The values for the specific heat ratio are shown for the unburned and burned mixture and for different compressor pressure ratios, π_c. The values are obtained from the C.E.A. code [70]. The table also shows the value of γ that is used in throughout the analysis.

Table 3.1. Specific heat ratio for reactants and products of a detonation process and used specific heat ratio for various fuel–air mixtures.

mixture	π_c	$\gamma_{reactants}$	$\gamma_{products}$	γ used
Hydrogen–air	1	1.4015	1.1638	1.4015
	20	1.4015	1.1887	
Methane–air	1	1.3883	1.1688	1.3883
	20	1.3883	1.1915	
Propane–air	1	1.3683	1.1661	1.3683
	20	1.3683	1.1887	

By comparing the values presented in Tab.3.1, it is seen that there is a great difference between the values presented, especially as the compressor pressure ratio increases. The data shows that considering different values for the specific heat ratio can influence the results. However, using the one–gamma model makes the analysis more simpler and applicable for a wide variety of fuels, and helps the creation of an analysis tool that does

not require the user to have detailed information about the chemical reaction as will be shown later.

Another assumption made about the mixture is that it is a stoichiometric mixture. A stoichiometric mixture is a mixture that has a fuel–air ratio $f = 1$. Using a stoichiometric mixture brings many advantages not only to detonation mode of combustion but also to deflagration mode of combustion. The first advantage is that the adiabatic flame temperature during the combustion is at its highest at stoichiometric condition. The adiabatic flame temperature is the maximum temperature that can be achieved for a given set of reactants. In addition, the CJ velocity, the pressure ratio and the temperature ratio are the highest at $f = 1$. Moreover, the detonation size cell is the smallest for a stoichiometric mixture. This can be seen in Figs. (3.1) and (3.2). Figure (3.1) shows the cell size vs. fuel–air ratio for different mixtures. Figure (3.2) shows the detonation cell size vs. fuel–air ratio for a hydrogen–air mixture. With a small detonation cell size, the deflagration-to-detonation transition (DDT) is improved and it increases the sensitivity of the mixture to detonation, decreases ignition delay, activation energy and the minimum and critical tube diameters. All of these factors improve the detonation process also.

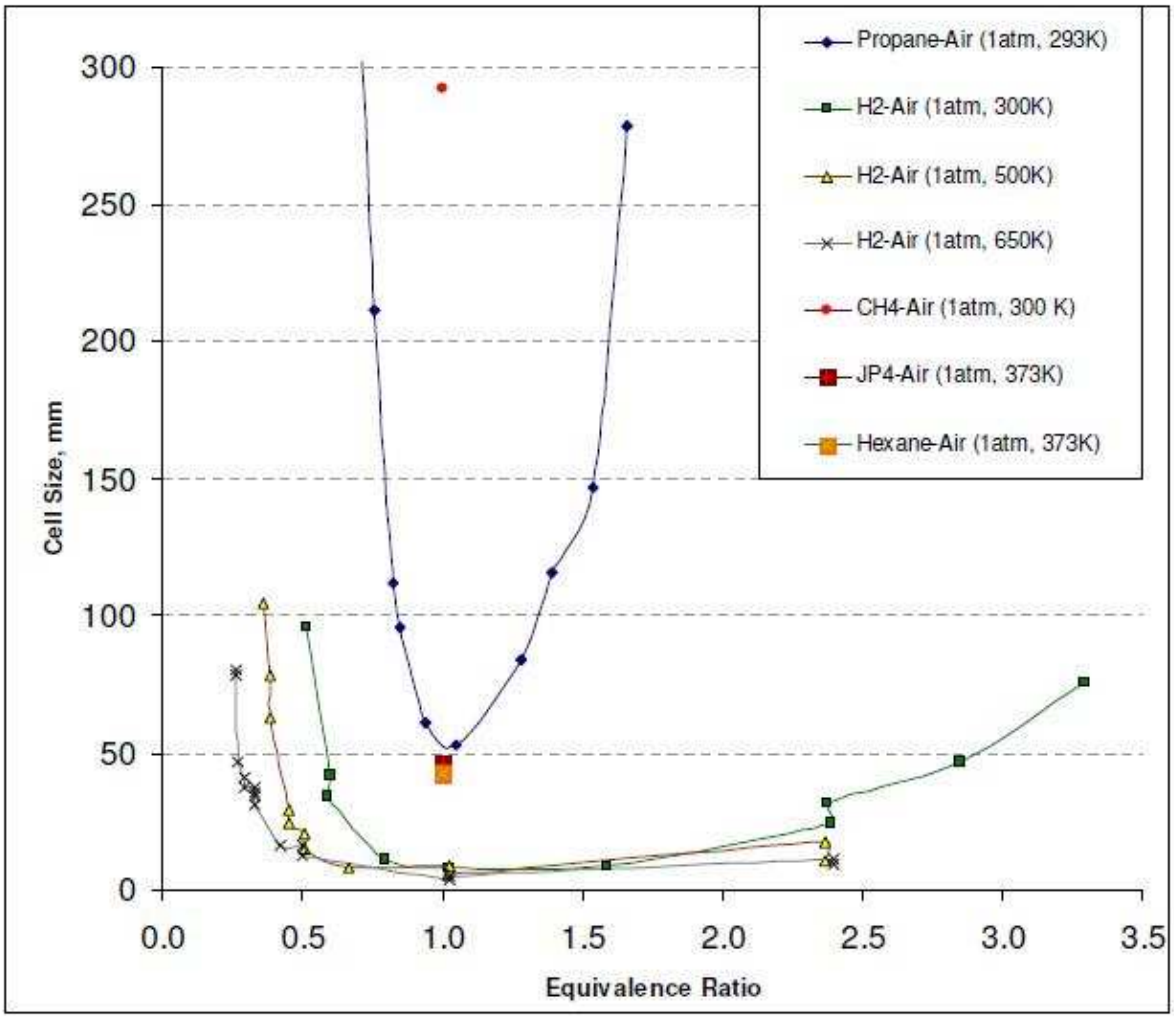

Figure 3.1. Detonation cell size vs. equivalence ratio for various fuel–air mixtures [1].

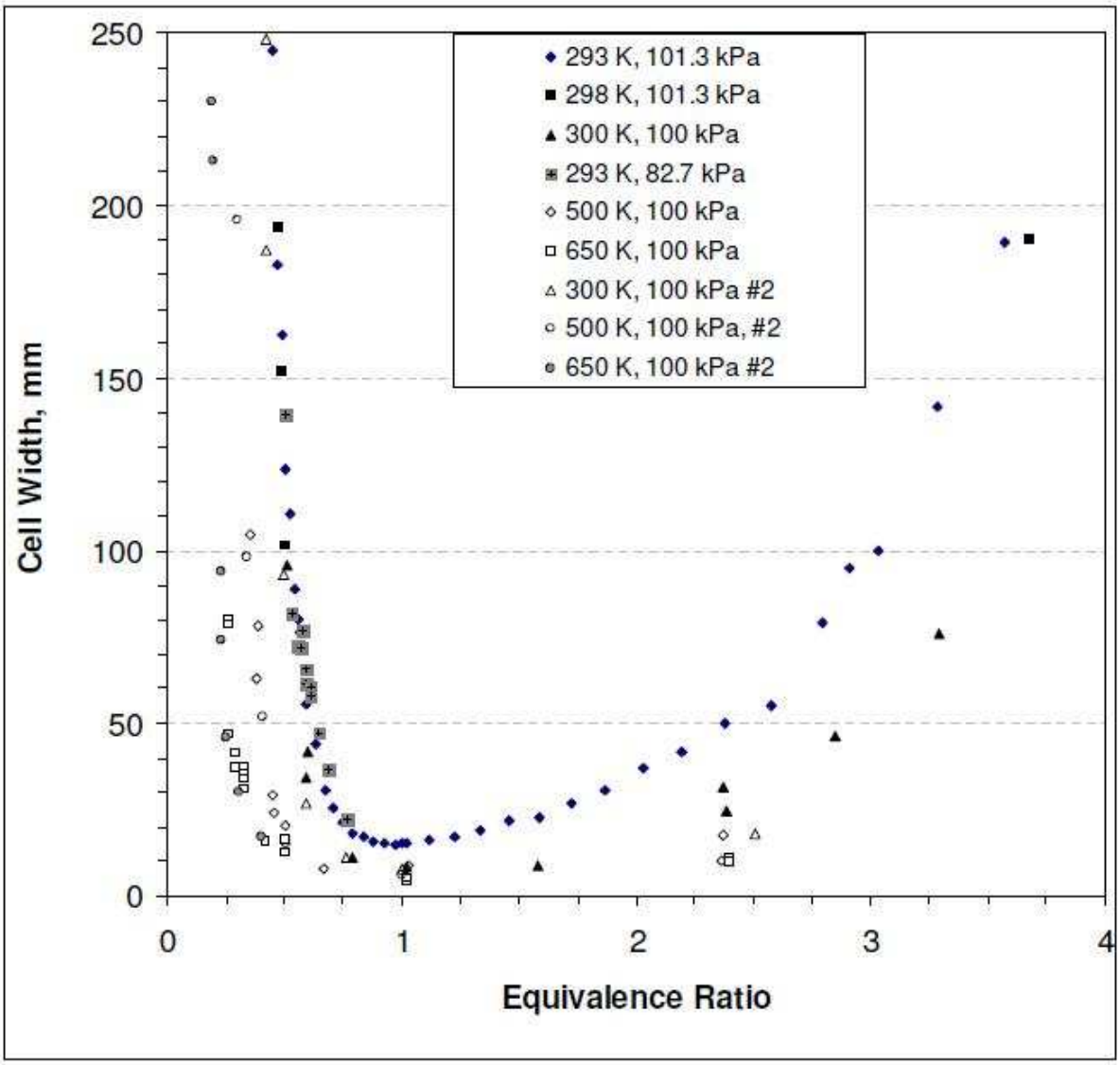

Figure 3.2. Detonation cell size vs. equivalence ratio for a hydrogen–air mixture [1].

3.3 Detonation vs. Diesel

The most common choice of an engine for a land based power production device would be the diesel engine. Diesel engines are used in small scale power generators, rated in the range of a few hundred Watts, medium scale power generators, rated in the range of a few kilowatts, and all the way up to large scale power generators, rated in the

megawatts. It is know that the energy efficiencies of diesel engines are between 35% and 40%. Compared to the less efficient gasoline based engines, diesel engines have lower fuel costs and burn the fuel more completely. Diesel engines are also used in locomotives, tanks and ships for direct shaft power for propulsion or to generate onboard electric power by means of an electric generator which turns an electric motor that drives the wheels or propeller. On the other hand, diesel engines are known to be very bulky and heavy and to have significant heat loss. Another disadvantage of diesel engines is that they require very complex components, such as very high pressure fuel injection systems for example.

The PDE cycle, having a higher theoretical efficiency than the Otto or diesel cycles, also promise other advantages for power production. PDEs have the potential of being more compact and even portable and theoretically are very simple in design. Another great advantage of PDEs is the possible use of a wide range of fuels, including hydrogen and methane. In addition, PDEs can have higher power to weight ratio.

Using PDEs for power production seems like a very straightforward option when taking into account all the advantages compared to the main stream options such as diesel engines. In the next chapter, an analysis of the detonation based system will be performed to establish how efficient PDEs can be and what conditions are necessary to ensure high efficiencies.

3.4 Thermodynamic Properties

Given a generic power cycle, represented by Fig. (3.3) one can explain how the thermodynamic states 0, 1, 2 and 3 can be determined, assuming complete thermodynamic equilibrium. Each process present in those cycles can be described as follows. From the initial state, an isentropic compression takes place ($0 \rightarrow 1$), followed by a heat addition process representing the detonation process ($1 \rightarrow 2$) and an isentropic expansion

$(2 \rightarrow 3)$ that takes the mixture to the initial pressure. The cycle ends with an isobaric heat release $(3 \rightarrow 0)$ that takes the mixture back to its initial state.

The processes described above are common in all the cycles studied, with the exception of the heat addition, also called, sensible heat or heat value which is the heat of reaction during the combustion.

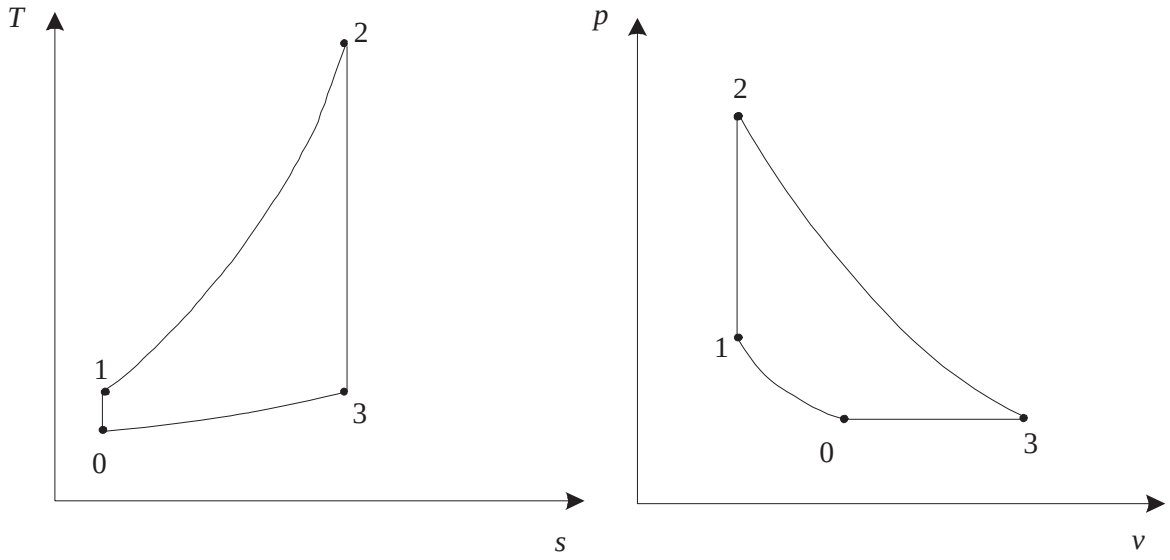

Figure 3.3. T–s and p–v diagrams of a generic power cycle.

State 0 is the initial state of the mixture. In the present analysis all the values are considered with respect to the initial values, e.g. v/v_0 and p/p_0. In the case of power production, a compressor can be utilized to accomplish an increase in pressure and temperature of the mixture prior to the combustion process.

Figures (3.4) and (3.5) show the p–v and T–s diagram for the ZND cycle, where the $(0 \rightarrow 1)$ process is assumed to follow the inert Rankine–Hugoniot curve according to the Eq. (2.9), assuming that the final pressure p_1 is that of the one achieved by

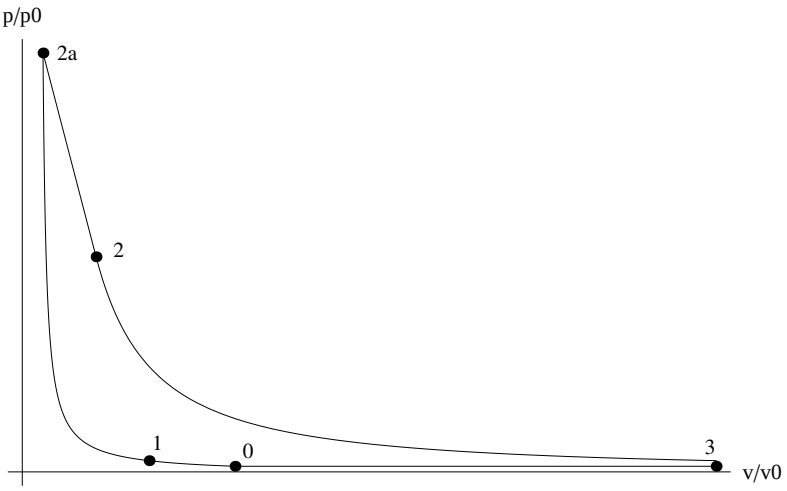

Figure 3.4. p–v diagram of a ZND cycle.

the compressor. Process $(1 \rightarrow 2)$ describes the heat addition or combustion process. For the ZND cycle this process can be divided in two specific parts. The first one is process $(1 \rightarrow 2a)$, where the mixture is taken from state 1 to state $2a$, called the von Neumann spike, through the inert Hugonior–Rankine curve. That process is identified as the leading shock wave, where no reaction takes place. The second process $(2a \rightarrow 2)$ is where the mixture is taken from state $2a$ to the CJ condition, state 2, located in the reactive Hugoniot curve and it is identified as the release of sensible heat in constant area and where the reaction takes place. The ZND cycle assumes that a straight line connects the two states. The CJ condition is that the Rayleigh line and the Hugoniot curve be tangent, so their slopes are equal at the CJ point. So, knowing the slope for the Hugoniot curve and knowing that the Rayleigh line connects the initial state to the CJ state and to the von Neumann spike, states $2a$ and 2 can then be determined. The slope is calculated by taking the derivative of the Hugoniot curve with respect to the specific volume and applying it to the initial state, to the CJ state and the von Neumann spike.

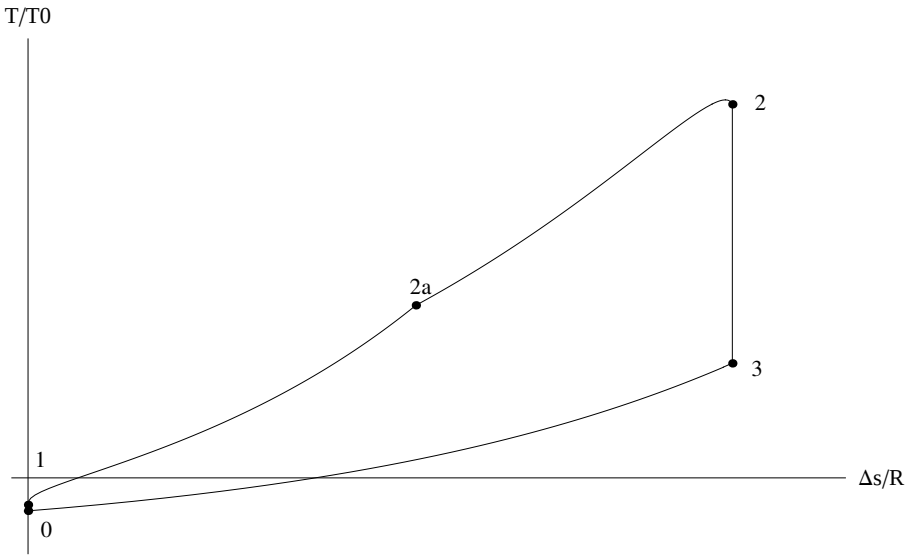

Figure 3.5. T–s diagram of a ZND cycle.

Process $(2 \rightarrow 3)$ is an isentropic Taylor expansion, where the final pressure p_3 is equal to the initial pressure p_0. Using the isentropic relations

$$\frac{T}{T_0} = \left(\frac{p}{p_0}\right)^{\frac{\gamma-1}{\gamma}} \tag{3.1}$$

$$\frac{T}{T_0} = \left(\frac{v}{v_0}\right)^{\gamma-1} \tag{3.2}$$

$$\frac{p}{p_0} = \left(\frac{v}{v_0}\right)^{\gamma} \tag{3.3}$$

and knowing that the entropy change for a calorically perfect gas is given by

$$\Delta s = c_v \ln \frac{T}{T_0} + R \ln \frac{v}{v_0} \tag{3.4}$$

$$\Delta s = c_p \ln \frac{T}{T_0} - R \ln \frac{p}{p_0} \tag{3.5}$$

the thermodynamic properties of state 3 can be determined. Process $(3 \rightarrow 0)$ is an isobaric heat release that takes the mixture to its initial state 0.

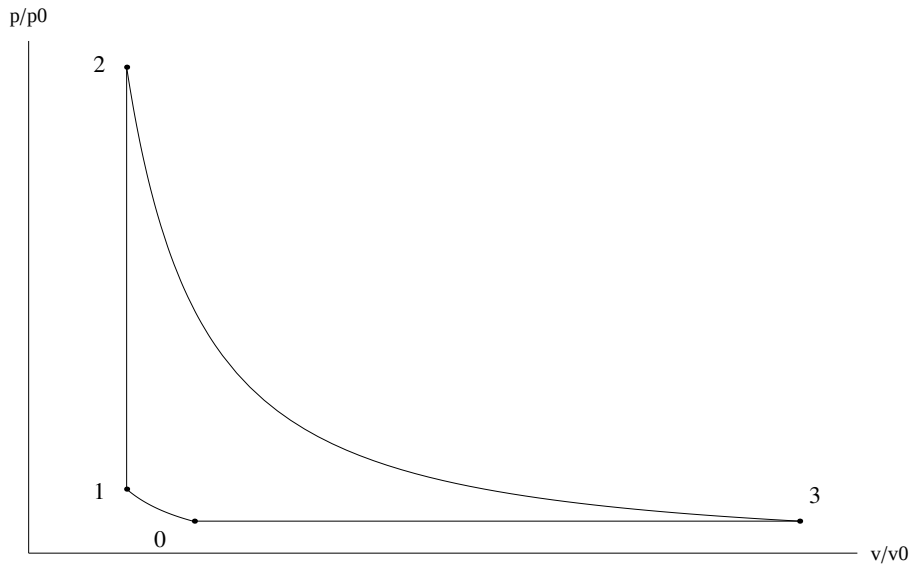

Figure 3.6. p–v diagram of a Humphrey cycle.

For the Humphrey cycle, process $(0 \rightarrow 1)$ is an isentropic compression. So assuming an initial compressor pressure ratio and using the isentropic relations given by Eqs. (3.1) to (3.3), state 1 can be determined. The main difference between the ZND and Humphrey cycles lies in the combustion process, since for the latter this process is assumed as a constant volume process. So, the heat addition process, $(1 \rightarrow 2)$, is assumed the same as the the heat addition obtained in the ZND cycle according to the equations for heat addition.

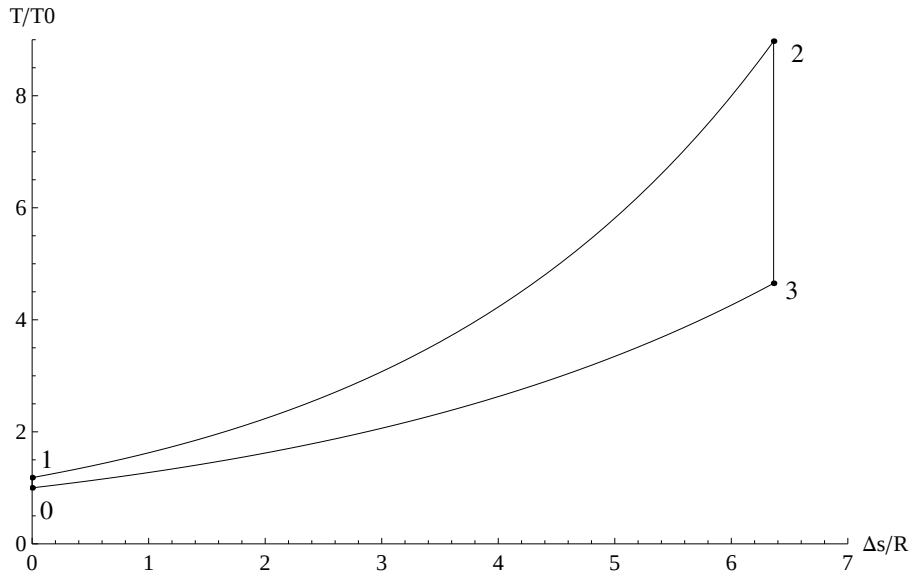

Figure 3.7. T–s diagram of a Humphrey cycle.

$$q = \Delta h \tag{3.6}$$

$$\Delta h = c_p \Delta T \tag{3.7}$$

$$q = c_p \Delta T \tag{3.8}$$

Given that

$$\alpha = \frac{q}{p_0 v_0} \tag{3.9}$$

and

$$\begin{aligned} \frac{c_v}{R} &= \frac{1}{\gamma - 1} \\ \frac{c_p}{R} &= \frac{\gamma}{\gamma - 1} \end{aligned} \tag{3.10}$$

the conditions for state 2 can be determined.

Processes $(2 \rightarrow 3)$ and $(3 \rightarrow 0)$ are exactly the same as the ones described for the ZND cycle.

To describe a deflagration mode of combustion, the Brayton cycle is adopted, and represented by Figs. 3.8 and 3.9. The main difference between the ZND, Humphrey and Brayton cycles, is that the latter assumes that the combustion $(1 \rightarrow 2)$ is a constant pressure process. All the other processes were previously described and the heat addition was the same as the ones used in the previous cycles.

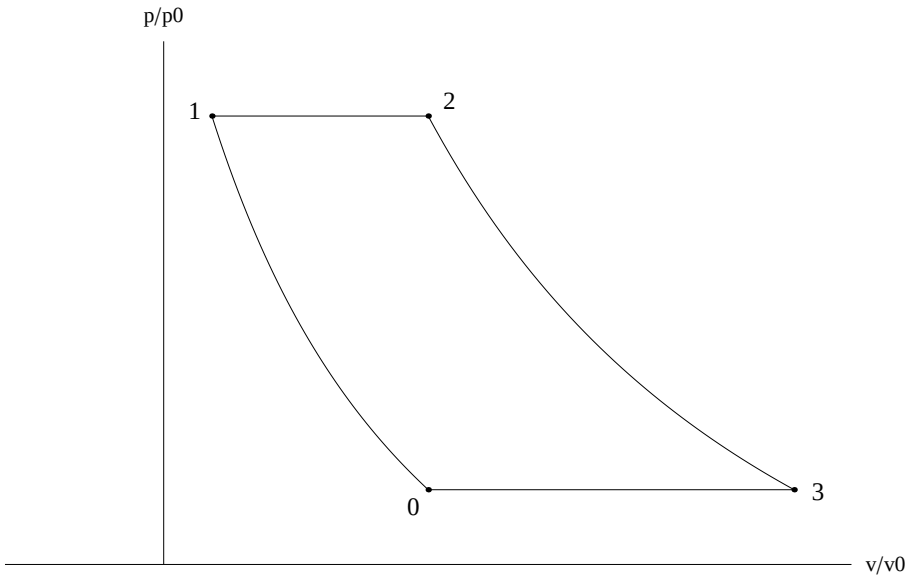

Figure 3.8. p–v diagram of a Brayton cycle.

For propulsion, the compressor in the detonation engines may be eliminated or have fewer stages (fan). For power production a compressor is used. The compressor is represented by process $(0 \rightarrow 1)$, which is driven by part of the useful work from the isentropic expansion process $(2 \rightarrow c)$.

The end of the Rayleigh heat addition is followed by a Taylor rarefaction. This rarefaction results in an isentropic expansion of the post-detonation products $(2 \rightarrow 2')$.

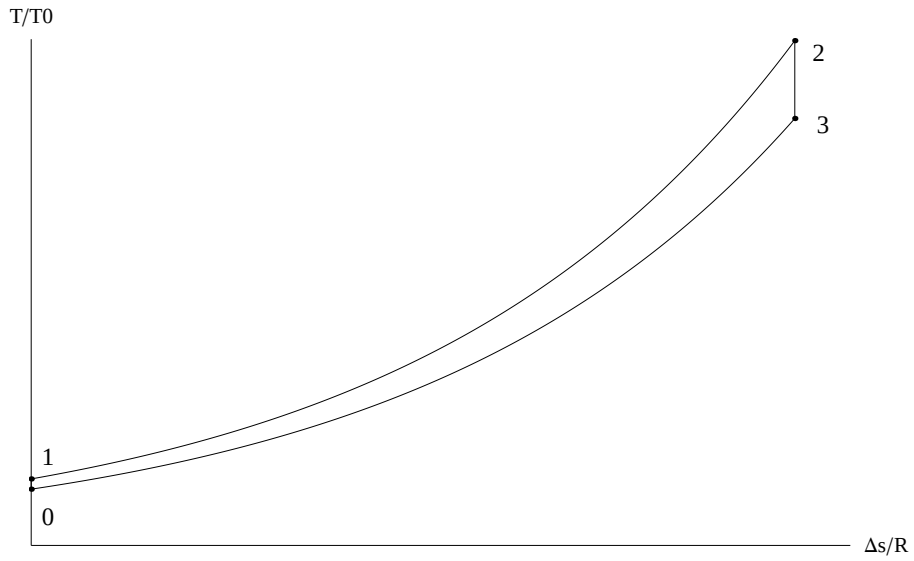

Figure 3.9. T–s diagram of a Brayton cycle.

This process is unable to produce shaft work output or increase the exhaust kinetic energy. The useful work output starts then from state $2'$, after the rarefaction process. Kentfield [62] showed that the temperature relationship for the ZND and Brayton cycles is $T_{2',ZND} = T_{2,Brayton}$ and the enthalpies relationship is $h_{2',ZND} = h_{2,Brayton}$. The heat addition is an adiabatic process without shaft work interaction.

3.5 Cycle Performance

In order to compute the thermal efficiency of the cycle, the energy input and output have to be identified. The heat addition or the heat of reaction q_{add} is defined as the heat removed to allow the combustion products to return to the initial temperature and pressure of reactants [61]. This means that q_{add} is the enthalpy change between the

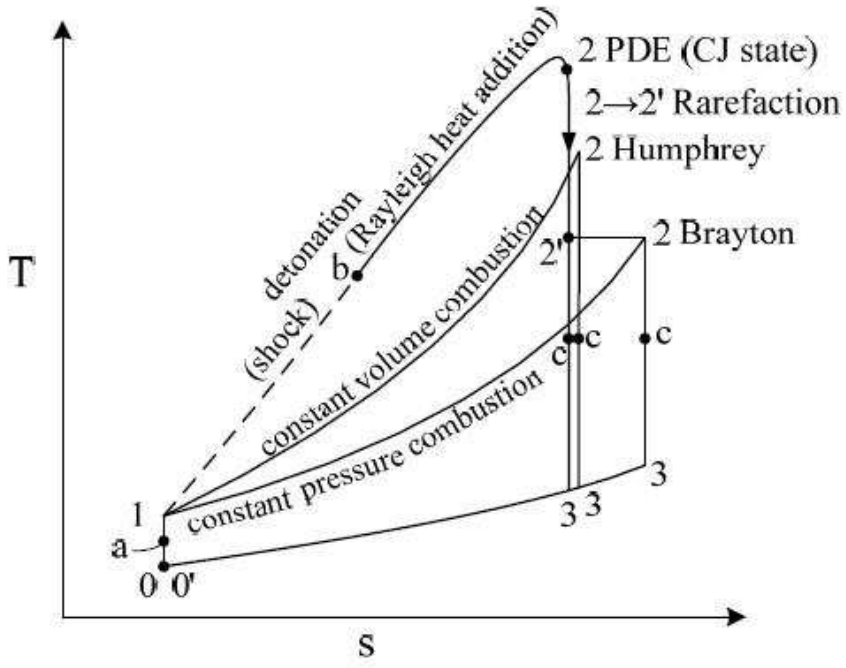

Figure 3.10. Comparison of T–s diagrams for various cycles.

reactants and the products both at the reactants' temperature and pressure (state 0), as given in Eq. (3.11).

$$\begin{aligned} q_{add} &= \dot{m}_f h_{PR} \\ &= \dot{m}_f \left(h_R - h_P \right) \end{aligned} \tag{3.11}$$

The h_R and h_P are the enthalpies of formation of the reactants and the products, respectively.

The heat rejected, q_{rej}, is the heat rejected through the exhausted flow (state 3) into the atmosphere (state 0) under a constant pressure process.

For power production, the performance of the cycle is based on the shaft work output defined as the specific work output W_{out} in kW per kg/s of air mass flow (kW/kg/s).

The work output is a portion of the heat addition, defined as $q_{add} - q_{rej}$. Using the previous definition, the thermal efficiency of the cycle is given by Eq. (3.12).

$$\eta_{th} = \frac{\text{work output}}{\text{heat addition}} = 1 - \frac{q_{\text{rejected}}}{q_{\text{added}}} = 1 - \frac{(1+f)\,(h_3 - h_0)}{f h_R} \tag{3.12}$$

The heat of reaction of unit mass of fuel (kJ/kg) is defined by Eq. (3.13).

$$\begin{aligned} h_{PR} &= \frac{1+f}{f}\,(h_{PR})_{mixture} \\ &= \frac{1}{f}\,(h_{PR})_{air} \end{aligned} \tag{3.13}$$

3.6 PDE Frequency

A PDE is modeled as a straight tube with a constant cross section. One end of the tube is closed and the other is open. For simplicity, gases are treated as polytropic. It is also assumed that viscous effects and thermal conduction are negligible and that the flow is one-dimensional.

Since PDEs operate cyclicly and due to the nonlinear nature of the detonation process, many of the thermodynamic properties used for cycle and performance analyses do not represent the real results with accuracy. One of the methods that the cyclic mode of operation can be accounted for is to make use of cycle averaged properties.

The Endo-Fujiwara model [60] is adopted here to average the cycle properties. For more detail on the model the original article can be accessed.

The model assumes an tube with one open end. The detonation wave is initiated at the closed end and propagates to the open end. When the detonation wave breaks out from the open end, a rarefaction wave starts to propagate from the open end toward the

closed end called the thrust wall. An analytical study is performed Endo-Fujiwara [60] to represent the decay pressure profile history at the thrust wall shown in Fig. (3.11). The period $0 \leq t \leq t_{plateau}$ is named the combustion phase. And, it is within that

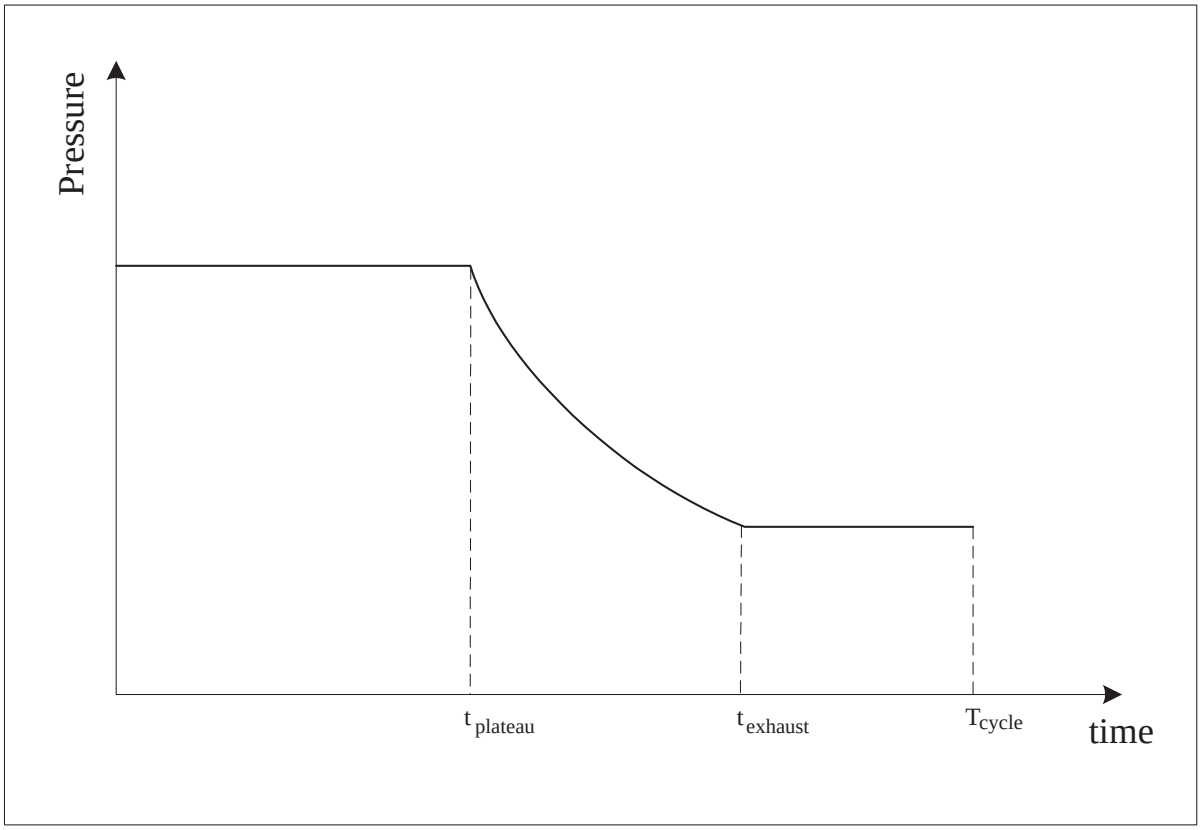

Figure 3.11. Detonation wave pressure profile.

phase that the whole detonation process takes place and the detonation wave exits the tube. At time $t = t_{plateau}$, another rarefaction wave is created and starts to propagate from the open end to the closed one. Through this rarefaction wave, the burned gas is exhausted from the open end of the tube. The exhaust of the burned gas lasts until time $t = t_{exhaust}$, called the exhaust phase. After time $t = t_{exhaust}$, the tube is recharged with

a fresh detonable mixture, and the recharging of the tube is completed at time $t = T_{cycle}$. The time $t_{exhaust} \leq t \leq T_{cycle}$ is named the filling phase.

The model start with the introduction of some PDE wave parameters, given by Eqs. (3.14) to (3.18).

$$k_1 = \frac{\gamma + 1}{2\gamma} \tag{3.14}$$

$$k_2 = \frac{\gamma - 1}{2\gamma} \tag{3.15}$$

$$k_3 = \frac{k_1}{k_2} \tag{3.16}$$

$$k_4 = \frac{2\left[(\gamma k_1)^{k_3} - 1\right]}{\gamma} k_2 \tag{3.17}$$

$$k_5 = 2k_1^{-k_3/2} \tag{3.18}$$

The time for the wave to reach the CJ position can be given by

$$t_{CJ} = \frac{L}{D_{CJ}} \tag{3.19}$$

and at the end of the combustion phase the time can be determined by Eq. (3.20), that represents the time at which plateau in pressure history at thrust wall ends.

$$t_{plateau} = k_5 t_{CJ} \tag{3.20}$$

Introducing a new set of parameters, given by Eqs. (3.21) to (3.24).

$$K_1 = k_4 \left[k_1^{k_1} M_{CJ}^{2k_2} \left(\frac{0.5\gamma}{\gamma} \right)^{k_2} - 1 \right] + k_5 \tag{3.21}$$

$$K_2 = \frac{k_4 \left[1 - \left(\frac{K_1 - k_5}{k_4} + 1 \right)^{-k_3} \right]}{k_3} \tag{3.22}$$

$$K_3 = \frac{K_2 \left(\frac{K_1 - k_5}{k_4} + 1 \right)^{\frac{1}{k_2}} - K_1}{\left(\frac{K_1 - k_5}{k_4} + 1 \right)^{\frac{1}{k_2}} - 1} \tag{3.23}$$

$$K_4 = \frac{K_3 \left[\left(\frac{K_1 - k_5}{k_4} + 1 \right)^{\frac{1}{k_2}} - 1 \right]}{M_{CJ}^2 \gamma} \tag{3.24}$$

where D_{CJ} is the ChapmanJouguet detonation speed.

The exhaust time, defined as the time when the pressure at the thrust wall is the same as the initial pressure, can be then determined as

$$t_{exhaust} = t_{CJ} K_1 \tag{3.25}$$

and the frequency of the detonation cycle can be obtained according to Eq. (3.26). For a given detonation process, this is the maximum frequency that a cycle can have in order to have a full detonation cycle developed.

$$freq_{max} = \frac{1}{t_{exhaust}} \tag{3.26}$$

The filling pressure can be given by

$$p_{fill} = \frac{M_{CJ}^2 \gamma k_1^{k_3} p_0}{2\gamma} \tag{3.27}$$

and the pressure profile during the exhaust time is determined by Eq. (3.28).

$$p_{plateau} = p_{fill} \left[\frac{k_4 t_{CJ}}{k_4 t_{CJ} + (t - t_{plateau})} \right]^{\frac{1}{k_2}} \tag{3.28}$$

And finally, the expression for total time of the detonation cycle T_{cycle} is given in Eq. (3.29).

$$T_{cycle} = \left[1 + (\gamma k_1)^{k_3} \right] 2t_{CJ} \tag{3.29}$$

The variables k_1 to k_5 and K_1 to K_5 are parameters that will aid in determining the flow properties, such as the pressures, and the times that constitute the various periods of the cycle. The model analytically determined the pressure history at the thrust wall, whose formulas were compared with numerical and experimental results. For the parameter described here, the numerical and experimental results used by Endo-Fujiwara [60] were well reproduced by the model for the decay pressure at the thrust wall. For more details on the model presented above, and how the properties and times are computed, please refer to the original article by Endo-Fujiwara [60].

CHAPTER 4

REGENERATION AND POWER PRODUCTION

In any heat engine, the heat rejected in the cycle through the exhaust gases has potentially useful energy that could be used for other purposes. The temperature of the exhaust gases from the PDE or the hybrid PDE-turbine system will undoubtedly be above the ambient temperature, and therefore, has valuable energy. This energy can be safely captured and harvested for useful work before being wasted permanently into the environment. In this chapter, two such methods are discussed. The results of a quantitative analysis of the increase in efficiencies due to the addition of regeneration is presented and discussed in the next chapter.

4.1 Regeneration

The heat from the exhaust gases can be fed back into the system by means of a regenerator. A regenerator is a heat exchanger that uses the hot exhaust gases to preheat the air coming out of the compressor before entering the combustor. In a gas turbine engine, regeneration helps to reduce the fuel required to heat the core flow through the combustor to the required maximum combustor temperature T_2. In multi-stage gas turbine compressors, there may be an intercooler in between the low pressure and high pressure compressors. The regenerator would be applied at the end of the final compressor stage or at the exit of the combustor. In a PDE, the compressor does not have to be as large or require as many stages and may be replaced with a fan which can be driven by a low pressure turbine. Thus, the extra energy in the flow can be captured with the high pressure turbine to run an electric power generator.

The use of a regenerator in a PDE-turbine system is illustrated in Fig. (4.1). Preheating the air using a regenerator has some extra benefits in a PDE in addition to a reduction in fuel usage. The energy required to ignite the fuel–air mixture will be lowered considerably whereby the life of the ignition system can be extended. If the fuel used is a liquid that has to be sprayed and mixed in with the air, preheating the air will aid in quicker vaporization of the liquid fuel. The regenerator can also be applied to preheat the liquid fuel to enhance the vaporization of the fuel. This will reduce the fuel–air mixing times and enhance the mixing, which is critical for a PDE since a properly mixed fuel–air mixture is required for a successful detonation. In addition, various detonation properties depend on the initial pressure and temperature of the reactants. The detonation cell size, ignition delays and DDT run up distance and time vary inversely with pressure and temperature [71, 1]. It is widely known that the cell size of a mixture is inversely related to the sensitivity of the mixture to detonation. Thus, a mixture with smaller cell size will be more sensitive to undergo detonation and have lower activation energy and ignition delays. Thus, higher the initial temperature and pressure of the mixture, the faster DDT will occur. Reference [72, 71] has a good collection of experimental data on hydrogen–air mixtures that show the inverse relationship of cell size with initial temperature and pressure. Thus, regeneration can help in bringing about successful and consistent detonations in a PDE.

Current state of the art of turbine technology places a ceiling on turbine inlet temperatures at about 1850 K due to material limitations. Thus, in a PDE, which produces much higher temperatures than deflagration based engines, it is important to limit the exit temperature of the flow leaving the combustor to protect the turbine blades. The turbine inlet temperature can be lowered by mixing cold air with the combustor core flow or by introducing regeneration at the exit of the combustor and before the turbine, shown as a dotted path in Fig. (4.1)[73]. Thus, unlike gas turbine engines in which

regeneration is always introduced at the end of the turbine, in PDE-hybrid systems, there are two possibilities for regeneration, before and after the turbine.

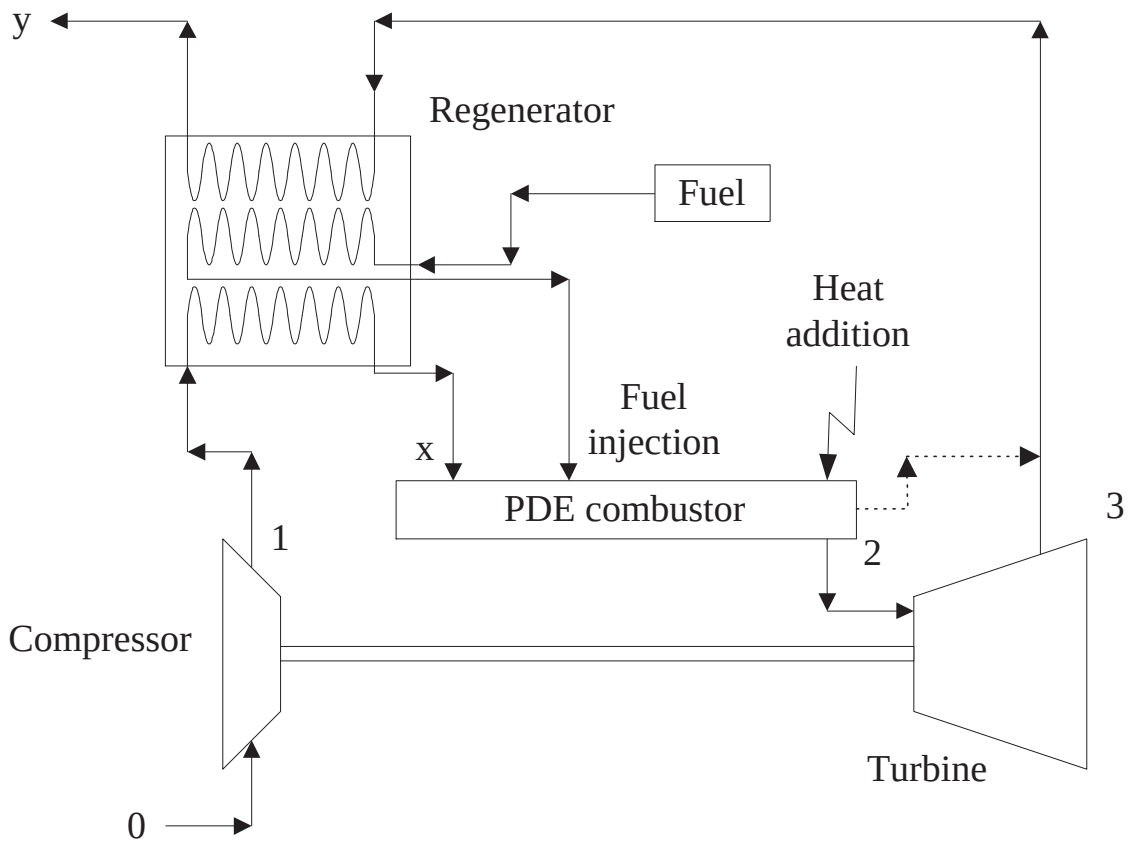

Figure 4.1. Schematic of a hybrid PDE with regeneration.

4.2 Cogeneration

The thermodynamic efficiency of a fuel can be maximized in a PDE system by using cogeneration. The waste heat from a PDE can be used for process heating or for steam generation in a cogenerative system, as illustrated in Fig. (4.2). Cogeneration is a method of using a heat engine to generate both power (thrust or shaft power) and

electricity. If the waste heat has temperatures is in excess of 100°C, the heat can be used to produce steam to run a steam turbine-generator system. Hot water can also be used for district heating (space heating or water heating for homes and industry) or for process heat for industrial applications. In addition, a third sub-system can be incorporated in a concept called trigeneration. This is the application of waste heat with temperatures in the range of 100 to 180°C in absorption chillers for refrigeration and air conditioning. Thus, a PDE's waste heat can be used for electricity, heating and cooling simultaneously, thereby extending the usefulness of a fuel.

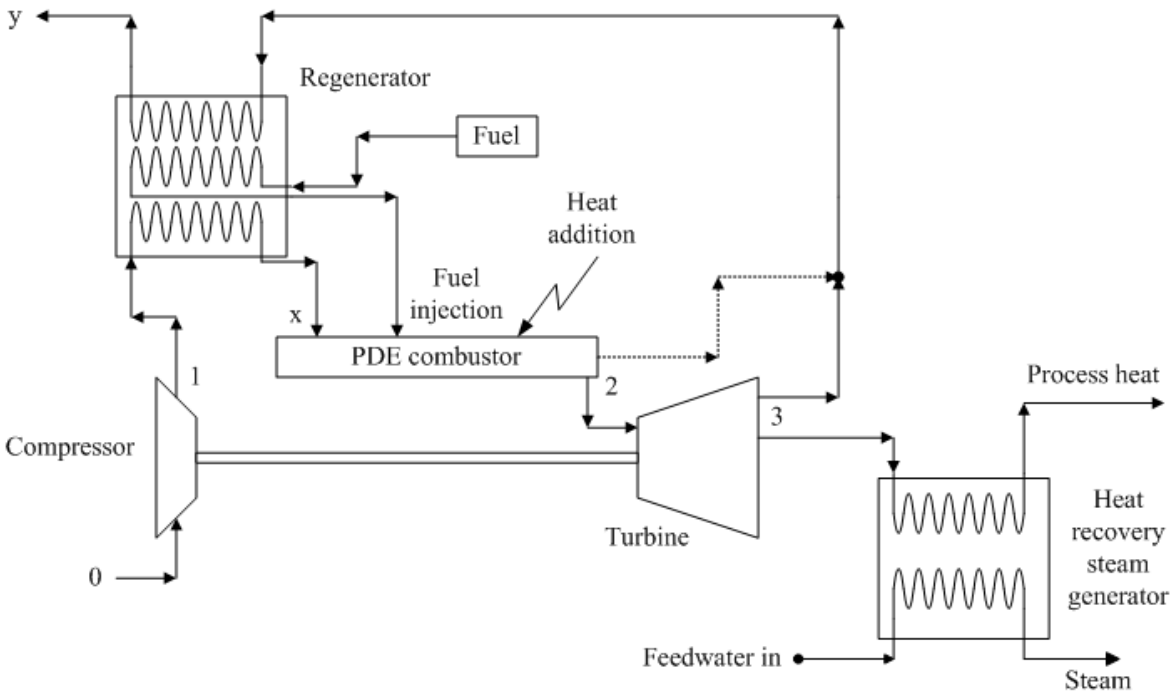

Figure 4.2. Schematic of a hybrid PDE with regeneration and cogeneration.

4.3 Power Production

When using PDEs for land based power production devices, a generator is added to the system in order to produce electricity. Figure (4.3) shows, schematically, how a generator is incorporated to a PDE to produce electric power. The first stage of the turbine is used to drive the compressor.

The next stages drive the electric generator through a transmission system consisting of a set of gears, shafts and other torque converting equipment. The addition of these components also bring added losses to the system that have to be considered when computing the efficiencies. The generator efficiency η_{gen} represents how much of the shaft power provided by the turbine is transformed into electrical power. The value of the generator efficiency is typically the same as the motor efficiency, since the generator is theoretically the inverse of a motor [74]. The efficiency of the shaft power transmission system is denoted by η_{shaft}. Thus, the total mechanical to electrical conversion efficiency can then be written as shown in Eq. (4.1).

$$\eta_{MEC} = \eta_{th}\ \eta_{shaft}\ \eta_{gen} \tag{4.1}$$

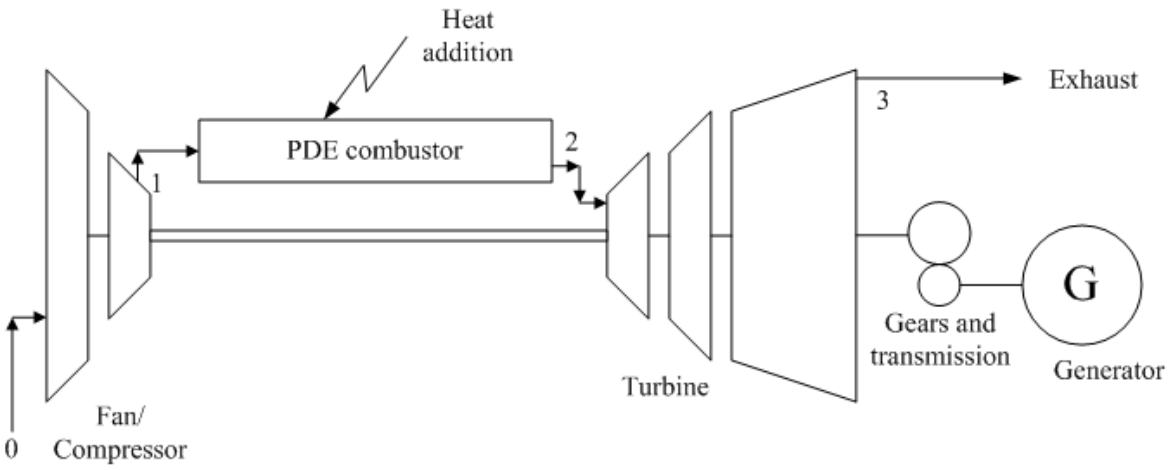

Figure 4.3. Schematic of a PDE for power production with a generator.

CHAPTER 5

RESULTS AND DISCUSSION

In this chapter, the results for the thermodynamic cycle analysis is presented in three different sections. In the first section, a comparison between the cycles adopted to represent the detonation process, ZND and Humphrey cycles, and a deflagration-based cycle, Brayton cycle, is presented. The best approximation for the detonation cycle is selected and its thermal and mechanical to electrical conversion efficiencies are studied and compared with the Brayton cycle. In the second section, The frequency of the PDE is taken into account and a model to compute the cycle thermal efficiency that includes the PDE frequency is explained. The third section of this chapter introduces the regeneration concept in the cycle analysis of the the ZND cycle. The efficiencies are computed and compared with the efficiencies of the cycle without regeneration.

5.1 Detonation Cycle

A generic model for the cycle analysis is developed using a *Mathematica* code [75] where the user only needs to provide the heat of reaction to be able to obtain the p–v and T–s diagrams for the Brayton, Humphrey and ZND cycles. The area enclosed by the cycle on a p–v diagram represents the work done by the system, which is the integral of the pressure with respect to the volume, while the area enclosed by the cycle on a T–s diagram represents the heat transfer to the system during the cycle.

All the state properties for each different cycle are determined without the need to change any of the parameters involved in the methodology. The state properties are associated to states 0,1, 2, 2a and 3. This is a very versatile approach where the

thermal and mechanical to electrical conversion efficiencies with respect to the compressor pressure ratio are generated. This approach can be used in many practical ways, such as a real time control of PDEs that can be performed by obtaining the equivalence ratio, f, from sensors located in the engine. By knowing this information, many detonation properties of the flow can be obtained with onboard computers such as determining the CJ condition and properties, and locating the von Neumann spike for each ZND cycle.

For the cycle analysis and to determine the efficiencies, the cycles have to be described and their state properties determined. In the PDE cycle described in Chapter 1, the fuel–oxidizer mixture enters the combustion chamber at standard atmospheric conditions. A pre-compression of the mixture can occur before the detonation is initiated and consequently the pressure and temperature in the combustion chamber can differ from the initial state. Then a triggering mechanism occurs and detonation is initiated. An isentropic expansion returns the flow to its initial conditions.

For propulsion applications, the system may not have a compressor or may have a fan, meaning that in the cycles analyzed here, the temperature at state 1 is the stagnation temperature of the freestream state 0. For power production that is land based, the rise in temperature and pressure ($0 \rightarrow 1$) are accomplished by means of a compressor.

Figures (5.1) and (5.2) show the p–v and t–s diagrams, respectively, for the Brayton, Humphrey and ZND cycles. The cycle heat addition can be modeled by different processes. One of the approximations commonly used is a constant volume process. When this is the case, the cycle is known as the Humphrey cycle [76, 3].

For the ZND cycle, the combustion process is modeled according to the ZND theory. In this model, the heat addition process ($1 \rightarrow 2a$) starts with an adiabatic compression by the leading shock followed by a Rayleigh-type, constant area, frictionless heat addition that ends at the CJ detonation state ($2a \rightarrow 2$). To determined the von Neumann and the CJ states is the most difficult and important task of determining the state properties

of the cycles. As mentioned in Chapter 3, the ZND theory assumes that a straight line, the Rayleigh line, connects the two states. The CJ condition is that the Rayleigh line and the Hugoniot curve be tangent, so their slopes with, respect to the specific volume, are equal at the CJ point. The CJ point can be determined by the tangent line to the reactive Hugoniot curve that intersects the initial state. This same line, the Rayleigh line, intersects the inert Hugoniot curve at the von Neumann spike.

For a power production device, part of the work produced during the isentropic expansion process ($2 \rightarrow 3$) is used to drive the compressor present in the process ($0 \rightarrow 1$), supplying a matching shaft work. For the part of the expansion that is left, a turbine is connected to a separate shaft that converts the enthalpy into useful shaft work. It is seen that the work cannot be extracted from the fluid right after state 2, since there is an rarefaction wave after the CJ state, and hence the work can only be extracted after the rarefaction process.

Since the models adopted to represent the PDE cycles were already discussed, a comparative analysis is developed. Both the ZND and Humphrey cycles represent detonation-based cycles. For a better understanding of the advantages and features of the detonation process and the PDE's for power production devices, a comparison with a deflagration-based cycle is made. The Brayton cycle is the choice to be used in this comparison. The processes in this cycle follow the ones described previously for the Humphrey and ZND cycle with the only variation being the process that represent the combustion ($1 \rightarrow 2$), which in the case of the Brayton cycle is considered a constant pressure process. Figures (3.8) and (3.9) show the Brayton cycle on a p–v and on a t–s diagram, respectively.

In addition, Figures (5.1) and (5.2) show the Humphrey, ZND and Brayton cycles in the same p–v and t–s diagrams. The fuel–oxidizer mixture adopted for this example is hydrogen–air. According to the CEA code [70], for an hydrogen–air mixture, the

properties are obtained as $\gamma = 1.4015$. The heat of reaction for hydrogen–air initially at STP is $q_{add} = 3.42$ MJ/kg. The heat addition is considered the same for the different cycles. The CEA code calculates chemical equilibrium product concentrations from any set of reactants and determines thermodynamic and transport properties of the product. The compression performed during the process $(0 \rightarrow 1)$ has a ratio of 2. The cycles are constructed in such a way that the heat addition is the same for all three different cycles. The cycle construction is absolutely dependent upon the value of q_{add} and γ for the mixture.

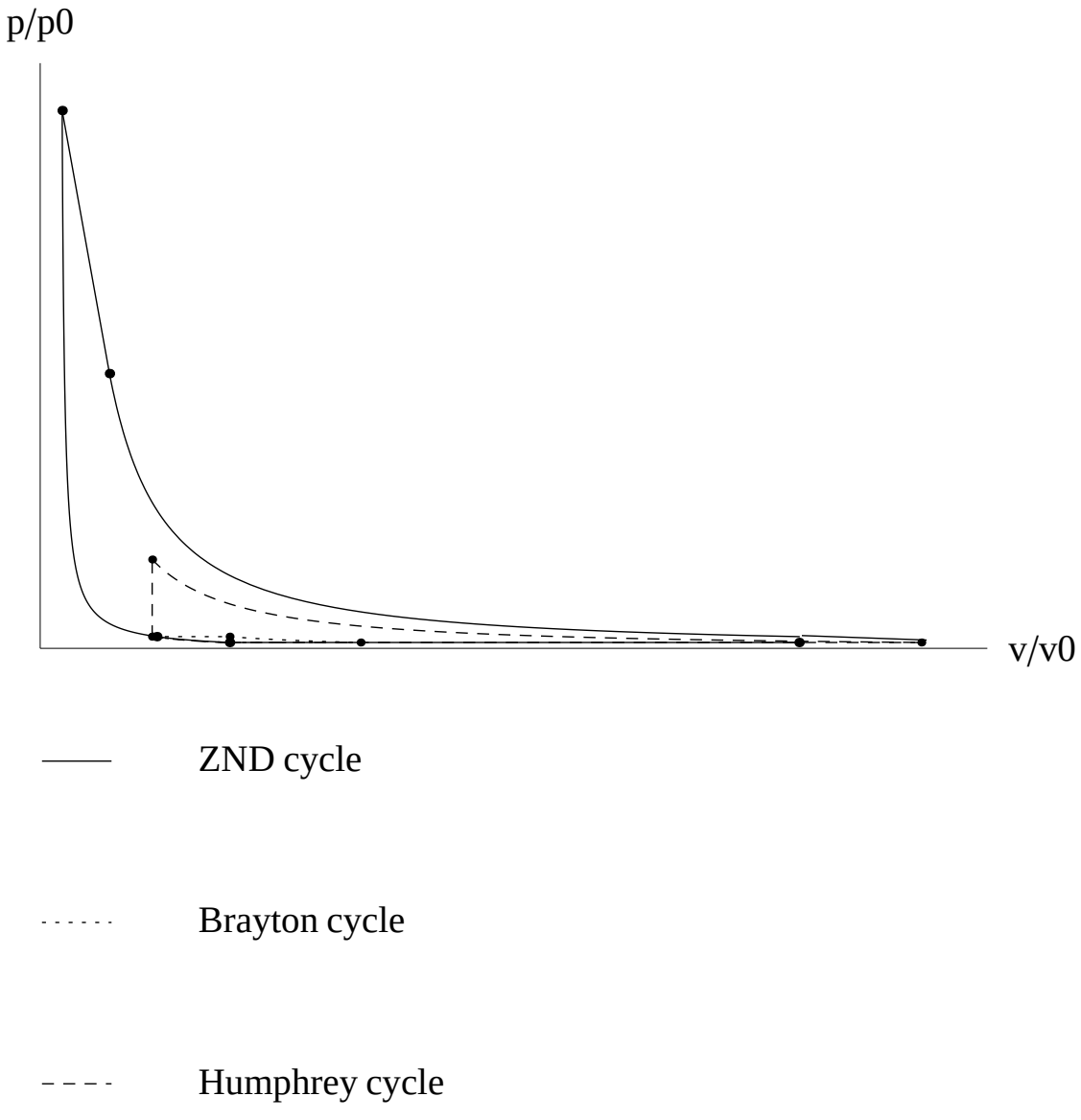

Figure 5.1. Comparison of various cycles on a p–v diagram.

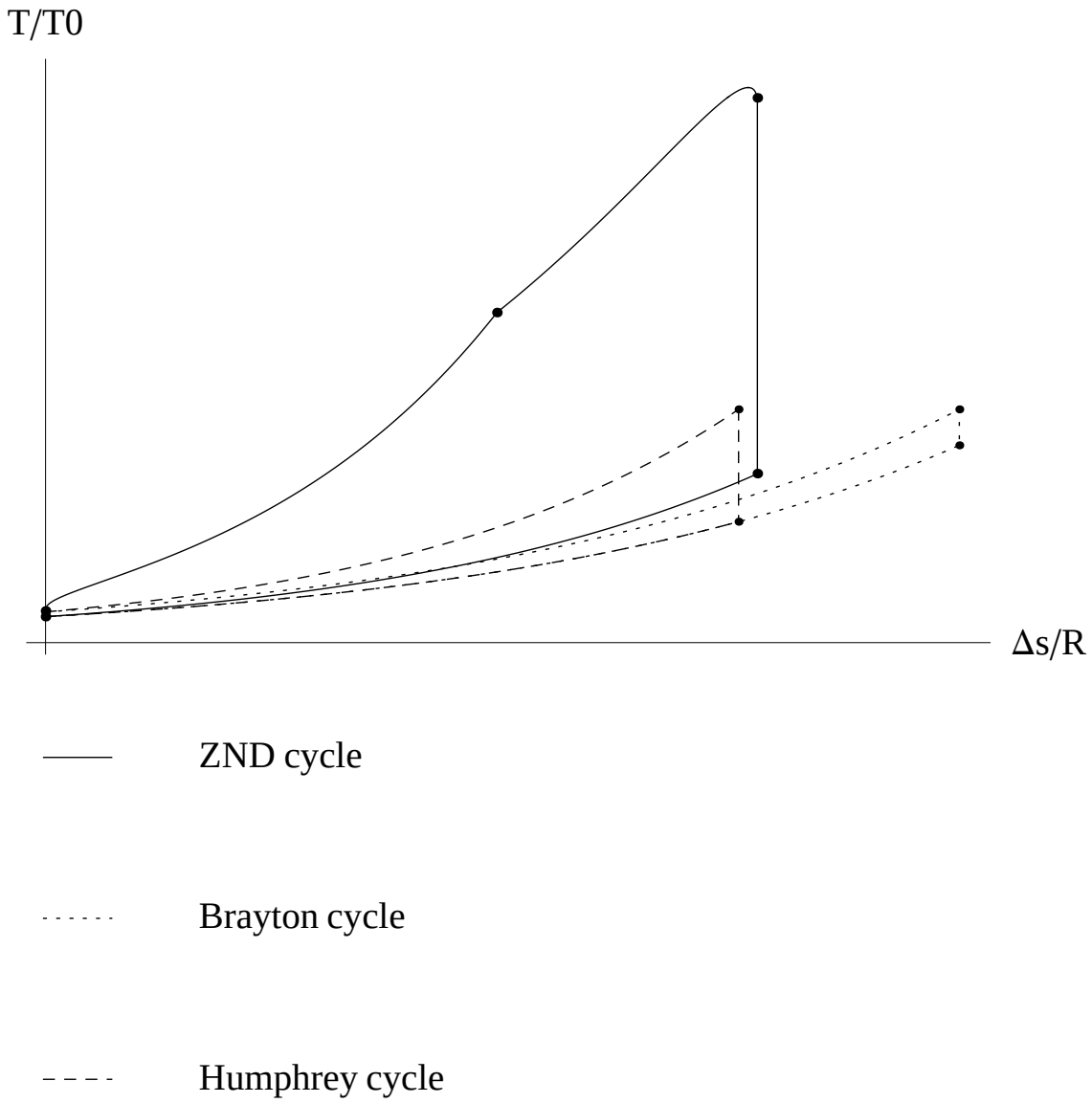

Figure 5.2. Comparison of various cycles on a T–s diagram.

By comparing the cycles provided in Figures (5.1) and (5.2), it is clear that the ZND has an area significantly greater than the Brayton and Humphrey cycles, both on p–v and on a t–s diagrams. This difference is especially large between the ZND and Brayton

cycles. The Brayton cycle, in the p–v diagram, is hardly visible when compared to the other cycles. From those observations it is possible to determine that, despite the fact that the heat addition is the same for the different cycles, the area under the p–v curve is much greater for the ZND cycle, implying that the ZND cycle has a much greater work done by the system than the other cycles. The reason for that can be attributed to the extremely high raise in pressure and temperature that the detonation process achieves for the ZND model of detonation. Another factor is the heat rejected, since the work is related to the difference between the heat addition and the heat rejection, the greater the heat rejection is the smaller the work output of the cycle is going to be. The heat rejection process is dependent on the cycle model.

It can also be seen that the Humphrey cycle is closer to the the Brayton cycle than the ZND cycle. Since the Brayton cycle represents the deflagration mode of combustion, then the ZND cycle is a closer representation of the real PDE cycle. This conclusion was expected based on the fact that a more complex mechanism for the combustion process is adopted by the ZND theory. For the analysis that follows, the Humphrey cycle will not be considered.

5.1.1 Efficiency

The thermal efficiencies for each cycle, ZND and Brayton, are compared according to Eq. (3.12). For every cycle, the thermal efficiency with respect to the compressor pressure ratio in process $(0 \rightarrow 1)$ is presented for three different fuel–oxidizer mixtures namely hydrogen–air, methane–air and propane–air.

The thermal efficiency is a measure of the usefulness of the heat of reaction, h_R, for each stoichiometric mixture. Table 5.1 shows the values of h_R for three fuel–air mixtures at stoichiometric condition used in this study.

Table 5.1. Heat of reaction for different fuel–air mixtures.

Fuel	heat of reaction unit mass of mixture h_R kJ/kg
Hydrogen (H_2)	3420.0
Methane (CH_4)	2757.7
Propane (C_3H_8)	2798.5

Figure (5.3) shows the thermal efficiency, η_{th}, with respect to the compressor pressure ratio for different fuel–air mixtures and Fig. (5.4) shows the Brayton cycle thermal efficiency, $\eta_{Brayton}$, with respect to the compressor pressure ratio for a hydrogen–air mixture. Typical compressor pressure ratios for a gas turbine range from 5 to 20, so in this analysis the efficiencies are computed for π_c ranging from 1 to 25. A compressor pressure ratio of 1 represents the case where there is no compressor added to the system and the pressure entering the combustion chamber is the same as the initial total pressure p_0. From the plots shown in Fig. (5.5) through (5.7), it is seen that that the thermal efficiency for the different fuel-air mixtures exhibit a very similar trends. It is expected that, with the increase in compressor pressure ratio, the thermal efficiency increases, given that increasing the pressure with which the mixture enters the combustor can improve the deflagration-to-detonation transition as well as increase the post-detonation pressure.

The results also show that $\eta_{th,PDE}$ is higher than $\eta_{th,Brayton}$ for low values of the compressor pressure ratio. This is also expected since in a PDE, the process of compressing the flow prior to heat addition is performed by the detonation wave which produces much higher increases in flow pressure and temperature with less entropy increase as compared to the compression stage in a Brayton cycle. This gain is especially significant at low compressor pressure ratios.

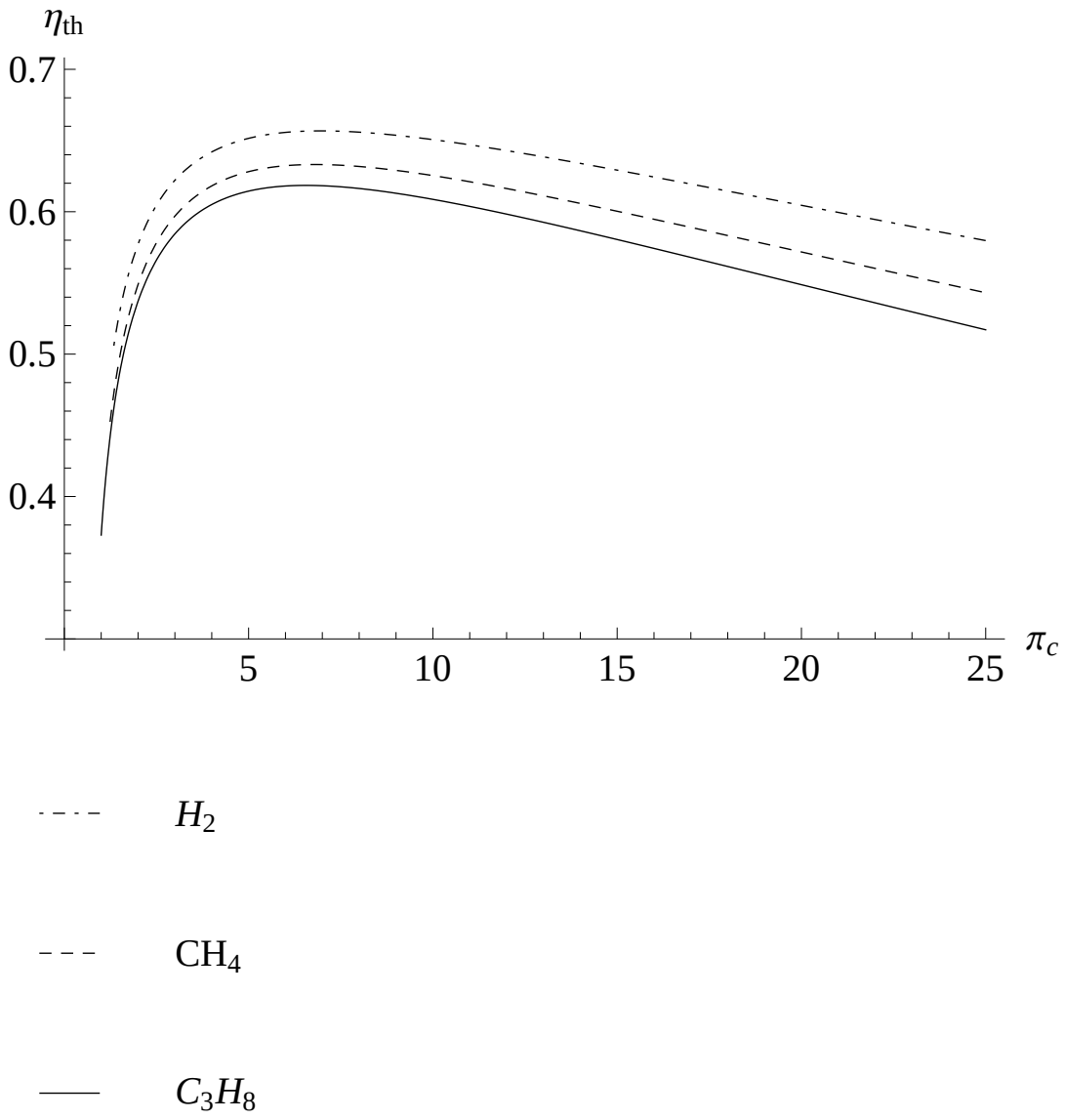

Figure 5.3. Thermal efficiency of a ZND cycle with respect to the compressor pressure ratio for various fuel–air mixtures.

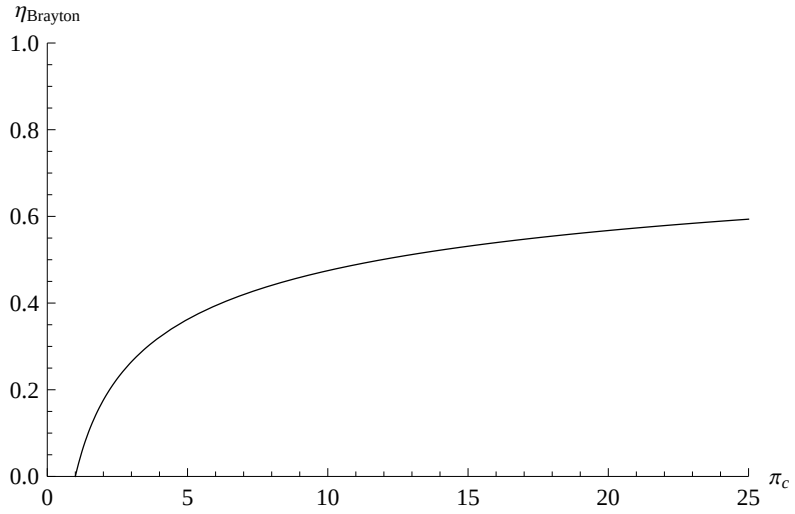

Figure 5.4. Brayton cycle thermal efficiency for hydrogen–air mixture.

For electrical power production, the efficiency of the process of converting the mechanical energy into electrical energy, η_{MEC}, can be calculated using Eq. (4.1) as follows. The electrical generator efficiency is taken as $\eta_{gen} = 95\%$ based on typical motor efficiencies [74], and the shaft efficiency $\eta_{shaft} = 95\%$ is also a typical value [77]. Thus, the total mechanical to electrical conversion efficiency is then found to be

$$\eta_{MEC} = 90.25\% \ \eta_{th} \tag{5.1}$$

Figures (5.5) to (5.7) show a comparison between the thermal efficiency and the mechanical to electric conversion efficiency for a ZND cycle, with respect to the compressor pressure ratio for a hydrogen–air, methane–air and propane–air mixtures, respectively. Again, the efficiency behavior does not vary significantly with the fuel–air mixture. One can see that as the compressor pressure ratio increases so does η_{MEC}, with a more rapid increase in lower compressor pressure ratios, until that is around $\pi_c = 7$. After that, increasing the pressure before the combustion process stops being advantageous. When

compared with the thermal efficiency, it is seen that the losses added to the system due to the addition of the generator and shaft power transmission system produce a decrease in efficiency, as expected. Figure (5.8) shows the thermal, mechanical to electrical conversion and Brayton efficiencies for stoichiometric hydrogen–air mixture.

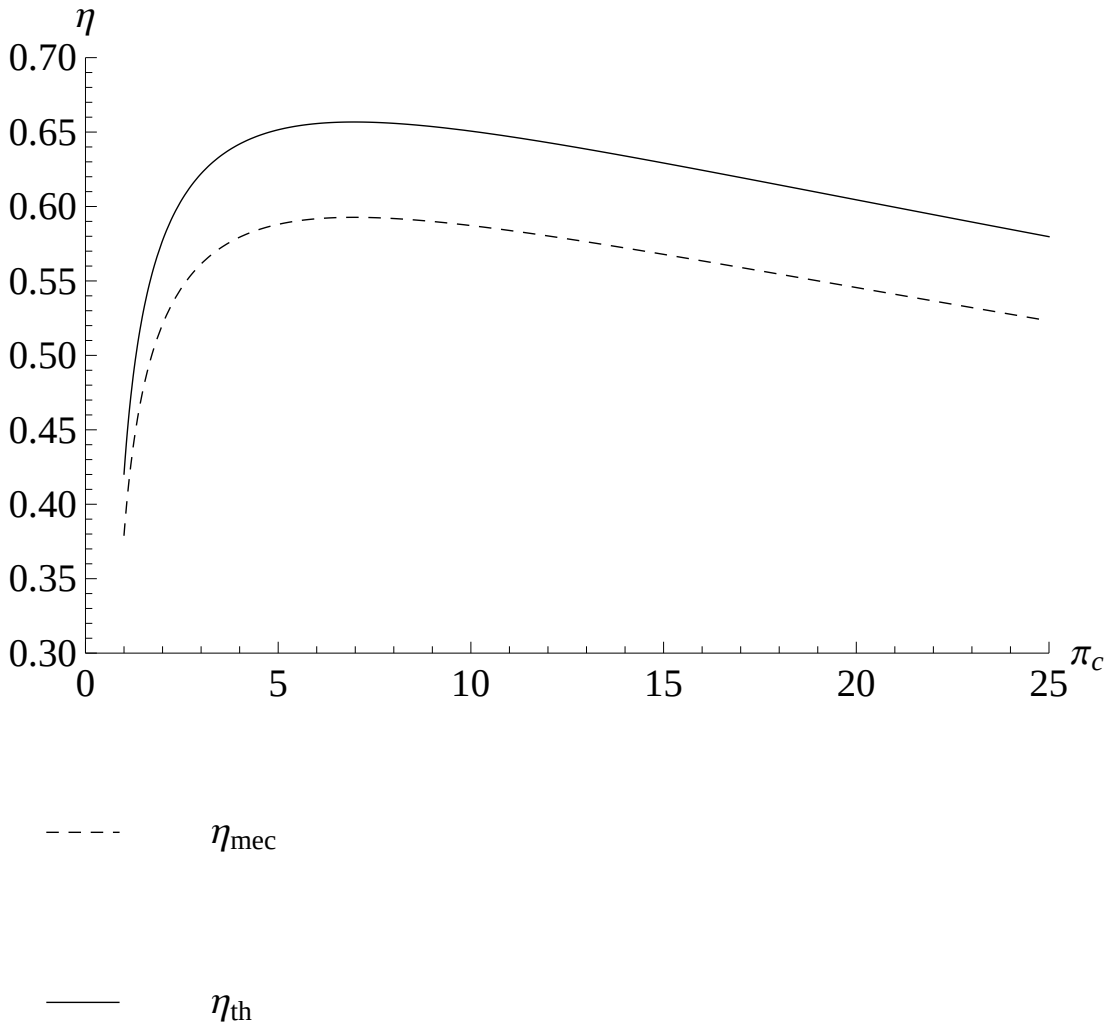

Figure 5.5. Cycle efficiency of a ZND cycle for hydrogen–air mixture.

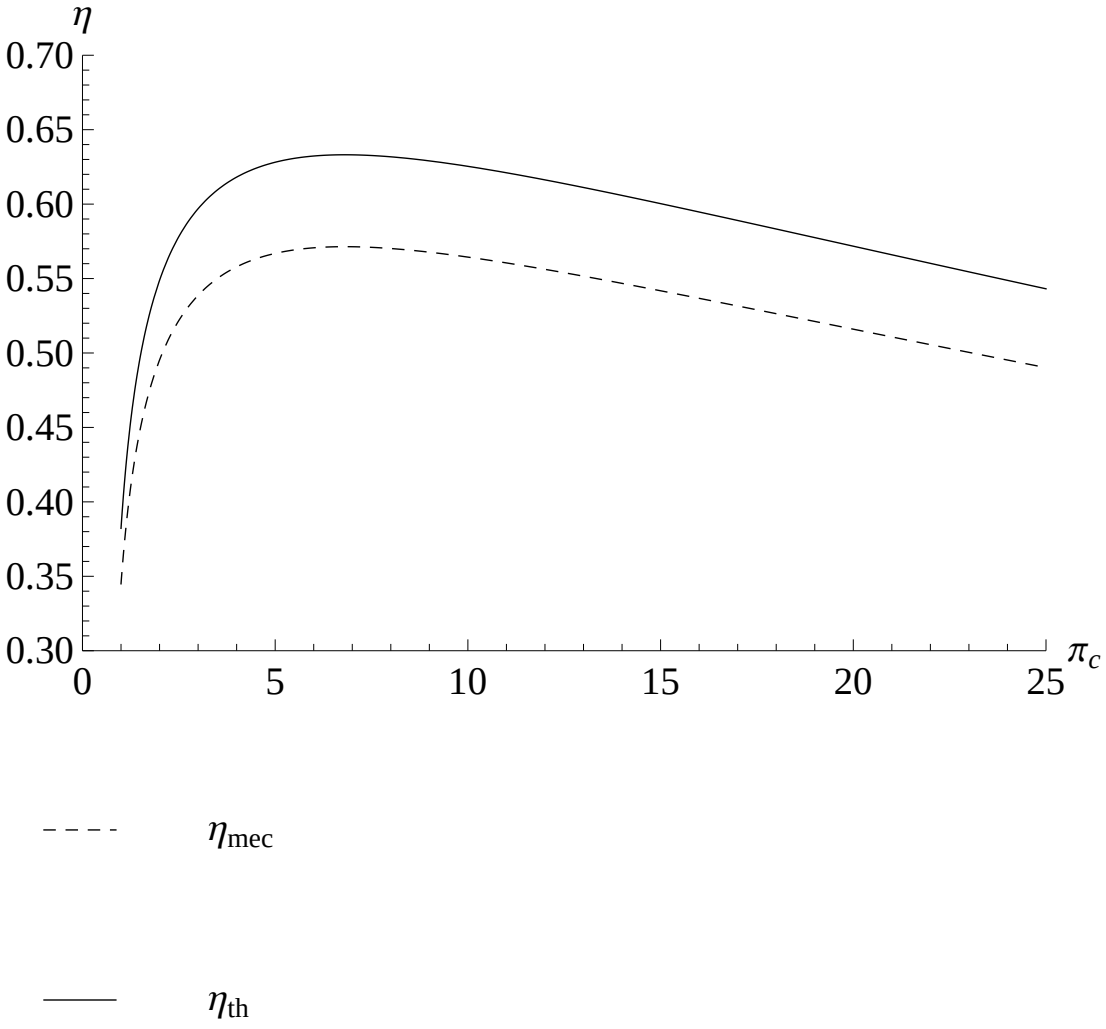

Figure 5.6. Cycle efficiency of a ZND cycle for methane–air mixture.

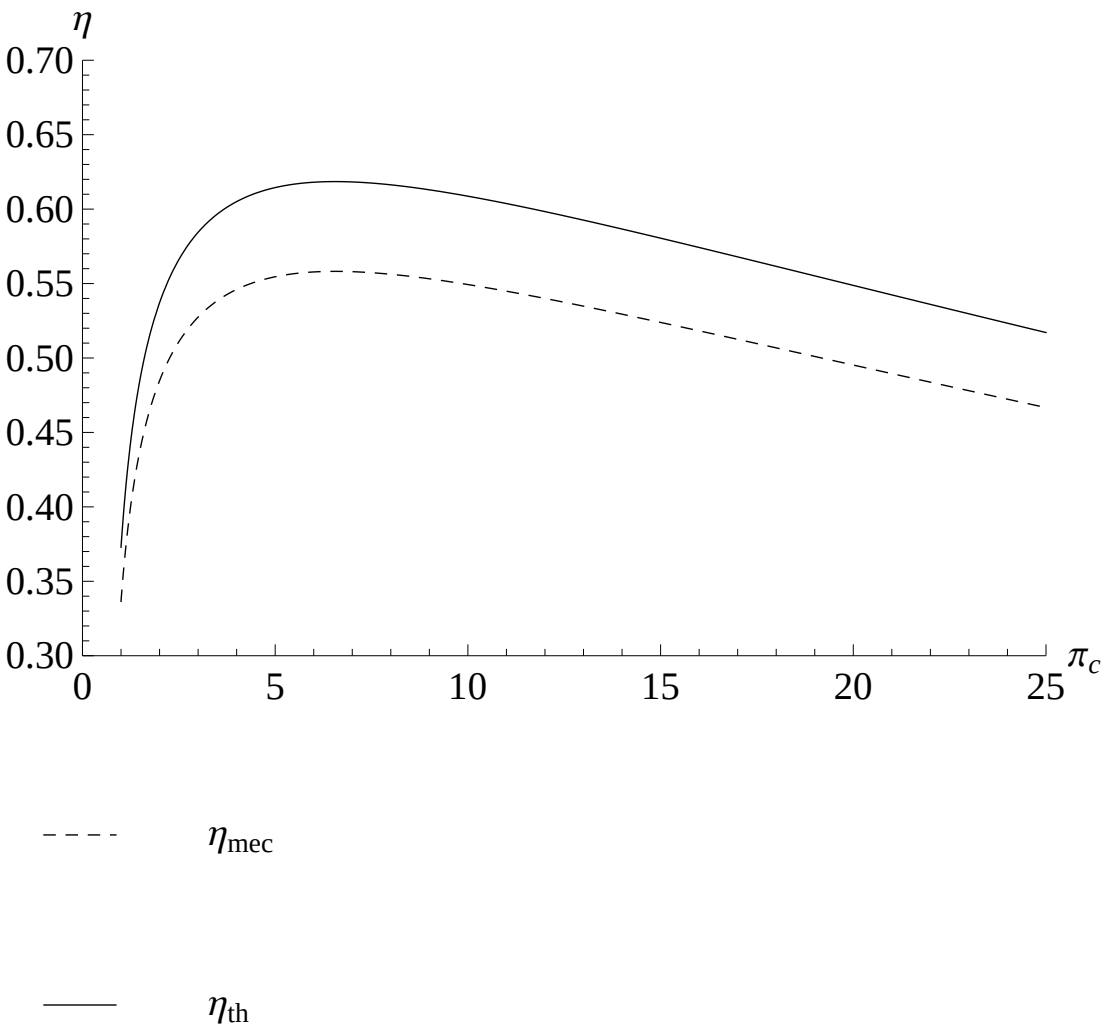

Figure 5.7. Cycle efficiency of a ZND cycle for propane–air mixture.

Figure (5.8) shows that the thermal and mechanical to electrical conversion efficiencies start decreasing when the compressor pressure ratio is around $\pi_c = 7$ and they become smaller than $\eta_{Brayton}$ for $\pi_c \cong 22$ for the thermal efficiency and $\pi_c \cong 17$ for the mechanical to electrical efficiency. This behavior can be explained by the way the efficiencies are calculated. Figures (5.9)and (5.10) show the temperatures T_1, T_2 and

T_3 and the pressures p_1, p_2 and p_3 with respect to the compressor pressure ratio. It is possible to observe the extremely high increase in temperature and pressure across the detonation process and how it is a linear increase. The linear behavior is a consequence of the modeling of the ZND cycle. State 2, called the CJ condition, is computed by means of a reactive Rankine–Hugoniot curve and a Rayleigh line. When observing those relations, it is possible to identify how the pressure and temperature are linearly related to the initial total pressure and temperature.

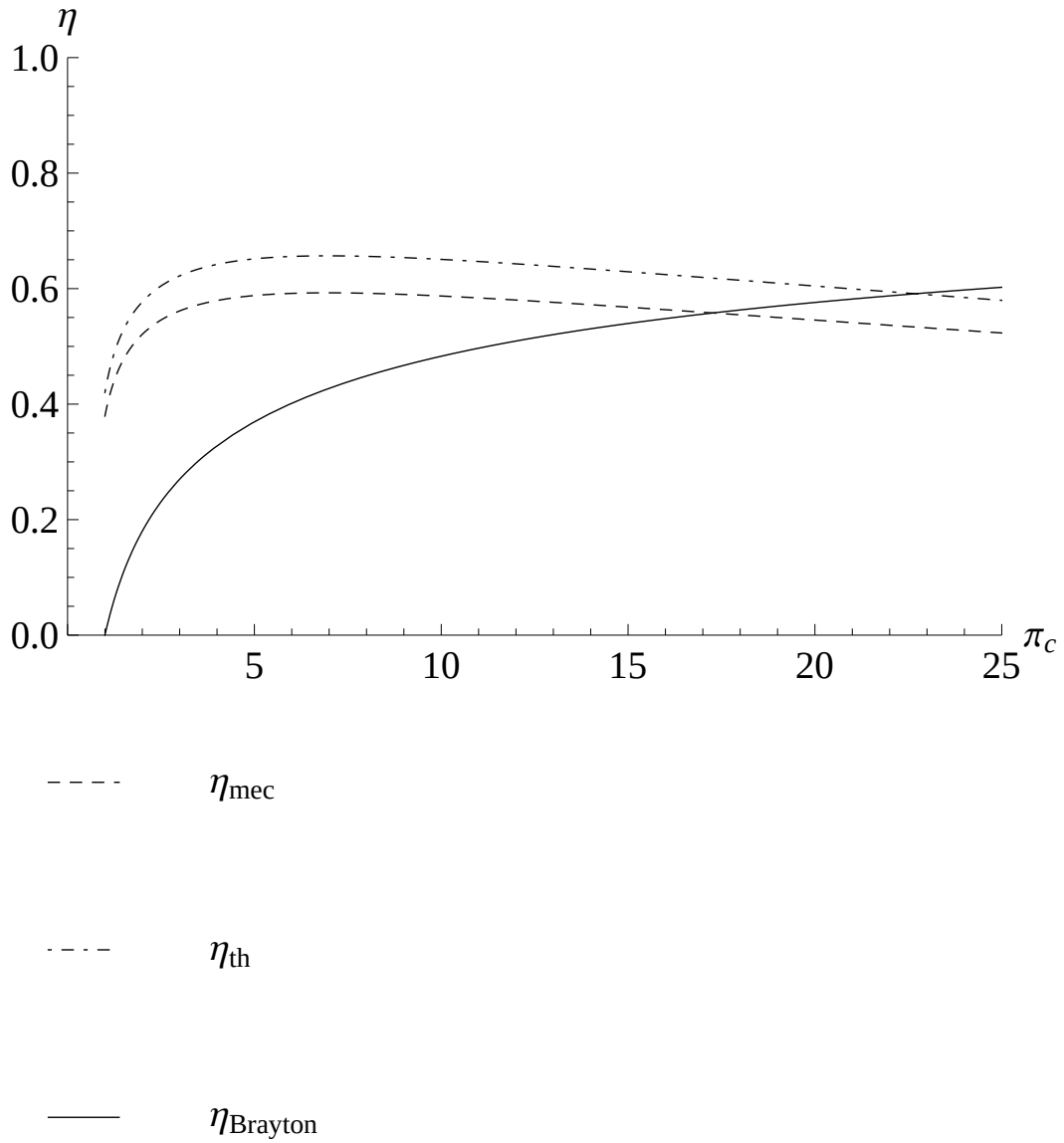

Figure 5.8. ZND thermal, mechanical to electrical conversion and Brayton efficiencies with respect to the compressor pressure ratio for a hydrogen–air mixture.

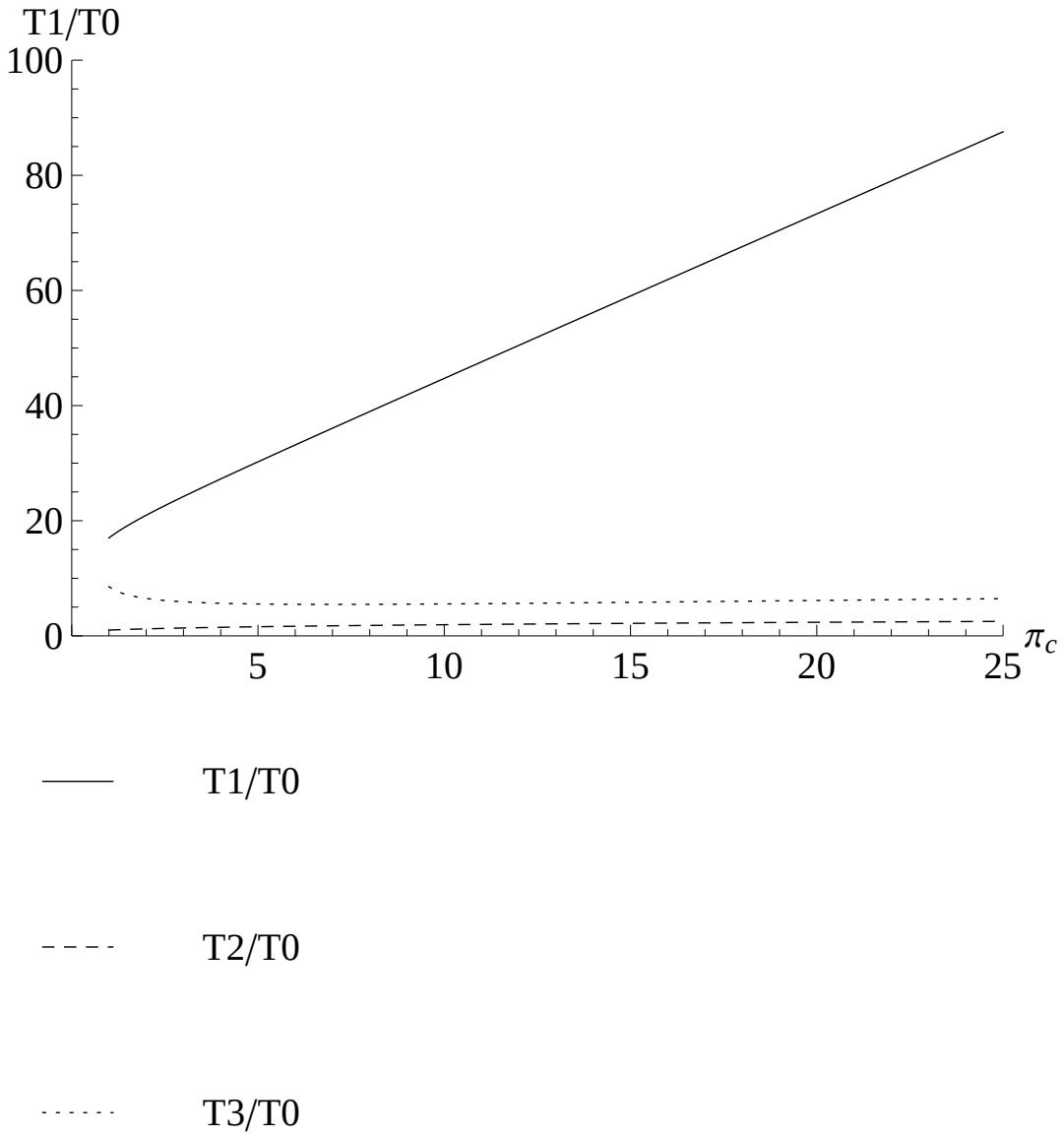

Figure 5.9. Temperatures of states 1, 2 and 3 with respect to the compressor pressure ratio for a hydrogen–air mixture in a ZND cycle.

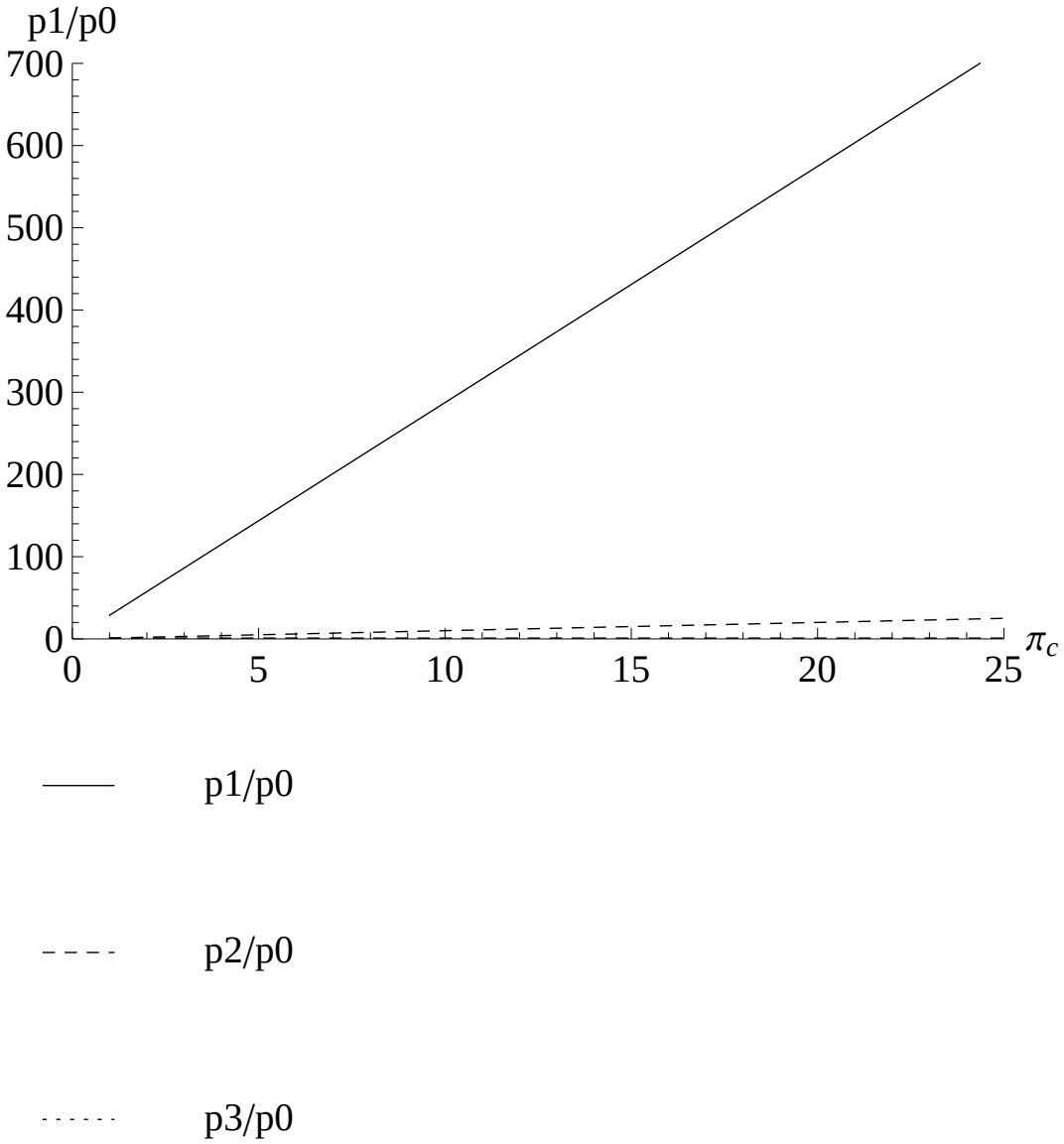

Figure 5.10. Pressures of states 1, 2 and 3 with respect to the compressor pressure ratio for a hydrogen–air mixture in a ZND cycle.

Figure (5.11) shows the thermal efficiency, entropy of state 3 and temperature T_3 with respect to the compressor pressure ratio. The process $(2 \rightarrow 3)$ is, as described before, an isentropic expansion that takes the flow from the combustor exit condition

to the initial total pressure. This means that there is an extremely large difference in pressures from state 2 to state 3, not taking into account the practical aspects of the turbine involved in the process. The entropy at state 2 and 3 are related to the pressure and temperature as can be seen in Fig. (5.11) . The temperature ratio follows the trend of the entropy curve and starts increasing at approximately $\pi_c = 7$. Since the thermal efficiency is given by Eq. (3.12), which can be described as

$$\eta_{th} = 1 - f(\frac{T_3}{T_0}) \tag{5.2}$$

the efficiency behavior is the inverse behavior of the thermal efficiency and the entropy. This means that the efficiency will start decreasing when $\pi_c = 7$.

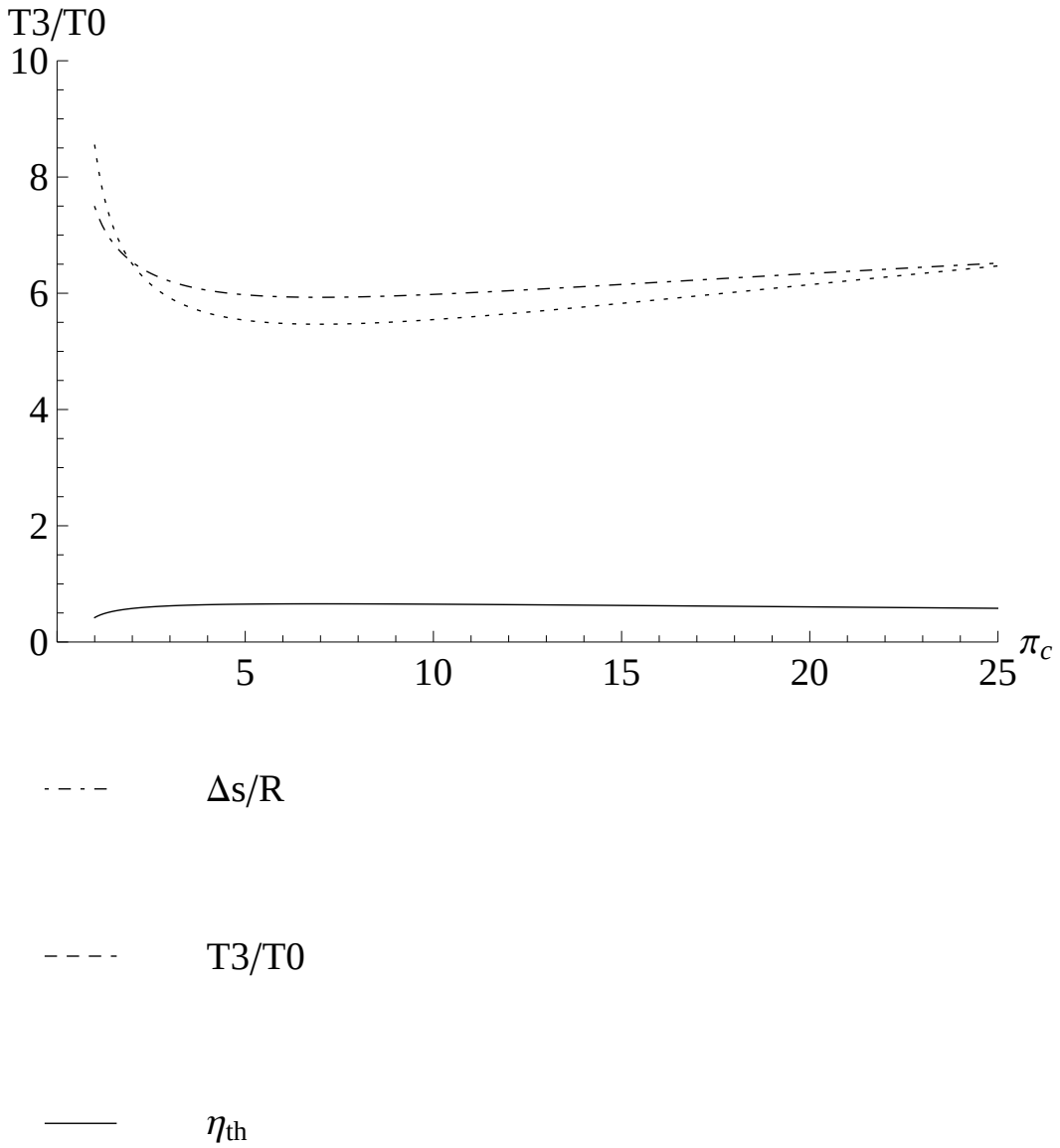

Figure 5.11. Study of efficiency behavior for hydrogen–air.

This behavior in the efficiency shows that there is a limit for which it is still advantageous to compress the mixture before the flow enters the combustion chamber. At $\pi_c = 7$, any further increase in compressor pressure ratio will cause very little improve-

ment in the final performance of the system and as the compressor pressure ratio is increased, the Brayton cycle thermal efficiency eventually becomes higher than that of the ZND cycle.

Tables 5.2 to 5.4 show the maximum, minimum and peak thermal efficiency values for a ZND and Brayton cycles for different fuel–air mixtures. The minimum efficiency is the value of the thermal efficiency when π_c is minimum in this analysis, or equal 1. The maximum efficiency is the value of the thermal efficiency when π_c is maximum in this analysis, or equal 25. And the peak efficiency is the maximum value of the thermal efficiency obtain within the studied range of π_c.

For the Brayton cycle, the thermal efficiency has its minimum at $\pi_c = 1$ and increases from there until π_c is maximum, meaning that the peak and maximum thermal efficiencies are the same. For the ZND cycle, it is observed that the peak thermal efficiencies occur at the same value of $\pi_c = 7$ for all the fuel–air mixtures studied. It is also observed that hydrogen–air presents the higher thermal efficiencies amongst all the fuel–air mixtures studied.

Table 5.2. Maximum, peak and minimum efficiencies for stoichiometric hydrogen–air mixture.

	$\eta_{Brayton}$	η_{th}	η_{MEC}
Peak	0.6023	0.6568	0.5927
π_c	25	7	7
Max	0.6023	0.5797	0.52326
π_c	25	25	25
Min	0	0.4202	0.3792
π_c	1	1	1

Table 5.3. Maximum, peak and minimum efficiencies for stoichiometric methane–air mixture.

	$\eta_{Brayton}$	η_{th}	η_{MEC}
Peak	0.5935	0.6331	0.5714
π_c	25	7	7
Max	0.5935	0.5431	0.4902
π_c	25	25	25
Min	0	0.3822	0.3449
π_c	1	1	1

Table 5.4. Maximum, peak and minimum efficiencies for stoichiometric propane–air mixture.

	$\eta_{Brayton}$	η_{th}	η_{MEC}
Peak	0.5795	0.6182	0.5580
π_c	25	7	7
Max	0.5795	0.5170	0.4667
π_c	25	25	25
Min	0	0.3729	0.3365
π_c	1	1	1

5.2 PDE Frequency

One of the challenges of this study is to incorporate the PDE frequency into this analysis. The thermal efficiency depends only on the work added to the system and the work extracted from the system. When looking closely, it can be concluded that for every cycle, the work added and extracted are always the same. Hence, the PDE efficiency for

power production would not change with the PDE frequency. However PDEs are pulsed engines and their frequencies need to be taken into account.

The PDE frequency is an important parameter when quantifying the efficiency of PDEs for thrust in propulsion, since it is known that the increase in frequency increases the thrust and power output [1] as well as the efficiency of PDEs for propulsion [78].

In order to be able to account for the frequency, an average process for the pressure, temperature and specific volume profiles as described in Chapter 3. The main difficulty of the Endo–Fujiwara model [60] is to average the pressure that changes during the decay of pressure for every detonation period, according to Fig. (3.11).

Another detail to be considered in this discussion is that, for every fuel–air mixture, there is a minimum period for the detonation wave to occur. Depending on the fuel-oxidizer mixture, the detonation wave has a minimum time to be able to travel, so that a minimum period is required for the detonation that is composed by a discontinuity to bring the pressure to the CJ point, after that the pressure profile stabilized and finally decreases to the initial state, followed by a purge and filling period. In this analysis, the purging is considered to take the same amount of time as the recharging of the tube. To determine the average pressure of the PDE cycle that includes the time for purging and recharge of the tube Eq. (5.3) is developed.

$$p_{cycle} = p_{average}\ f_{PDE}\ t_{exhaust} + p_0\,(1 - f_{PDE}\ t_{exhaust}) \tag{5.3}$$

Where p_{cycle} is the pressure average for the cycle that includes the time for the purging and recharging of the tube, $p_{average}$ is the pressure average of the cycle that does not include the time for the purging and recharging of the tube, $t_{exhaust}$ is the cycle period that does not include the time for the purging and recharging of the tube and f_{PDE} is the PDE frequency.

The maximum attainable frequency of a PDE is the inverse of the minimum attainable period of a PDE that can be calculated by adding the period that takes the detonation to start, develop and decay to the time for purging and filling the tube. In computing the minimum period, the time related to detonation delay is not considered.

Knowing the minimum period for the detonation to occur will directly imply that there is a maximum frequency for which each fuel-air mixture can be analyzed with the certainty that there is enough time to allow the detonation to go through all the processes described earlier. Also the maximum frequency will guarantee that the detonation cell size will be achieved.

Figure (5.12) shows the efficiency vs. the PDE frequency, using the average thermodynamic properties mentioned above. It is seen that the maximum frequency for each mixture varies as mentioned above. So, even though the efficiencies increase with the increasing of the detonation frequency, there is no reason to evaluate up to a frequency that is bigger that the one that the mixture is able to accommodate. It is seen that increasing the frequency of the PDE is a very beneficial approach to the performance of the cycle. Furthermore, the efficiencies present here are much lower than the ones showed in Fig. (5.3), which is expected due to the averaging method just described.

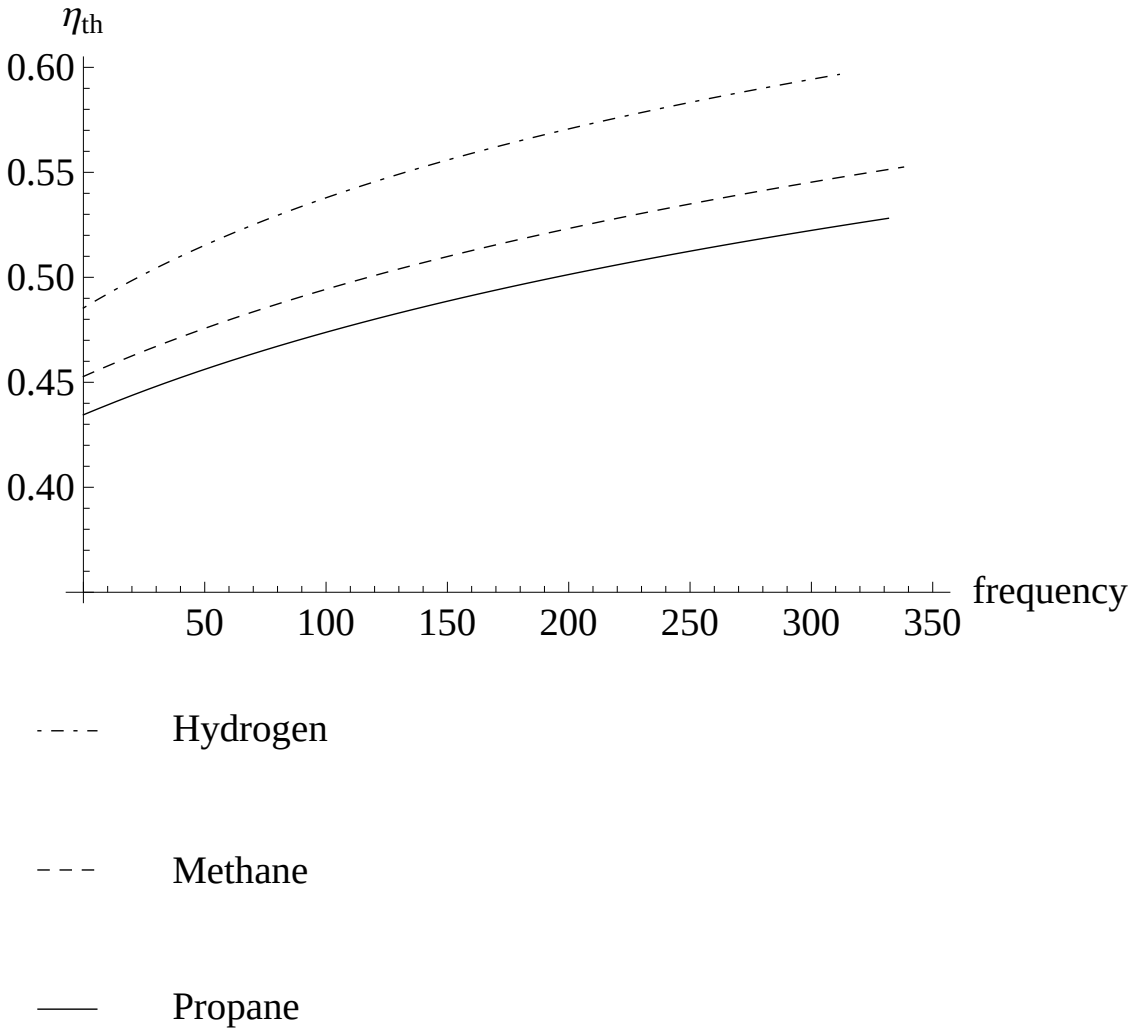

Figure 5.12. ZND efficiency with respect to the PDE frequency.

Table 5.5 shows the parameters involved in the calculation of the pressure average and the cycle frequencies and times. It can be seen that the plateau region is the longest region of the cycle, followed by the exhaust time. The maximum frequencies can be determined for each fuel–air mixtures as 351 Hz for hydrogen–air, 308 Hz for methane–air and 300 Hz for propane–air.

This practical operating frequency range of PDEs agrees with what has been seen on the literature regarding experimental work using detonation for propulsion. Those studies claim that in order for the PDE cycle to be competitive with conventional turbojet/turboramjet systems, they will be required to operate in the 75-100 Hz range with near stoichiometric fuel–air mixtures. It is expected that for power production the range need not be the same but similar to that for propulsion [79, 80, 81].

Table 5.5. Frequency parameters.

Parameter	H_2	CH_4	C_3H_8
t_{CJ}	0.0003894s	0.0004422s	0.0004526s
$t_{plateau}$	0.001236s	0.001405s	0.001441s
$t_{exhaust}$	0.002846s	0.003241s	0.003332s
f_{max}	351.33Hz	308.52Hz	300.10Hz
p_{fill}/p_0	7.518	7.532	7.553
T_{cycle}	0.003105s	0.003518s	0.003589s
$p_{average}/p_0$	4.083	4.089	4.099
M_{CJ}	4.353	4.362	4.374

5.3 Regeneration

A regenerator is nothing more than a heat exchanger. To design or predict the performance of a heat exchanger, it is essential to determine the heat lost to the surroundings for the analyzed configuration. We can define a parameter to quantify the percentage of losses or gains. Such parameter may readily be obtained by applying overall energy balances for hot and cold fluids. If Q_e is the heat emitted from the hot fluid, meanwhile Q_a the heat absorbed by the cold fluid (neglecting potential and kinetic energy changes);

$$Q_e = \dot{m}_h \left(h_{h,i} - h_{h,o}\right) = \dot{m}_h c_{p_h} \left(T_{h,i} - T_{h,o}\right)$$
$$Q_a = \dot{m}_c \left(h_{c,i} - h_{c,o}\right) = \dot{m}_c c_{p_c} \left(T_{c,i} - T_{c,o}\right) \tag{5.4}$$

where, $\dot{m}_h$, $\dot{m}_c$ mass flow rate of hot and cold fluid, respectively; $h_{h,i}$, $h_{h,o}$ inlet and outlet enthalpies of hot fluid, respectively; $h_{c,i}$, $h_{c,o}$ inlet and outlet enthalpies of cold fluid, respectively; $T_{h,i}$, $T_{h,o}$ inlet and outlet temperatures of hot fluid, respectively; $T_{c,i}$, $T_{c,o}$ inlet and outlet temperatures of cold fluid, respectively; and c_{p_h}, c_{p_c}specific heats of hot and cold fluid, respectively.

It is possible to determine the temperature at which the heat transfer between exhaust and incoming gases occurs. If that temperature is named T_x, then the efficiency for the cycle with regeneration is described by Eq. (5.5). The thermodynamic states in this equation follow the ones presented in Fig. (3.4).

$$\eta_{regen} = \frac{(T_2 - T_3) - (T_1 - T_0)}{T_2 - T_x} \tag{5.5}$$

$$\eta_{regenerator} = 50\% \tag{5.6}$$

$$\eta_{reg} = \frac{T_x - T_1}{T_3 - T_1} \tag{5.7}$$

$$\eta_{th} = \frac{(T_2 - T_3) - (T_1 - T_0)}{T_2 - T_x} \tag{5.8}$$

Carnot cycle efficiency for T_0 and T_3

$$\eta_{carnot} = 1 - \frac{T_0}{T_3} \tag{5.9}$$

The concept of using the energy wasted through the exhaust gases is explored here. The regeneration method is used, meaning that the heat coming from the high

temperature exhaust gases are used to pre-heat the air–fuel mixture before it enters the combustion chamber. Some of the advantages of regeneration are not only the energy savings but especially the improvement in the combustion process due to the preheating of the mixture before it enters the combustion chamber. For detonation, increasing the temperatures with which the mixtures enters the combustor, can aid in the DDT process which guarantees that detonation takes place. It is important to keep in mind that over preheating the mixture can cause premature detonation if the temperature of the mixture reaches the auto-ignition temperature and it necessary to ensure that the fuel and oxidizer are not mixed in the heat exchanger In this section, some results of the regeneration study are presented.

There are two modes of regeneration that are studied in the present work. In the first mode, the exhaust gases exiting the turbine are redirected to the regenerator heat exchanger, as shown in Fig. (4.1). In the second mode, the hot flow is extracted directly from the combustion chamber, before entering the turbine, and then redirected to the regenerator, as shown by the dotted line in Fig. (4.1). After the hot gas goes through the primary circuit in the heat exchanger, it is then sent to the turbine from the location marked as (y) in Fig. (4.1) and (4.2).

In Figs. (5.13) and (5.14) the regeneration process is shown in a T–s diagram for a Brayton and for a ZND cycle, where the mixture after the turbine is used for regeneration. In Fig. (5.13) the process of regeneration can be explained better. In that cycle the process $(y \rightarrow 0)$ is the heat rejected, processes $(3 \rightarrow y)$ and $(1 \rightarrow x)$ is the heat saved or regenerated and process $(x \rightarrow 2)$ is the heat addition.

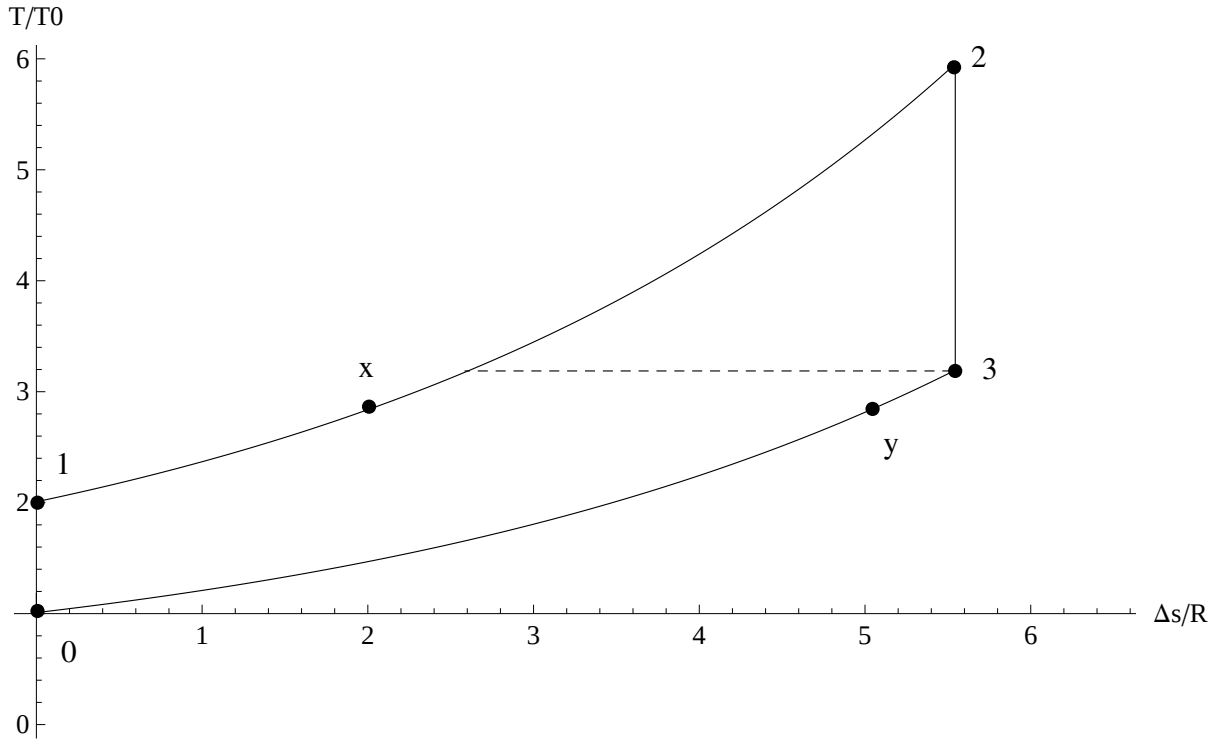

Figure 5.13. Regenerative Brayton cycle.

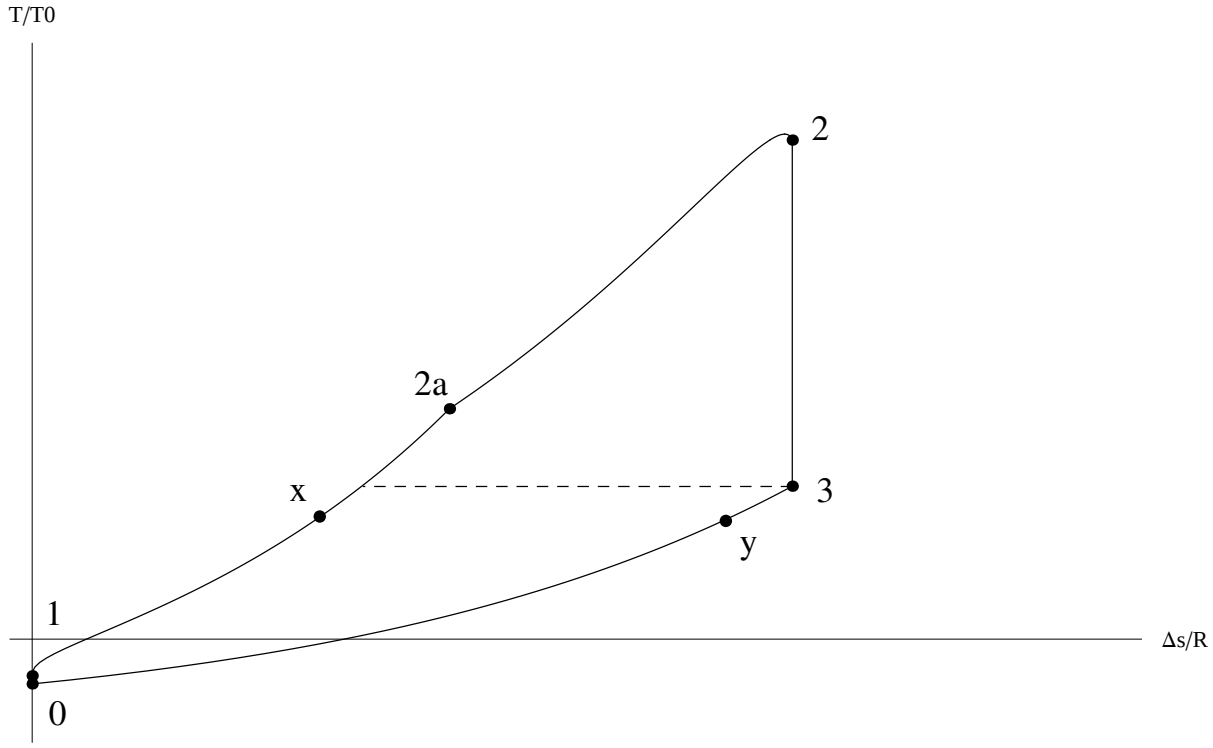

Figure 5.14. ZND cycle with regeneration at the turbine exhaust.

The regenerator efficiency is considered at $\eta_{reg} = 0.5$, which means that only 50% of the exhaust heat can be reused back in the system. The regeneration study is only applied to the ZND cycle, since it was established as the model closest to a real detonation cycle.

Table 5.7 shows the efficiency results for the first type of regenerative cycle compared with the efficiencies before regeneration. The compressor pressure ratio is taken as 2. The increase in efficiency is evident. The influence of the air–fuel mixture is very small when the efficiencies are analyzed.

Figure (5.15) shows a comparison of the thermal, mechanical to electrical conversion, Brayton and regenerative efficiency with respect to the compressor pressure ratio.

Table 5.6. Carnot efficiency.

Fuel	Carnot Efficiency
Hydrogen (H_2)	84.05%
Methane (CH_4)	81.53%
Propane (C_3H_8)	81.71%

Table 5.7. Efficiency for the ZND cycle with a regenerator.

Fuel	Efficiency w/ regeneration	Efficiency w/o regeneration
Hydrogen (H_2)	77.73%	51.96%
Methane (CH_4)	76.64%	50.12%
Propane (C_3H_8)	76.72%	50.24%

An increase in efficiency is clear, as expected, since more of the heat is being captured before it can be wasted. It is seen that the regenerative efficiency does not drop for the compressor pressure ratio range studied. This shows a great improvement in the behavior shown by the other efficiencies, making the device much more efficient than one that uses deflagration as mode of combustion.

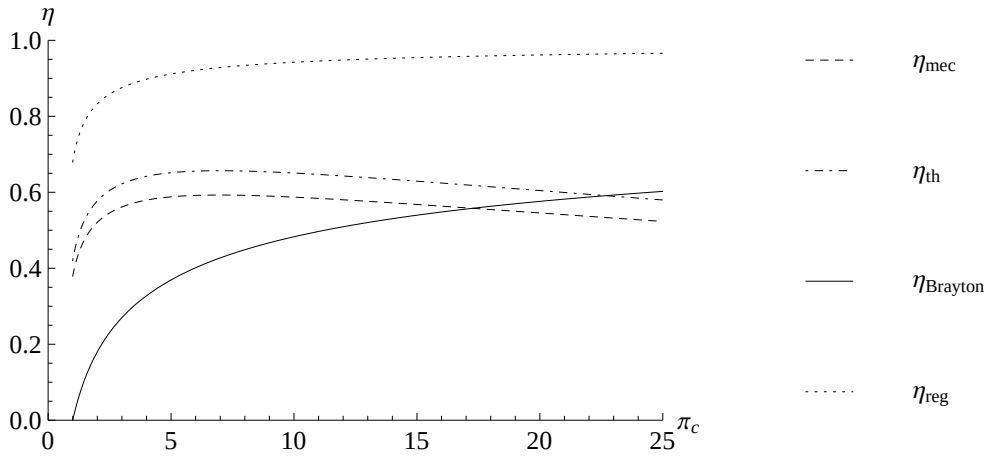

Figure 5.15. Efficiency of ZND cycle with regeneration compared with other efficiencies.

For the second type of regeneration in Fig. (5.16), the temperature of the exhaust taken is $T_{2'}$ which is equal to $T_{2,Brayton}$ according to Fig. (3.10) in Chapter 3. It is important to note that after the regeneration takes place, T_x cannot be higher than T_2a or premature detonation will occur.

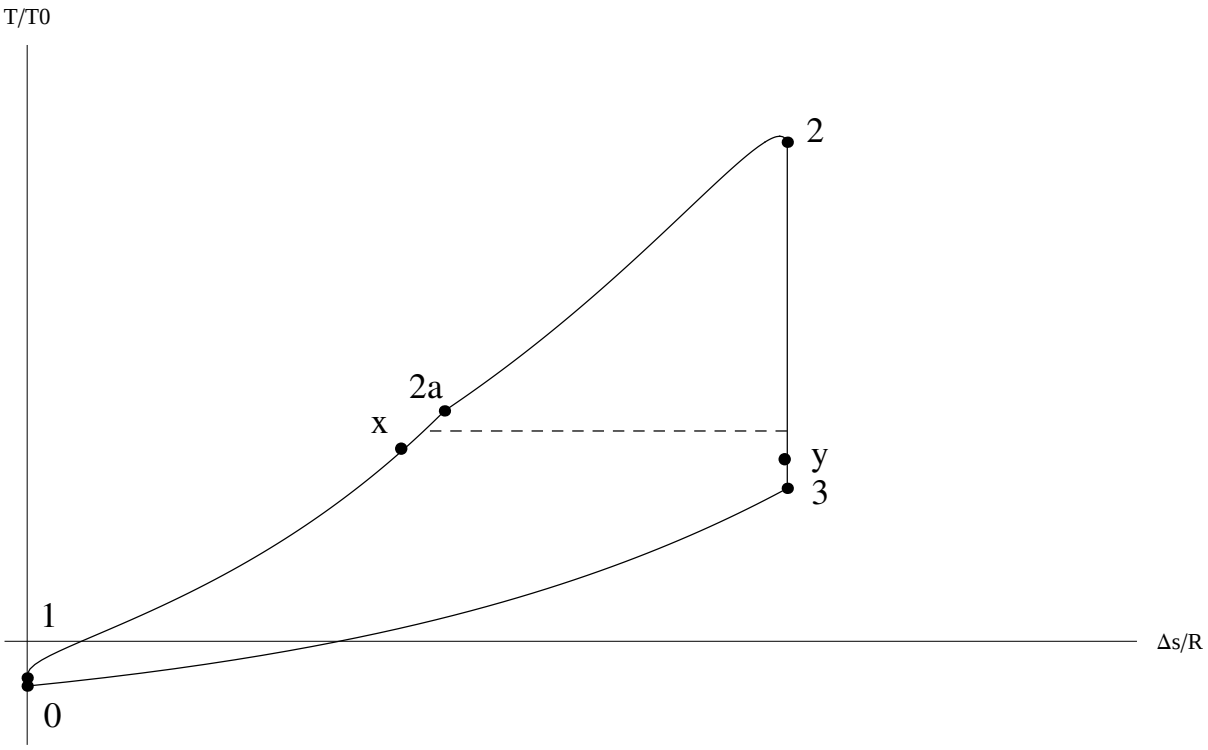

Figure 5.16. ZND cycle with regeneration at the combustor exhaust.

For the second type of regeneration the detonation process will be improved since mixture enters the combustor at a higher temperature. However, the overall efficiency will be dropped since the temperature the enters the turbine decreases. Of course, the turbine properties will be a determining factor as well, due to material constraints, as discussed in Chapter 4. In that case, using the second type of regeneration is preferable, since the flow would have to be cooled before entering the turbine and that energy would be wasted.

The benefit of using a regenerator is clear from the results shown. One disadvantage of using the regenerator is the increase in complexity of the system, with added equipment. One of the great advantages of using a PDE for power production is its simplicity and portability and one has to take into account the benefits and disadvantages of adding a regeneration system to the cycle.

All the calculation performed above were developed in *Mathematica* [75] and can be seen in detail in Appendix A.

CHAPTER 6

CONCLUSION

A thermodynamic cycle analysis was performed to study the application and feasibility of using PDEs for power production. Two different cycles were used to approximate the real PDE cycle: the ZND cycle and the Humphrey cycle. The Humphrey cycle assumes that the detonation process is a constant volume combustion, while the ZND cycle assumes that the combustion process follows the ZND theory where there is a leading shock wave followed by a reaction zone. Both cycles were compared with a deflagration–based cycle, namely Brayton cycle. A generic method was developed to, given the fuel–air mixture, provide the state properties and the p–v and t–s diagrams, for each cycle, and to provide information on the CJ condition and the von Neumann spike properties for the ZND cycle.

To compare the cycles mentioned above a p–v diagram and a t–s diagram were generated for each cycle and compared. The results showed that, as expected, the ZND cycle is the best cycle to represent a real PDE cycle.

The thermal and mechanical to electrical conversion efficiencies of the two detonation cycles were also studied and compared to each other and to those of the Brayton cycle.

The mechanical to electrical conversion efficiencies were computed for the three mixtures for the ZND and Brayton cycles. The mechanical to electrical conversion efficiency curves follow those of the thermal efficiency, however it has lower values, due to the losses associated with gearing, transmission and with the generator.

The analysis demonstrates that it is more advantageous to use PDEs over the gas turbine engines, for propulsion and power generation at low compressor pressure ratios.

The need for low compression ratios in PDEs eliminates the need for heavy compressor machinery, allowing them to operate with just a fan or few compressor stages making PDEs lighter, more compact, less complex and therefore more cost effective than other engines. This also means that more shaft work can be derived from the exhaust flow through the use of more turbine stages, which can be then used for power generation.

- The maximum attainable frequency for a mixture was determined for hydrogen, methane and propane–air mixtures, based on the detonation period and the times for purging and recharging of the tube.
- The maximum frequencies found were 351 Hz for hydrogen–air, 308 Hz for methane-air and 300 Hz for propane–air by a 1 m long constant area combustor.
- When averaging the flow properties throughout the cycle, there is a small decrease in efficiency as compared to efficiencies based on CJ properties alone.
- A regeneration study is presented to analyze how the use of exhaust gases can improve the performance of the system.
- For a hydrogen–air mixture, the thermal efficiency increases from 52%, for a cycle without regeneration, to 78% for the regenerative cycle.
- For a methane–air mixture, the thermal efficiency increases from 50%, for a cycle without regeneration, to 77% for the regenerative cycle.
- For a propane–air mixture the thermal efficiency increases from 50%, for a cycle without regeneration, to 77% for the regenerative cycle.
- The efficiency is considerably larger when regeneration is introduced. Regeneration can be added to the flow after the turbine, similar to gas turbine engines, or right after the combustor and prior to the turbine to protect the turbine blades from

the extremely high detonation temperatures. Post detonation temperatures can surpass the maximum limit of current turbines, which is about 1850 K.

- The regenerative thermal efficiencies for the PDE surpass those of the Brayton cycle for the range of compressor pressure ratios studied.
- Regeneration will require the use of more equipment than the original PDE-turbine hybrid system, which can compromise the simplicity and portability of the system.
- Regenerative heating of the air and fuel to the combustor can aid in promoting DDT and to lower ignition energy and delay. The addition of regeneration into the system was shown to be a great improvement on the system performance.
- The pulsed nature of PDE operation makes frequency an important parameter to be studied. It is important to show the influence of frequency on the efficiencies of the ZND cycle.
- The analysis shows that PDEs are a more advantageous choice of engines for power production over the deflagrative based engines.

6.1 Recommendations and Future Work

The results show clearly that the use of detonation is advantageous for power production. There are many improvements in the analysis that can make the results more realistic and more practical.

The next step in expanding this analysis is to make use of a two–gamma model, that some studies have shown to be worth considering for this type of analysis. The second suggestion is to do a qualitative analysis of cogeneration, that will capture more of the useful energy left in the exhaust. Many configurations of a cogeneration system are possible,. The exhaust could directly be used for process heat or to create steam in a boiler, which can then be used for various processes. The exhaust heat can also be used for heating and cooling, the latter using a vapor-compression refrigeration system.

Lastly, the effects of the high temperatures of the detonation products on the turbine blades can be mitigated by vitiating the hot core flow with cold air. This can be done by means of a bypass system or ejector augmentation. Bypass in a gas turbine is known to increase power and efficiency. A cycle analysis on the effects of bypass and ejector augmentation on a PDE-turbine hybrid system would be very advantageous.

APPENDIX A

CODE

Initial data and other variables

pic is the compression ratio

$H_2 = 3\,420\,000;$
$CH_4 = 2\,757\,700;$
$C_2\,H_4 = 3\,004\,200;$
$C_3\,H_8 = 2\,798\,500;$

q = 2 798 500;

pic = 2;

pp0 = 101 325; vv0 = 0.997668;

$\alpha 1$ = 0; vinitial = 1; pinitial = 1; Tinitial = 1; sinitial = 0; γ = 1.318541;

hprm = q / 1000; Rf = 0.2183; Rair = 0.2869; $R = \frac{Rf + Rair}{2}$; $hpr[f\_] := \frac{1 + f}{f}$ hprm;

p0[πc_] := pinitial πc

q

2 798 500

$\alpha = \frac{q}{p0\ v0}$

$\alpha 2 = Solve\left[\frac{q}{pp0\ vv0} == xxx,\ xxx\right][[1]][[1,\ 2]]$

27.6836

Hugoniot

$\mu = \sqrt{\frac{\gamma - 1}{\gamma + 1}}$

0.37066

$v0[\pi c\_] := Solve\left[\left(\frac{p0[\pi c]}{pinitial} + \mu^2\right)\left(\frac{v}{vinitial} - \mu^2\right) == 1 - \mu^4 + 2\,\mu^2\,\alpha 1,\ v\right][[1]][[1,\ 2]]$

v0[2]

0.596418

plot0[πc_] := ListPlot[{{v0[πc], p0[πc]}}, PlotStyle −> {Black, Thick}]

plot0b = ListPlot[{{sinitial, Tinitial}}, PlotStyle −> {Black, Thick}]

$$\text{eq1}[\alpha\_, \pi c\_] := \text{Solve}\left[\left(\frac{p}{p0[\pi c]} + \mu^2\right)\left(\frac{v}{v0[\pi c]} - \mu^2\right) == 1 - \mu^4 + 2\,\mu^2\,\alpha,\ p\right][[1]][[1,\ 2]]$$

ZND pressure

pznd[πc_] := eq1[α1, πc]

pznd[1]

$$\frac{0.981124 - 0.137389\,(-0.137389 + 1.\,v)}{-0.137389 + 1.\,v}$$

CJ point

$$m[\pi c\_] := \partial_v\ \text{eq1}[\alpha 2,\ \pi c] \text{ // Simplify}$$

$$\text{vcj}[\pi c\_] := \text{Solve}\left[\frac{\text{eq1}[\alpha 2,\ \pi c] - p0[\pi c]}{v - v0[\pi c]} == m[\pi c],\ v\right][[1]][[1,\ 2]]$$

pcj[πc_] := eq1[α2, πc] /. v −> vcj[πc]

pcj[1]

19.1882

m1[πc_] := m[πc] /. v −> vcj[πc]

m1[2]

−145.833

plot2[πc_] := ListPlot[{{vcj[πc], pcj[πc]}}, PlotStyle −> {Black, Thick}]

plot2[1]

ZND specific volume

m1

m1

$$\text{vznd}[\pi c\_] := \text{Solve}\left[\frac{\text{eq1}[\alpha 1,\ \pi c] - \text{pcj}[\pi c]}{v - \text{vcj}[\pi c]} == m1[\pi c],\ v\right][[1]][[1,\ 2]]$$

vznd[2]

0.0975396

pznd[πc_] := eq1[α1, πc] /. v −> vznd[πc]

pznd[2]

74.7527

Plot line from ZND to CJ point

m1

m1

p0 − m1 vznd

p0 − m1 vznd

line[πc_] := Solve[{p0[πc] == a + b v0[πc], pcj[πc] == a + b vcj[πc]}, {a, b}][[1]];

pp[v_, πc_] := a + b v /. line[πc];

plot3[πc_] := ListPlot[{{vznd[πc], pznd[πc]}}, PlotStyle −> {Black, Thick}]

plot3[2]

Inert Hugoniot curve

plot1[πc_] := Plot[eq1[α1, πc] /. v −> aa,
{aa, vznd[πc], vinitial}, PlotRange −> {{0, 1}, {0, pznd[πc]}}, PlotStyle −> {Black}]

plot1[2]

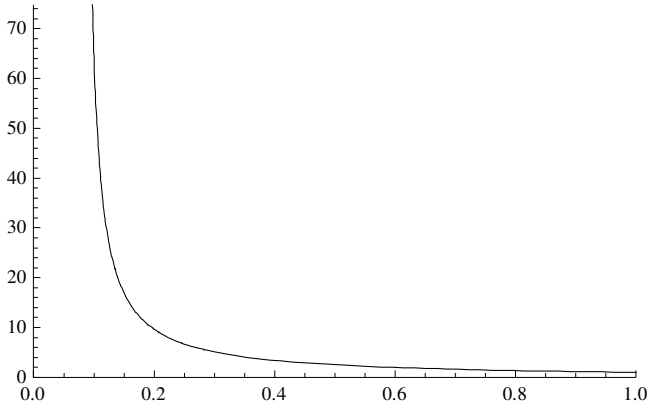

Line from ZND to CJ point

vcj[1]

0.581771

pp[v, 1]

44.4886 − 43.4886 v

plot6[πc_] := Plot[pp[v, πc] /. v −> aa, {aa, vznd[πc], vcj[πc]}, PlotStyle −> {Black}]

plot6[1]

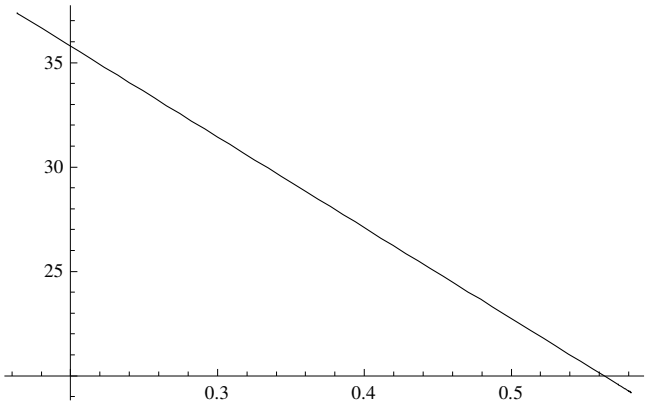

Taylor expansion

ptaylor = pinitial

1

$$\left(\frac{\text{ptaylor}}{\text{pcj}[\pi c]}\right) == \left(\frac{\text{vcj}[\pi c]}{\text{v}}\right)^{\gamma} \text{// Simplify;}$$

$$\text{vtaylor}[\pi c\_] := \text{Solve}\left[\left(\frac{\text{ptaylor}}{\text{pcj}[\pi c]}\right) == \left(\frac{\text{vcj}[\pi c]}{\text{v}}\right)^{\gamma}, \text{v}\right][[1]][[1, 2]]$$

vtaylor[3]

5.66234

$$\text{graph}[\text{v\_}, \pi c\_] := \text{Solve}\left[\left(\frac{\text{p}}{\text{pcj}[\pi c]}\right) == \left(\frac{\text{vcj}[\pi c]}{\text{v}}\right)^{\gamma}, \text{p}\right][[1]][[1, 2]]$$

graph[vcj[1], 1]

19.1882

$$\text{vtaylor}[\pi c\_] := \text{Solve}\left[\left(\frac{\text{p0}[\pi c]}{\text{pcj}[\pi c]}\right) == \left(\frac{\text{vcj}[\pi c]}{\text{v}}\right)^{\gamma}, \text{v}\right][[1]][[1, 2]]$$

vtaylor[1]

5.46793

```
plot7[πc_] := ListPlot[{{vtaylor[πc], ptaylor}}, PlotStyle -> {Black}]

plot7[1]

graph[vcj[1], 1]

19.1882

plot4[πc_] := Plot[graph[v, πc] /. v -> aa, {aa, vcj[πc], vtaylor[πc]},
    PlotRange -> {{0, vtaylor[πc]}, {0, pcj[πc]}}, AxesLabel -> {v/v0, p/p0}, PlotStyle -> {Black}]

plot4[3]
```

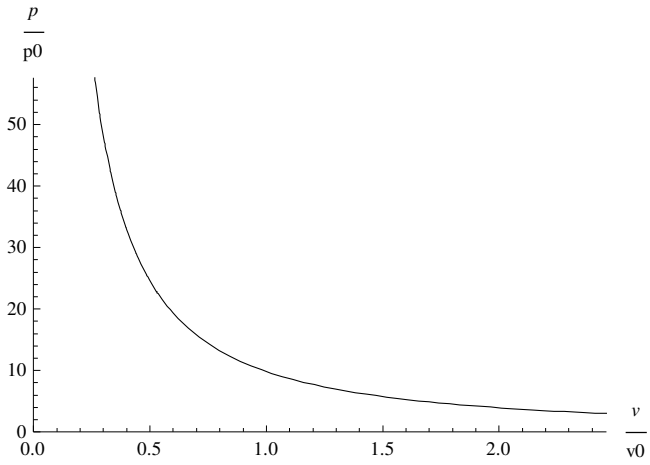

Heat release

```
plot5[πc_] := Plot[ptaylor, {aa, vinitial, vtaylor[πc]}, PlotStyle -> {Black}]

plot5[1]
```

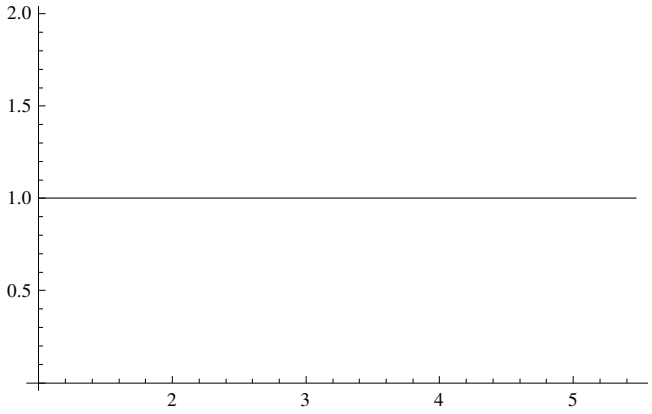

Plots

Initial point

CJ point

ZND point

Taylor expansion

End of taylor expansion point

Ideal PDE cycle

```
pv1 = Show[plot0[pic], plot1[pic], plot2[pic], plot3[pic],
    plot4[pic], plot5[pic], plot6[pic], plot7[pic], AxesLabel -> {"v/v0", "p/p0"},
    Epilog -> {PointSize[0.015], Point[{vinitial, pinitial}], Point[{v0[pic], p0[pic]}], Point[{vcj[pic], pcj[pic]}],
        Point[{vznd[pic], pznd[pic]}], Point[{vtaylor[pic], ptaylor}]}, PlotLabel -> "p-v diagram"]
```

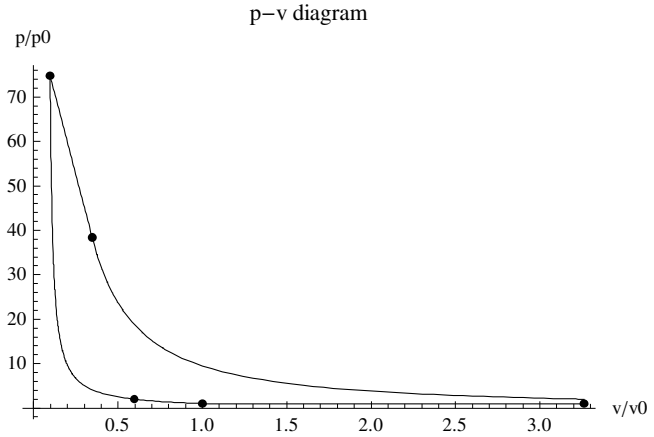

T - s diagrams

trying to use table values

```
s0 = sinitial;
```

$$T0 = \text{Solve}\left[\frac{\gamma}{\gamma - 1}\,\text{Log}\left[\frac{x}{\text{Tinitial}}\right] - \text{Log}\left[\frac{p0[pic]}{\text{pinitial}}\right] == 0,\ x\right][[1]][[1,\ 2]]$$

1.18229

$$\text{Tt0}[p\_,\ v\_,\ \pi c\_] := \text{Tinitial}\ \frac{p}{\text{pinitial}}\ \frac{v}{\text{vinitial}}$$

$$\text{T0}[\pi c\_] := \text{Tt0}[p0[\pi c],\ v0[\pi c],\ \pi c]$$

$$\text{Tt}[p\_,\ v\_,\ \pi c\_] := T0\ \frac{p}{p0[\pi c]}\ \frac{v}{v0[\pi c]}$$

$$\text{eq2}[\alpha\_,\ \text{v\_},\ \pi\text{c\_}] := \text{Solve}\left[\left(\frac{\text{p}}{\text{p0}[\pi\text{c}]} + \mu^2\right)\left(\frac{\text{v}}{\text{v0}[\pi\text{c}]} - \mu^2\right) == 1 - \mu^4 + 2\,\mu^2\,\alpha,\ \text{p}\right][[1]][[1,\ 2]]$$

$$\text{eq2}[\alpha 1,\ \text{v},\ 1]$$

$$\frac{0.981124 - 0.137389\,(-0.137389 + 1.\,\text{v})}{-0.137389 + 1.\,\text{v}}$$

$$\text{pressure}[\pi\text{c\_}] := \text{Table}[\text{eq2}[\alpha 1,\ \text{v},\ \pi\text{c}]\ /.\ \text{v} \to \text{aa},\ \{\text{aa},\ \text{v0}[\pi\text{c}],\ \text{vznd}[\pi\text{c}],\ -0.02\}];$$

$$\text{volume}\,[\pi\text{c\_}] := \text{Table}[\text{aa},\ \{\text{aa},\ \text{v0}[\pi\text{c}],\ \text{vznd}[\pi\text{c}],\ -0.02\}];$$

$$\text{pvb}[\pi\text{c\_}] := \text{Table}[\{\text{volume}[\pi\text{c}][[\text{i}]],\ \text{pressure}[\pi\text{c}][[\text{i}]]\},\ \{\text{i},\ 1,\ \text{Length}[\text{pressure}[\pi\text{c}]]\}];$$

$$\text{plot1bb}[\pi\text{c\_}] := \text{ListLinePlot}[\text{pvb}[\pi\text{c}],\ \text{PlotStyle} \to \{\text{Black}\}]$$

$$\text{plot1bb}[1]$$

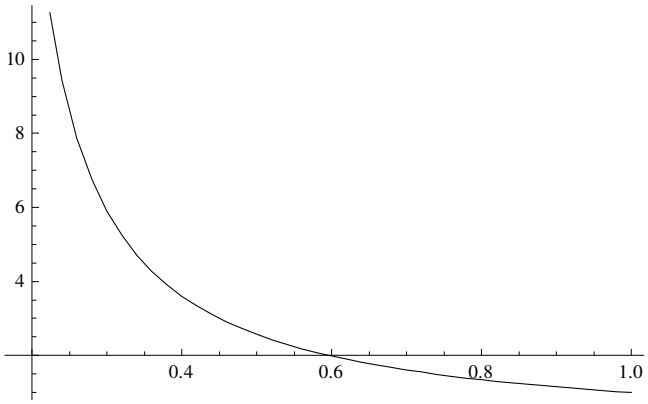

change here

$$\text{temperature}[\pi\text{c\_}] := \text{Table}\left[\text{T0}\ \frac{\text{pressure}[\pi\text{c}][[\text{i}]]\ \text{volume}[\pi\text{c}][[\text{i}]]}{\text{p0}[\pi\text{c}]\ \text{v0}[\pi\text{c}]},\ \{\text{i},\ 1,\ \text{Length}[\text{pressure}[\pi\text{c}]]\}\right];$$

change here

$$\text{entropy}[\pi\text{c\_}] := \text{Table}\left[\frac{\gamma}{\gamma - 1}\,\text{Log}\left[\frac{\text{temperature}[\pi\text{c}][[\text{i}]]}{\text{T0}}\right] - \text{Log}\left[\frac{\text{pressure}[\pi\text{c}][[\text{i}]]}{\text{p0}[\pi\text{c}]}\right],\ \{\text{i},\ 1,\ \text{Length}[\text{temperature}[\pi\text{c}]]\}\right];$$

$$\text{ts}[\pi\text{c\_}] := \text{Table}[\{\text{entropy}[\pi\text{c}][[\text{i}]],\ \text{temperature}[\pi\text{c}][[\text{i}]]\},\ \{\text{i},\ 1,\ \text{Length}[\text{temperature}[\pi\text{c}]]\}];$$

$$\text{plotinitial} = \text{ListPlot}[\{\{\text{sinitial},\ \text{Tinitial}\},\ \{\text{s0},\ \text{T0}\}\},\ \text{PlotStyle} \to \{\text{Black},\ \text{Thick}\}]$$

ZND point

$$\text{eq3}[\alpha\_,\ \text{p\_},\ \pi\text{c\_}] := \text{Solve}\left[\left(\frac{\text{p}}{\text{p0}[\pi\text{c}]} + \mu^2\right)\left(\frac{\text{v}}{\text{v0}[\pi\text{c}]} - \mu^2\right) == 1 - \mu^4 + 2\,\mu^2\,\alpha,\ \text{v}\right][[1]][[1,\ 2]]$$

```
eq3[α1, p, 1]
```

$$\frac{1.\,(0.981124 + 0.137389\,(0.137389 + p))}{0.137389 + p}$$

```
Ts[p_, πc_] := Tt[p, eq3[α1, p, πc], πc]

Tznd[πc_] := Ts[pznd[πc], πc]

Tznd[2]

7.22689

ps[T_, πc_] := Solve[Ts[p, πc] == T, p][[2]][[1, 2]]

ps[T, 2]
```

$$3.68727 \times 10^{-35}\left(-1.97399 \times 10^{35} + 1.66963 \times 10^{35}\,T + 1.66963 \times 10^{35}\sqrt{1.39781 - 2.27532\,T + 1.\,T^2}\right)$$

change here

$$\Delta sR[T\_, \pi c\_] := \frac{\gamma}{\gamma - 1}\,\text{Log}\left[\frac{T}{\text{Tinitial}}\right] - \text{Log}\left[\frac{ps[T, \pi c]}{\text{pinitial}}\right] // \text{Simplify}$$

```
ΔsR[Tcj[1], 1]
```

$$4.13931\,\text{Log}[Tcj[1]] - \text{Log}\left[-3.63931 + 3.07819\,Tcj[1] + 3.07819\sqrt{1.39781 - 2.27532\,Tcj[1] + 1.\,Tcj[1]^2}\right]$$

```
entropy[πc_] := Table[ΔsR[T, πc], {T, T0, Tznd[πc], 0.1}];

temp[πc_] := Table[aa, {aa, T0, Tznd[πc], 0.1}];

Tsdiag[πc_] := Table[{entropy[πc][[i]], temp[πc][[i]]}, {i, 1, Length[temp[πc]]}];

plot1b[πc_] := ListLinePlot[Tsdiag[πc], PlotStyle -> {Black}]

ListPlot[{{1, 1}}, PlotStyle -> {Black, Thick}]

Show[plot1b[pic], ListPlot[{{0, 1}, {s0, T0}}, PlotStyle -> {Black, Thick}], PlotRange -> {{0, 8}, {0, 5}}]

ΔsRznd[πc_] := ΔsR[Tznd[πc], πc]

ΔsRznd[1]

4.56573

plotznd[πc_] := ListPlot[{{ΔsRznd[πc], Tznd[πc]}}, PlotStyle -> {Black, Thick}]

plotznd[1]

Show[plotznd[pic], plot1b[pic],
  ListPlot[{{0, 1}, {s0, T0}}, PlotStyle -> {Black, Thick}], PlotRange -> {{0, 10}, {0, 10}}]
```

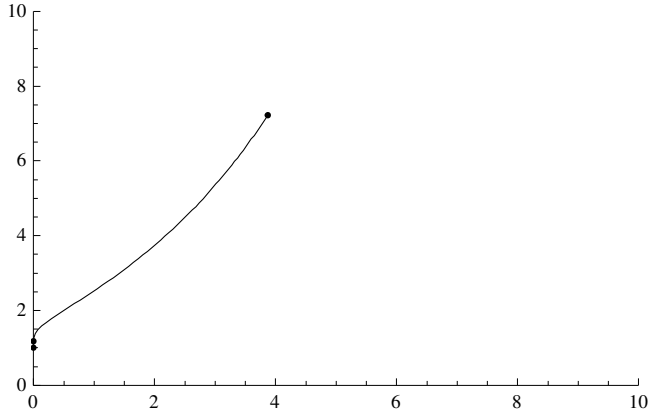

Chapman – Jouguet point

Finding the pressure and entropy for CJ point

$$\text{Ttz}[p\_,\ v\_,\ \pi c\_] := \text{Tznd}[\pi c]\ \frac{p}{\text{pznd}[\pi]}\ \frac{v}{\text{vznd}[\pi c]}$$

$$\text{Tcj}[\pi c\_] := \text{Tt0}[\text{pcj}[\pi c],\ \text{vcj}[\pi c],\ \pi c]$$

Tcj[1]

11.1631

$$\text{Ts2}[p\_,\ \pi c\_] := \text{Tt}[p,\ \text{eq3}[\alpha 2,\ p,\ \pi c],\ \pi c]$$

Ts2[p, 2]

$$\frac{0.591146\ (8.58795 + 0.137389\ (0.137389 + 0.5\ p))\ p}{0.137389 + 0.5\ p}$$

$$\text{ps2}[T\_,\ \pi c\_] := \text{Solve}[\text{Ts2}[p,\ \pi c] == T,\ p][[2]][[1,\ 2]]$$

change here

$$\Delta\text{sR2}[T\_,\ \pi c\_] := \frac{\gamma}{\gamma - 1}\ \text{Log}\left[\frac{T}{\text{Tinitial}}\right] - \text{Log}\left[\frac{\text{ps2}[T,\ \pi c]}{\text{pinitial}}\right] // \text{Simplify}$$

$$\Delta\text{sRcj}[\pi c\_] := \Delta\text{sR2}[\text{Tcj}[\pi c],\ \pi c]$$

$$\text{plotcj}[\pi c\_] := \text{ListPlot}[\{\{\Delta\text{sRcj}[\pi c],\ \text{Tcj}[\pi c]\}\},\ \text{PlotStyle} \rightarrow \{\text{Black},\ \text{Thick}\}]$$

plotcj[1]

Equation for the line from ZND to CJ

$$\text{vv}[p\_,\ \pi c\_] := \frac{p - a}{b} /. \text{line}[\pi c]$$

```
Ts3[p_, πc_] := Tt[p, vv[p, πc], πc]
ps3[T_, i_, πc_] := Solve[Ts3[p, πc] == T, p][[i]][[1, 2]]
test[πc_] := Solve[Ts3[p, πc] == T, p]
test[1]
```

$$\left\{\left\{p \to 18.3916\left(1.20948 - 0.329765\sqrt{13.452 - 1.\,T}\right)\right\},\ \left\{p \to 18.3916\left(1.20948 + 0.329765\sqrt{13.452 - 1.\,T}\right)\right\}\right\}$$

```
equalT[πc_] := Solve[test[πc][[1]][[1, 2]] == test[πc][[2]][[1, 2]], T][[1]][[1, 2]]
equalT[1]
```

13.452

```
ps3[Tcj[1], 1, 1]
```

13.0687

```
pss3[T_, i_, πc_] := ps3[T, i, πc]
```

change here

$$\Delta sr3a[T\_, \pi c\_] := \frac{\gamma}{\gamma - 1}\,\text{Log}\left[\frac{T}{\text{Tinitial}}\right] - \text{Log}\left[\frac{\text{pss3[T, 1, }\pi c]}{\text{pinitial}}\right] \text{// Simplify}$$

$$\Delta sr3b[T\_, \pi c\_] := \frac{\gamma}{\gamma - 1}\,\text{Log}\left[\frac{T}{\text{Tinitial}}\right] - \text{Log}\left[\frac{\text{pss3[T, 2, }\pi c]}{\text{pinitial}}\right] \text{// Simplify}$$

$$\Delta sR3[T\_, \pi c\_] := \frac{\gamma}{\gamma - 1}\,\text{Log}\left[\frac{T}{\text{Tinitial}}\right] - \text{Log}\left[\frac{\text{pss3[T, 2, }\pi c]}{\text{pinitial}}\right] \text{// Simplify}$$

```
ΔsR2[Tcj[1], 1]
```

7.99035

```
ΔsR3[Tznd[1], 1]
```

4.56573

```
equalT[1]
```

13.452

```
entropy3[πc_] := Table[ΔsR3[T, πc], {T, Tznd[πc], Tcj[πc] + 0.0495, 0.1}];
entropy3a[πc_] := Table[Δsr3a[T, πc], {T, equalT[πc], Tcj[πc], −0.01}];
entropy3b[πc_] := Table[Δsr3b[T, πc], {T, equalT[πc], Tcj[πc], −0.01}];
temp3[πc_] := Table[aa, {aa, Tznd[πc], Tcj[πc] + 0.0495, 0.1}];
```

temp3a[πc_] := Table[aa, {aa, equalT[πc], Tcj[πc], −0.01}];

temp3b[πc_] := Table[aa, {aa, equalT[πc], Tcj[πc], −0.01}];

Tsdiag3[πc_] := Table[{entropy3[πc][[i]], temp3[πc][[i]]}, {i, 1, Length[temp3[πc]]}];

Tsdiag3a[πc_] := Table[{entropy3a[πc][[i]], temp3a[πc][[i]]}, {i, 1, Length[temp3a[πc]]}];

Tsdiag3b[πc_] := Table[{entropy3b[πc][[i]], temp3b[πc][[i]]}, {i, 1, Length[temp3b[πc]]}];

plot1b3[πc_] := ListLinePlot[Tsdiag3[πc], PlotStyle −> {Black}]

pp1 = plot1b3[pic]

plot1b3a[πc_] := ListLinePlot[Tsdiag3a[πc], PlotStyle −> {Black}]

pp2 = plot1b3a[pic]

plot1b3b[πc_] := ListLinePlot[Tsdiag3b[πc], PlotStyle −> {Black}]

pp3 = plot1b3b[pic]

Show[pp1, pp2, pp3]

plot2show = Show[plot1b[pic], pp1, pp2, pp3, plotznd[pic], plotcj[pic], PlotRange −> {{0, 10}, {0, 15}}]

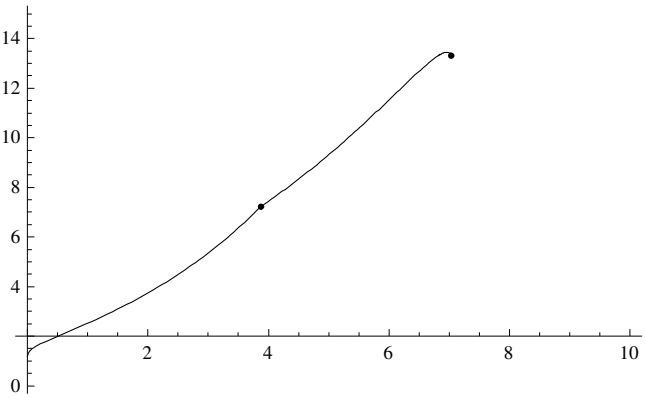

End of Taylor expansion point

$$\text{Ttt}[p\_,\ v\_,\ \pi c\_] := \text{Tcj}[\pi c]\ \frac{p}{\text{pcj}[\pi]}\ \frac{v}{\text{vcj}[\pi c]}$$

$$\text{vtaylor2} = \text{Solve}\left[\text{Tcj}[\text{pic}]\ \frac{\text{ptaylor}}{\text{pcj}[\text{pic}]}\ \frac{v}{\text{vcj}[\text{pic}]} == \text{Ttaylor}[\text{pic}],\ v\right][[1]][[1,\ 2]]$$

1. Ttaylor[2]

vtaylor[pic]

3.26117

ΔsRtaylor[πc_] := ΔsRcj[πc]

Ttaylor[πc_] := Ttt[ptaylor, vtaylor[πc], πc]

$$\text{Ttaylor}[\pi c\_] := \text{Solve}\left[\frac{\gamma}{\gamma - 1}\,\text{Log}\left[\frac{x}{\text{Tinitial}}\right] - \text{Log}\left[\frac{\text{ptaylor}}{\text{pinitial}}\right] == \Delta\text{sRtaylor}[\pi c],\, x\right][[1]][[1,\, 2]]$$

Ttaylor[pic]

5.46856

plottaylor[πc_] := ListPlot[{{ΔsRtaylor[πc], Ttaylor[πc]}}, PlotStyle −> {Black, Thick}]

temp4[πc_] := Table[aa, {aa, Ttaylor[πc], Tcj[πc], 0.01}];

entropy4[πc_] := Table[ΔsRtaylor[πc], {T, Ttaylor[πc], Tcj[πc], 0.01}];

plot4b[πc_] :=
  ListLinePlot[Table[{entropy4[πc][[i]], temp4[πc][[i]]}, {i, 1, Length[temp4[πc]]}], PlotStyle −> {Black}]

plot2showb = Show[ListLinePlot[{{ΔsRtaylor[pic], Ttaylor[pic]}, {ΔsRcj[pic], Tcj[pic]}}, PlotStyle −> {Black}],
    ListPlot[{{ΔsRtaylor[pic], Ttaylor[pic]}, {ΔsRcj[pic], Tcj[pic]}}]]

plot2showc = ListLinePlot[{{s0, T0[pic]}, {sinitial, Tinitial}}]

Heat release (array)

Length[vtable[pic]]

1

vtable[pic][[21]]

vtable[2][[21]]

ΔsRtaylor[pic]

7.03275

$$\frac{\gamma}{\gamma - 1}\,\text{Log}\left[\frac{\text{Ttaylor[pic]}}{\text{Tinitial}}\right] - \text{Log}\left[\frac{\text{ptaylor}}{\text{pinitial}}\right]$$

7.03275

$$\frac{\gamma}{\gamma - 1}\,\text{Log}\left[\frac{\text{Tcj[pic]}}{\text{Tinitial}}\right] - \text{Log}\left[\frac{\text{pcj[pic]}}{\text{pinitial}}\right]$$

7.06903

$$\frac{1}{\gamma - 1}\,\text{Log}\left[\frac{\text{Ttable[pic][[21]]}}{\text{Tinitial}}\right] + \text{Log}\left[\frac{\text{vtable[pic][[21]]}}{\text{vinitial}}\right]$$

3.13931 Log[Ttable[2][[21]]] + Log[vtable[2][[21]]]

vtaylor[pic]

3.26117

```
ptable[πc_] := Table[ptaylor, {aa, vinitial, vtaylor2, 0.1}];

vtable[πc_] := Table[aa, {aa, vinitial, vtaylor2, 0.1}];

Ttable[πc_] := Table[Tt[ptaylor, vtable[πc][[i]], πc], {i, 1, Length[ptable[πc]]}];

Δstable[πc_] := Table[γ/(γ - 1) Log[Ttable[πc][[i]]/Tinitial] - Log[ptable[πc][[i]]/pinitial], {i, 1, Length[ptable[πc]]}];

plot5b[πc_] :=
  ListLinePlot[Table[{Δstable[πc][[i]] + 0.00001, Ttable[πc][[i]]}, {i, 1, Length[Ttable[πc]]}], PlotStyle -> {Black}]

ListPlot[
  {{sinitial, Tinitial}, {s0, T0[pic]}, {ΔsRcj[pic], Tcj[pic]}, {ΔsRznd[pic], Tznd[pic]}, {ΔsRtaylor[pic], Ttaylor[pic]}}]

Show[plot2show, plot2showb]
```

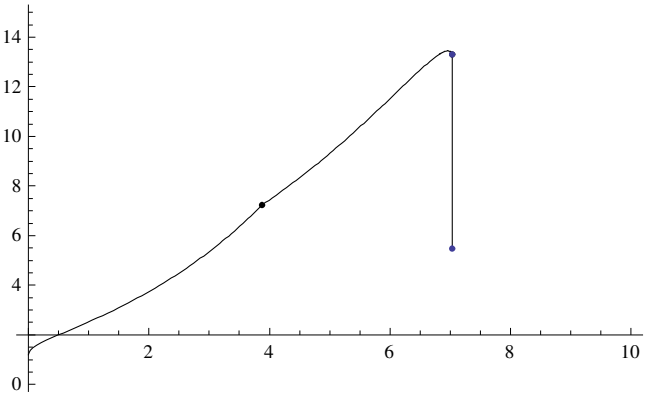


```
plot2showd = Show[plot5b[pic], PlotRange -> {{0, 10}, {0, 15}}]
```

vtaylor[pic]

3.26117

```
ts1 = Show[plot2show, plot2showb, plot2showc, plot2showd, ListPlot[{{s0, T0[pic]}, {sinitial, Tinitial}}],
    Epilog -> {PointSize[0.01], Point[{sinitial, Tinitial}], Point[{s0, T0}], Point[{ΔsRcj[pic], Tcj[pic]}],
      Point[{ΔsRznd[pic], Tznd[pic]}], Point[{ΔsRtaylor[pic], Ttaylor[pic]}]},
    AxesLabel -> {"Δs/R", "T/T0"}, PlotLabel -> "T−s diagram"]
```

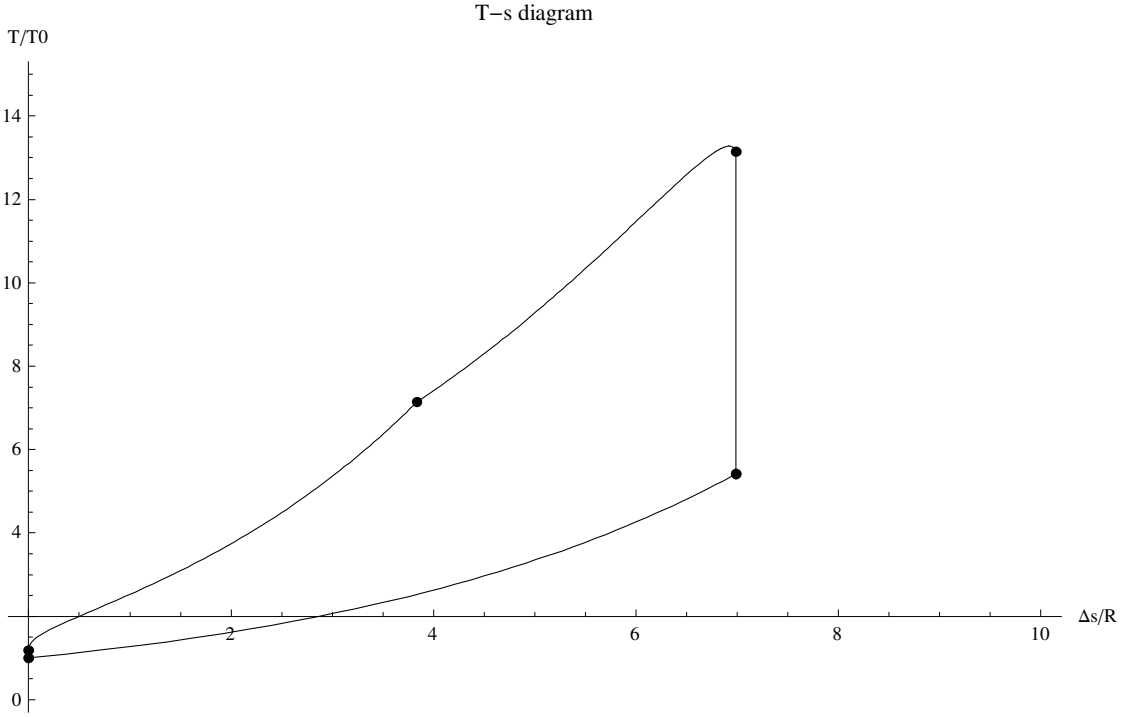

$$\eta_{th}[f\_, \pi c\_] := 1 - \frac{\left((1 + f)\, R\, \frac{\gamma}{\gamma - 1}\, (\text{Tinitial}\ 298)\left(\frac{\text{Ttaylor}[\pi c]}{\text{Tinitial}} - 1\right)\right)}{f\ \text{hpr}[f]}$$

$\eta_{th}[1, \text{pic}]$

0.502469

```
leg3 = Graphics[Legend[{{Graphics[{Line[{{0, 0}, {1, 0}}]}], Style["H2", FontFamily → "Times",  FontSize → 14]},
      {Graphics[{Dashed, Line[{{0, 0}, {1, 0}}]}], Style["CH4", FontFamily → "Times",  FontSize → 14]},
      {Graphics[{Dotted, Line[{{0, 0}, {1, 0}}]}], Style["C2H4", FontFamily → "Times",  FontSize → 14]},
      {Graphics[{DotDashed, Line[{{0, 0}, {1, 0}}]}], Style["C3H8", FontFamily → "Times",  FontSize → 14]}},
    LegendShadow → None, LegendBorder → None], ImageSize → 180]
```

efficiency4 = Plot[$\eta_{th}[1, \pi c]$, {πc, 1, 5}, AxesLabel → {"π_c", "η_{th}"}, PlotStyle → {DotDashed, Black}]

```
eff = Show[efficiency1, efficiency2, efficiency3, efficiency4]
```

```
GraphicsRow[{Show[eff, ImageSize −> 400, AxesStyle −> {"Times", 14}, LabelStyle −> {"Times", 14}], leg3},
  Spacings −> −80]
```

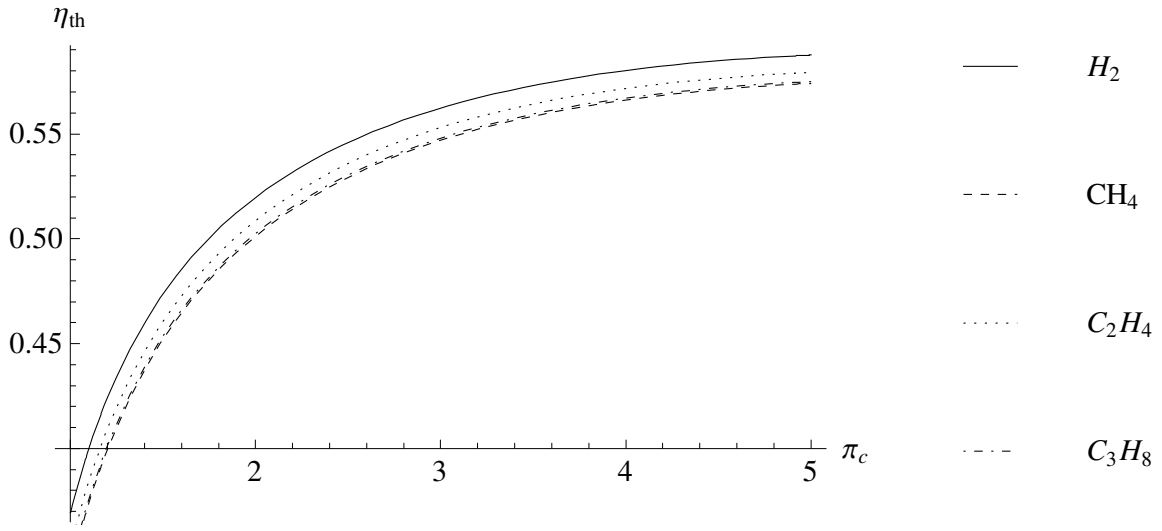


```
plot4[πc_] := Plot[graph[v, πc] /. v -> aa, {aa, vcj[πc], vtaylor2},
    PlotRange -> {{0, vtaylor2}, {0, pcj[πc]}}, AxesLabel -> {v/v0, p/p0}, PlotStyle -> {Black}]

plot4[pic]

Heat release

plot5[πc_] := Plot[ptaylor, {aa, vinitial, vtaylor2}, PlotStyle -> {Black}]

plot5[pic]

Plots

Initial point

CJ point

ZND point

Taylor expansion

End of taylor expansion point

Ideal PDE cycle

pv1 = Show[plot0[pic], plot1[pic], plot2[pic],
    plot3[pic], plot4[pic], plot5[pic], plot6[pic], AxesLabel -> {"v/v0", "p/p0"},
    Epilog -> {PointSize[0.01], Point[{vinitial, pinitial}], Point[{v0[pic], p0[pic]}], Point[{vcj[pic], pcj[pic]}],
        Point[{vznd[pic], pznd[pic]}], Point[{vtaylor2, ptaylor}]}, PlotLabel -> "p-v diagram"]
```

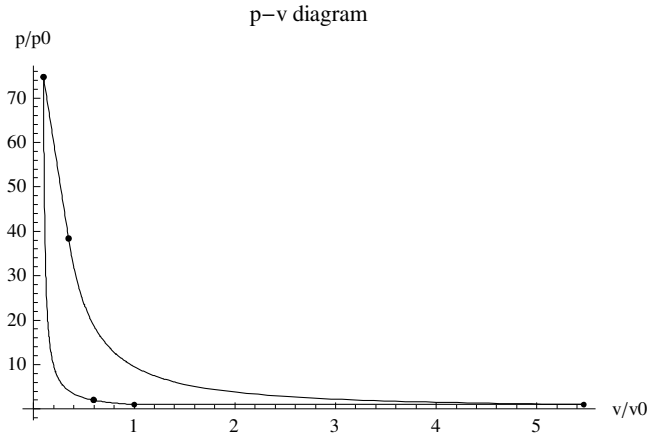

Decay pressure distribution (from Endo and Fujiwara paper, A simplified analysis on a pulse detonation Engine model)

$L = 1;\ V = 1000.;\ Dcj = \sqrt{2\left(\gamma^2 - 1\right) q}$

2247.6

$tfill = L/V$

0.001

$$Mcj = \sqrt{\frac{\gamma - 1}{2\,\gamma} + \frac{\gamma + 1}{2\,\gamma}\,\frac{pcj[pic]}{p0[pic]}}$$

4.12204

$$k1 = \frac{\gamma + 1}{2\,\gamma};\ k2 = \frac{\gamma - 1}{2\,\gamma};\ k3 = \frac{k1}{k2};\ k4 = \frac{2\left((\gamma\, k1)^{k3} - 1\right)}{\gamma\, k2};\ k5 = 2\, k1^{\frac{-k3}{2}};$$

$$tcj = \frac{L}{Dcj}$$

0.00044492

$tplateau = k5\, tcj$

0.00142161

$$K1 = k4\left(k1^{k1}\, Mcj^{2\,k2}\left(\frac{0.5\,\gamma}{\gamma}\right)^{k2} - 1\right) + k5$$

6.98823

texhaust = tcj K1

0.0031092

maxfreq = 1 / texhaust

321.626

$$K2 = \frac{k4\left(1-\left(\frac{K1-k5}{k4}+1\right)^{-k3}\right)}{k3}+k5$$

5.37051

$$K3 = \frac{K2\left(\frac{K1-k5}{k4}+1\right)^{1/k2}-K1}{\left(\frac{K1-k5}{k4}+1\right)^{1/k2}-1}$$

4.67578

$$K4 = \frac{K3\left(\left(\frac{K1-k5}{k4}+1\right)^{1/k2}-1\right)}{Mcj^2\,\gamma}$$

0.485982

$$pfill = \frac{Mcj^2\,\gamma\,k1^{k3}\,p0[pic]}{2\,\gamma}$$

6.65708

$$pplat[t\_] := pfill\left(\frac{k4\,tcj}{k4\,tcj+(t-tplateau)}\right)^{1/k2}$$

$$Tcycle = \left(1+(\gamma\,k1)^{k3}\right)2\,tcj$$

0.00349893

```
decay = Table[{t, pplat[t]}, {t, tplateau, texhaust, 0.000001}];
decayline = ListLinePlot[decay, AxesLabel -> {"t", "p/p0"}, PlotStyle -> {Black}]
platline = Plot[pplat[tplateau], {t, 0, tplateau}, PlotStyle -> {Black}]
fill = Plot[p0[pic], {t, texhaust, Tcycle}, PlotStyle -> {Black}]
profile = Show[platline, decayline, fill, PlotRange -> {{0, Tcycle}, {0, 8}}, AxesLabel -> {"t", "p/p0"}]
```

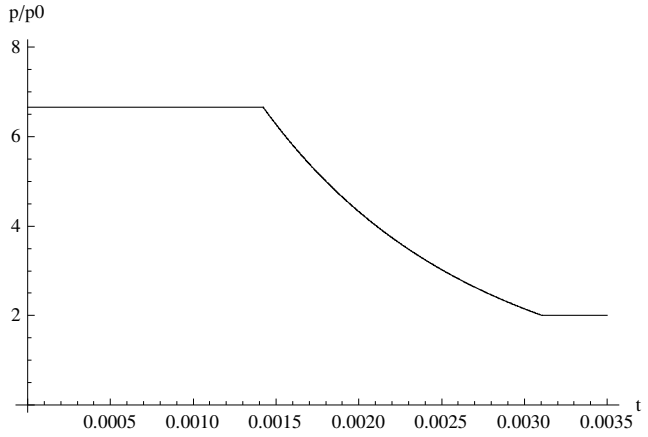

plateau = Table[{t, pplat[tplateau]}, {t, 0, tplateau, 0.0001}];

$$\text{paverage} = \left(\frac{1}{\text{texhaust} - \text{tplateau}} \int_{\text{tplateau}}^{\text{texhaust}} \text{pplat[t]}\, dt \right)$$

3.81784

pcycle[fr_] := paverage fr texhaust + p0[pic] (1 − fr texhaust)

Plot[pcycle[f], {f, 0, 300}]

$$\text{vave[fr\_]} := \text{Solve}\left[\left(\frac{\text{pcycle[fr]}}{\text{p0[pic]}} + \mu^2 \right)\left(\frac{\text{v}}{\text{v0[pic]}} - \mu^2 \right) == 1 - \mu^4 + 2\,\mu^2\,\alpha 2,\ \text{v}\right][[1]][[1,\ 2]]$$

$$\text{Tave[fr\_]} := \text{T0}\ \frac{\text{pcycle[fr]}}{\text{p0[pic]}}\ \frac{\text{vave[fr]}}{\text{v0[pic]}}$$

$$\text{Taverage[fr\_]} := \text{Solve}\left[\frac{\gamma}{\gamma - 1}\,\text{Log}\left[\frac{\text{x}}{\text{T0}}\right] - \text{Log}\left[\frac{\text{pcycle[fr]}}{\text{p0[pic]}}\right] == 0,\ \text{x}\right][[1]][[1,\ 2]]$$

Plot[Tave[f], {f, 0, 10 000}]

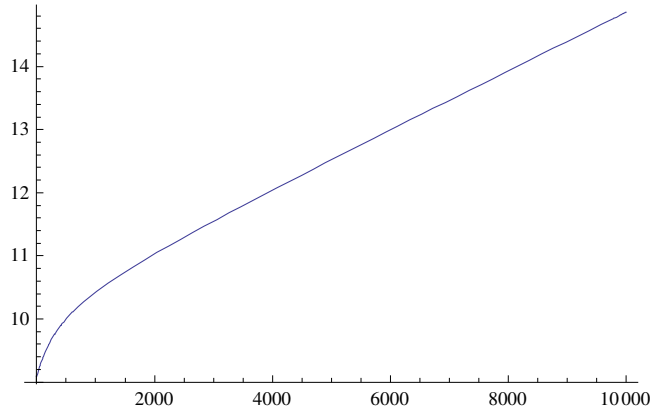

Tave[10]

9.12375

Ttaylor[pic]

5.46856

```
eff[fr_, f_] :=
  R γ (1 + f)/(γ - 1) (Tinitial 298) 1/(f hpr[f]) ((Tave[fr]/Tinitial - Ttaylor[pic]/Tinitial) - (T0/Tinitial - Tinitial/Tinitial))
```

```
Needs["PlotLegends`"]
```

```
leg = Graphics[Legend[{{Graphics[{DotDashed, Line[{{0, 0}, {1, 0}}]}],
        Style["Hydrogen", FontFamily -> "Times", FontSize -> 14]},
      {Graphics[{Dashed, Line[{{0, 0}, {1, 0}}]}], Style["Methane", FontFamily -> "Times", FontSize -> 14]},
      {Graphics[{Line[{{0, 0}, {1, 0}}]}], Style["Ethane", FontFamily -> "Times", FontSize -> 14]},
      {Graphics[{Dotted, Line[{{0, 0}, {1, 0}}]}], Style["Propane", FontFamily -> "Times", FontSize -> 14]}},
    LegendShadow -> None, LegendBorder -> None], ImageSize -> 100]
```

```
efftherm3 = Plot[eff[t, 1], {t, 0, maxfreq}, PlotStyle → {DotDashed, Black},
   AxesLabel → {"frequency", "η_th"}, AxesStyle → {"Times", 14}, LabelStyle → {"Times", 14}]
```

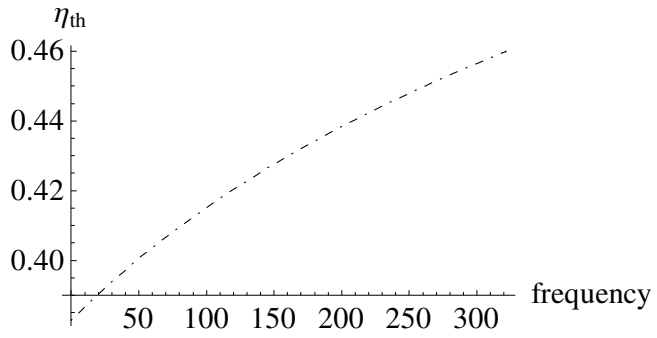

3

3

GraphicsRow[{Show[efftherm, efftherm2, efftherm3, efftherm4, ImageSize −> 400,
AxesStyle −> {"Times", 14}, LabelStyle −> {"Times", 14}], leg}, Spacings −> −150]

Show[efftherm, efftherm2, efftherm3, efftherm4]

Regeneration

ηreg is the efficiency of the regenerator. This is an assumption.

Tbr = Tb2[pic]

7.68797

ηreg = 0.5;

Tcj[pic]

13.3158

Ty2

10.9408

$$\text{Tx} = \text{Solve}\left[\eta\text{reg} == \frac{\text{x} - \text{T0}}{\text{Ttaylor[pic]} - \text{T0}}, \text{x}\right][[1]][[1, 2]]$$

3.32542

$$\text{Tx2} = \text{Solve}\left[\eta\text{reg} == \frac{\text{x} - \text{T0}}{\text{Tbr} - \text{T0}}, \text{x}\right][[1]][[1, 2]]$$

4.43513

px = p

p

Show[ts1]

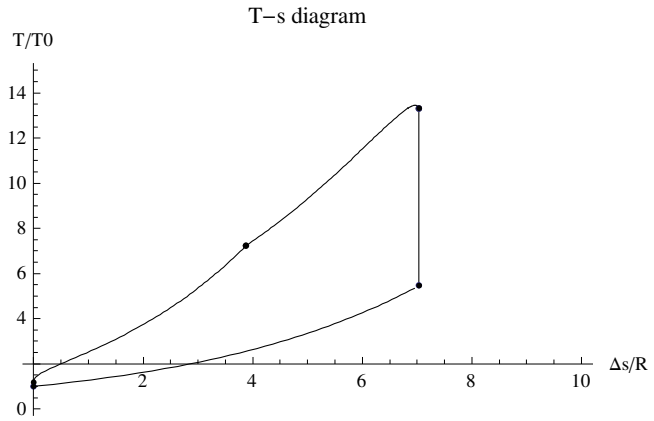

p0

p0

p0[pic]

2

pznd[pic]

74.7527

px = Solve[Ts[x, pic] == Tx, x][[2]][[1, 2]]

26.8075

px2 = Solve[Ts[x, pic] == Tx2, x][[2]][[1, 2]]

40.4226

vx = Solve[Tt[px, x, pic] == Tx, x][[1]][[1, 2]]

0.125155

vx2 = Solve[Tt[px2, x, pic] == Tx2, x][[1]][[1, 2]]

0.110698

sx = ΔsR[Tx, pic]

1.6851

sx2 = ΔsR[Tx2, pic]

2.46636

point = {{vx, px}}; point2 = {{sx, Tx}};

point2 = {{vx2, px2}}; point2 = {{sx2, Tx2}};

ff = ListPlot[point];

ff2 = ListPlot[point2];

regp = Show[pv1, ff]

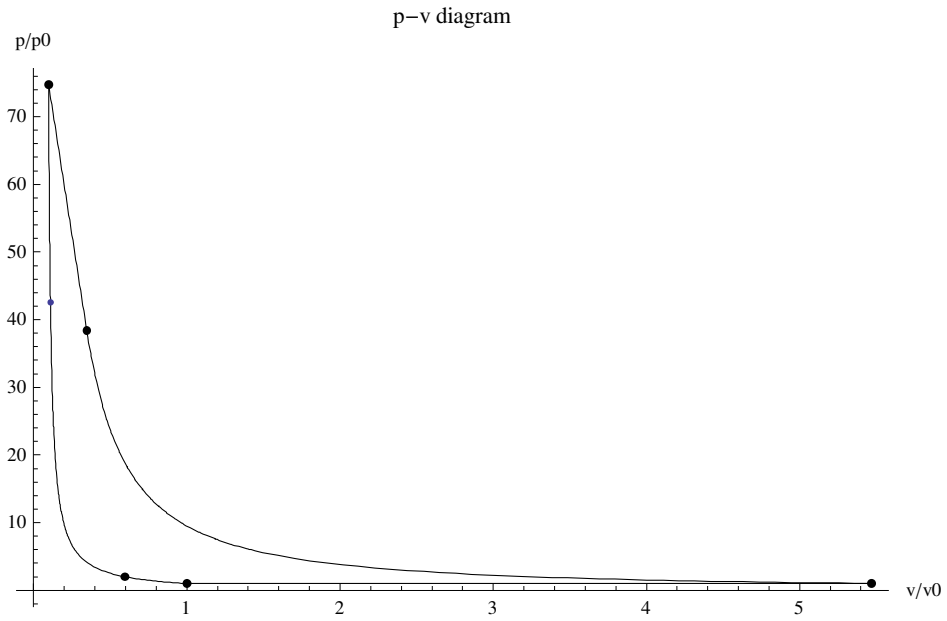

Show[ts1, ff2]

Tx − T0

2.14313

Ty = Solve[Ty − Ttaylor[pic] == Tx − T0, Ty][[1]][[1, 2]]

7.61169

Ty2 = Solve[Ty2 − Tbr == Tx2 − T0, Ty2][[1]][[1, 2]]

10.9408

Ty = T0

1.18229

$$vy = \text{Solve}\left[Ty == \text{Tinitial}\ \frac{y}{\text{vinitial}},\ y\right][[1]][[1,\ 2]]$$

1.18229

$$sy = \frac{\gamma}{\gamma - 1}\ \text{Log}\left[\frac{Ty}{\text{Tinitial}}\right] - \text{Log}\left[\frac{\text{pinitial}}{\text{pinitial}}\right]$$

0.693147

```
dd = ListPlot[{{vy, pinitial}}]
dd2 = ListPlot[{{sy, Ty}}]
regT = Show[ts1, dd2]
```

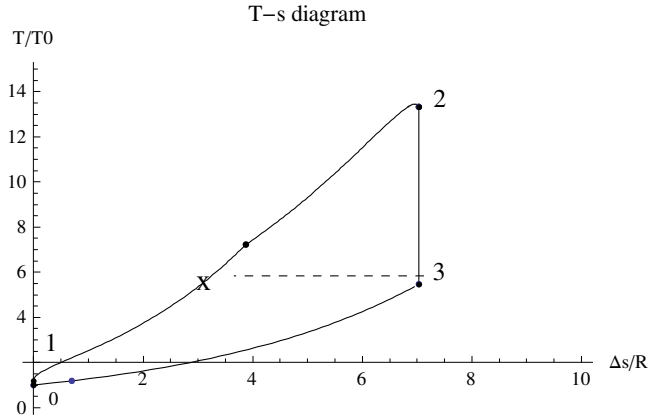


```
Show[pv1, dd]
```

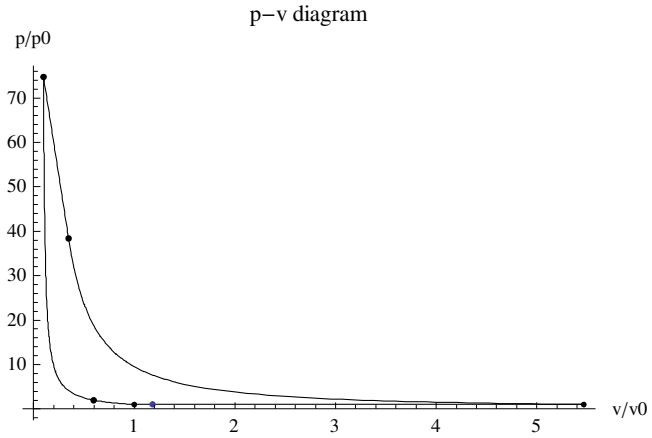

$$\eta\text{th} = \frac{(\text{Tcj[pic]} - \text{Ttaylor[pic]}) - (\text{T0} - \text{Tinitial})}{\text{Tcj[pic]} - \text{Tx}}$$

0.767233

$$\eta\text{th} = \frac{(\text{T0} - \text{Tinitial})}{\text{Tcj[pic]} - \text{Tx}}$$

0.0182468

$$1 - \left(\frac{\text{T0}}{\text{Ttaylor[pic]}}\right)\text{pic}^{\frac{\gamma-1}{\gamma}}$$

0.744391

$$\eta\text{th2} = \frac{(\text{Ty2} - \text{Ttaylor[pic]}) - (\text{T0} - \text{Tinitial})}{\text{Tcj[pic]} - \text{Tx2}}$$

0.477732

$$\eta\text{th2} = \frac{(\text{T0} - \text{Tinitial})}{\text{Tcj[pic]} - \text{Tx2}}$$

0.0205268

$$1 - \left(\frac{\text{T0}}{\text{Tbr}}\right)\text{pic}^{\frac{\gamma-1}{\gamma}}$$

0.818182

$$\text{Carnot} = 1 - \frac{\text{T0}}{\text{Ttaylor[pic]}}$$

0.783802

$$\text{Carnot2} = 1 - \frac{\text{T0}}{\text{Tbr}}$$

0.846215

Brayton Cycle

```
Clear[x, pb0, vb0, pb1, vb1, pb2, vb2, Tb0, Tb1, Tb2]
Rmixture = 0.396;
pic = 4;
```

$\alpha 1 = 0$; vbinitial = vinitial; pbinitial = pinitial; Tbinitial = Tinitial; sbinitial = sinitial; $\gamma = 1.318541$;

$$\text{Rf} = 0.2183;\ \text{Rair} = 0.2869;\ \text{R} = \frac{\text{Rf} + \text{Rair}}{2};\ \text{hpr}[\text{f\_}] := \frac{1 + \text{f}}{\text{f}}\ \text{hprm};$$

Isentropic compression

$$\text{sb0} = \text{sbinitial}$$

0

$$\text{pb0}[\pi\text{cc\_}] := \text{pbinitial}\,\pi\text{cc}$$

$$\text{eq1b}[\pi\text{cc\_}] := \frac{\text{x}}{\text{Tbinitial}} == \left(\frac{\text{pb0}[\pi\text{cc}]}{\text{pbinitial}}\right)^{\frac{\gamma-1}{\gamma}}$$

$$\text{Tb0}[\pi\text{cc\_}] := 3\ \text{Solve}[\text{eq1b}[\pi\text{cc}],\ \text{x}][[1]][[1,\ 2]]$$

$$\text{eq2b}[\pi\text{cc\_}] := \frac{\text{pb0}[\pi\text{cc}]}{\text{pbinitial}} == \left(\frac{\text{vbinitial}}{\text{x}}\right)^{\gamma}$$

$$\text{vb0}[\pi\text{cc\_}] := \text{Solve}[\text{eq2b}[\pi\text{cc}],\ \text{x}][[1]][[1,\ 2]]$$

$$\text{pb1}[\pi\text{cc\_}] := \text{pb0}[\pi\text{cc}]$$

$$\text{vb1}[\pi\text{cc\_}] := \text{vbinitial}$$

$$\text{Tb1}[\pi\text{cc\_}] := \frac{\text{pb1}\,[\pi\text{cc}]\ \text{vb1}[\pi\text{cc}]}{\text{Rmixture}}$$

$$\text{Tb1}[\pi\text{cc\_}] := \text{Tb0}\,[\pi\text{cc}]\left(1 + \alpha 2\ \frac{(\gamma - 1)}{\gamma}\right)$$

$$\text{sb1}[\pi\text{cc\_}] := \frac{\gamma}{\gamma - 1}\ \text{Log}\left[\frac{\text{Tb1}[\pi\text{cc}]}{\text{Tb0}[\pi\text{cc}]}\right] - \text{Log}\left[\frac{\text{pb1}[\pi\text{cc}]}{\text{pb0}[\pi\text{cc}]}\right]$$

$$\text{pb2}[\pi\text{cc\_}] := \text{pbinitial}$$

$$\text{vb2}[\pi\text{cc\_}] := \text{Solve}\left[\frac{\text{pb2}[\pi\text{cc}]}{\text{pb1}[\pi\text{cc}]} == \left(\frac{\text{vb1}[\pi\text{cc}]}{\text{x}}\right)^{\gamma},\ \text{x}\right][[1]][[1,\ 2]]$$

$$\text{Tb2}[\pi\text{cc\_}] := \frac{\text{pb2}[\pi\text{cc}]\ \text{vb2}[\pi\text{cc}]}{\text{Rmixture}}$$

$$\text{Tb2}[\pi\text{cc\_}] := \text{Solve}\left[\frac{\gamma}{\gamma - 1}\ \text{Log}\left[\frac{\text{TTb2}}{\text{Tb1}[\pi\text{cc}]}\right] - \text{Log}\left[\frac{\text{pb2}[\pi\text{cc}]}{\text{pb1}[\pi\text{cc}]}\right] == 0,\ \text{TTb2}\right][[1]][[1,\ 2]]$$

Tb2[pic]

7.22629

$$\text{sb2}[\pi\text{cc\_}] := \text{sb1}[\pi\text{cc}]$$

vb0[pic]

0.349453

vppoints = ListPlot[{{vbinitial, pbinitial}, {vb0[pic], pb0[pic]}, {vb1[pic], pb1[pic]}, {vb2[pic], pb2[pic]}}, PlotStyle −> {Black}, PlotMarkers −> {"∗", 15}]

stpoints = ListPlot[{{sbinitial, Tbinitial}, {sb0[pic], Tb0[pic]}, {sb1[pic], Tb1[pic]}, {sb2[pic], Tb2[pic]}}, PlotStyle −> {Black}, PlotStyle −> {Black}, PlotMarkers −> {"∗", 15}]

Isentropic relations

$$\frac{p}{p0} = \left(\frac{v0}{v}\right)^{\gamma}$$

$$\text{line1} = \text{Plot}\left[\text{pbinitial}\left(\frac{\text{vbinitial}}{\text{vv}}\right)^{\gamma}, \{\text{vv}, \text{vbinitial}, \text{vb0[pic]}\}, \text{PlotStyle} \to \{\text{Dotted}, \text{Black}\}\right]$$

line2 = Plot[pb0[pic], {vv, vb0[pic], vb1[pic]}, PlotStyle −> {Dotted, Black}]

$$\text{line3} = \text{Plot}\left[\text{pb1[pic]}\left(\frac{\text{vb1[pic]}}{\text{vv}}\right)^{\gamma}, \{\text{vv}, \text{vb1[pic]}, \text{vb2[pic]}\}, \text{PlotStyle} \to \{\text{Dotted}, \text{Black}\}\right]$$

line4 = Plot[pbinitial, {vv, vb2[pic], vbinitial}, PlotStyle −> {Dotted, Black}]

pvbrayton = Show[vppoints, line1, line2, line3, line4, AxesLabel −> {"v/v0", "p/p0"}, AxesStyle −> {"Times", 12}, LabelStyle −> {"Times", 12}, PlotRange −> {{0, 3}, {0, 3}}]

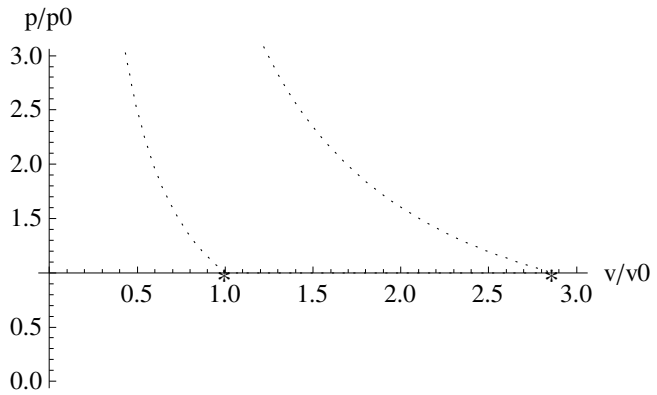

st = Table[{sbinitial, tt}, {tt, Tbinitial, Tb0[pic], 0.00001}];

st2 = Table[{sb1[pic], tt}, {tt, Tb1[pic], Tb2[pic], −0.00001}];

line1b = ListLinePlot[st, PlotStyle −> {Dotted, Black}]

line2b = ListLinePlot[st2, PlotStyle −> {Dotted, Black}]

```
Tplot[ss_, πcc_] := Solve[γ/(γ - 1) Log[tt/Tb0[πcc]] + sb0 == ss, tt][[1]][[1, 2]]

stplot = Table[{ss, Tplot[ss, pic]}, {ss, sb0, sb1[pic], 0.001}];

line3b = ListLinePlot[stplot, PlotStyle -> {Dotted, Black}]

Tplot2[ss_] := Solve[γ/(γ - 1) Log[tt/Tbinitial] + sbinitial == ss, tt][[1]][[1, 2]]

stplot2 = Table[{ss, Tplot2[ss]}, {ss, sbinitial, sb1[pic], 0.001}];

line4b = ListLinePlot[stplot2, PlotStyle -> {Dotted, Black}]

tsbrayton =
  Show[stpoints, line1b, line2b, line3b, line4b, AxesLabel -> {"Δs/R", "T/T0"}, AxesStyle -> {"Times", 12},
    LabelStyle -> {"Times", 12}, PlotRange -> {{0, 8}, {0, 8}}, Axes -> {True, True}]

plot

line1 = Plot[pbinitial (vbinitial/vv)^γ, {vv, vbinitial, vb0[pic]}, PlotStyle → {Dotted, Black}]

line2 = Plot[pb0[pic], {vv, vb0[pic], vb1[pic]}, PlotStyle -> {Dotted, Black}]

line3 = Plot[pb1[pic] (vb1[pic]/vv)^γ, {vv, vb1[pic], vb2[pic]}, PlotStyle → {Dotted, Black}]

line4 = Plot[pbinitial, {vv, vb2[pic], vbinitial}, PlotStyle -> {Dotted, Black}]

pvbrayton = Show[vppoints, line1, line2, line3, line4, AxesLabel -> {"v/v0", "p/p0"},
    AxesStyle -> {"Times", 12}, LabelStyle -> {"Times", 12}, PlotRange -> {{0, 3}, {0, 3}}]
```

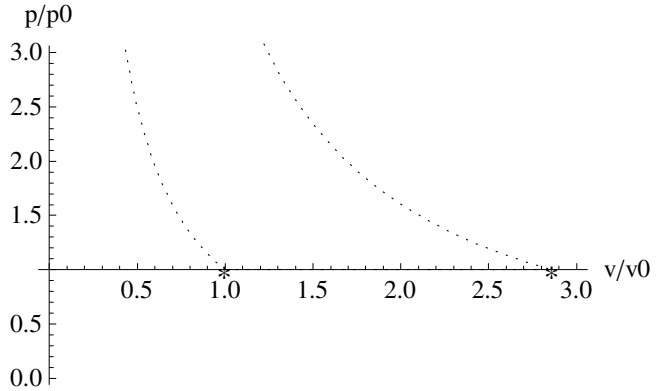


```
st = Table[{sbinitial, tt}, {tt, Tbinitial, Tb0[pic], 0.00001}];

st2 = Table[{sb1[pic], tt}, {tt, Tb1[pic], Tb2[pic], -0.00001}];
```

```
line1b = ListLinePlot[st, PlotStyle -> {Black}]

line2b = ListLinePlot[st2, PlotStyle -> {Black}]

Tplot[ss_, πcc_] := Solve[γ/(γ - 1) Log[tt/Tb0[πcc]] + sb0 == ss, tt][[1]][[1, 2]]

stplot = Table[{ss, Tplot[ss, pic]}, {ss, sb0, sb1[pic], 0.001}];

line3b = ListLinePlot[stplot, PlotStyle -> {Black}]

Tplot2[ss_] := Solve[γ/(γ - 1) Log[tt/Tbinitial] + sbinitial == ss, tt][[1]][[1, 2]]

stplot2 = Table[{ss, Tplot2[ss]}, {ss, sbinitial, sb1[pic], 0.001}];

line4b = ListLinePlot[stplot2, PlotStyle -> {Black}]

tsbrayton = Show[line1b, line2b, line3b, line4b, AxesLabel -> {"Δs/R", "T/T0"}, AxesStyle -> {"Times", 12},
    LabelStyle -> {"Times", 12}, PlotRange -> {{0, 10}, {0, 10}}, Axes -> {True, True}]
```

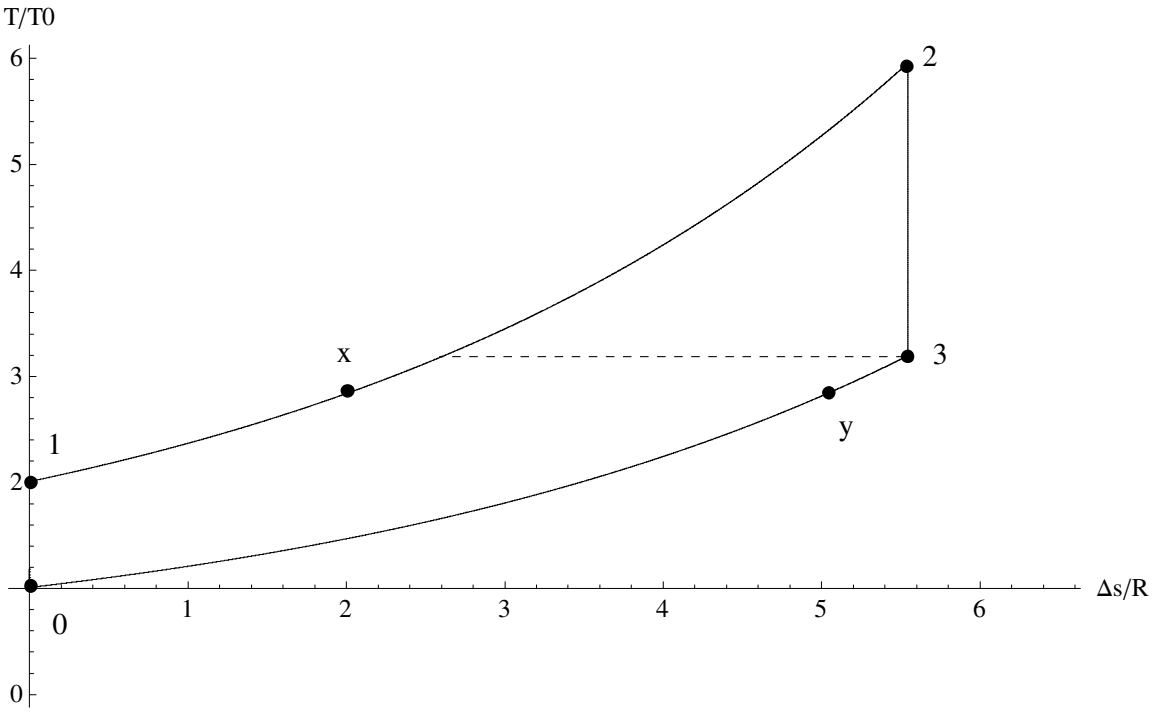

Humprey Cycle

Rmixture = 0.396;

pic = 2;

$\alpha 1$ = 0; vhinitial = vinitial; phinitial = pinitial; Thinitial = Tinitial; shinitial = sinitial; γ = 1.318541;

$$Rf = 0.2183;\ Rair = 0.2869;\ R = \frac{Rf + Rair}{2};\ hpr[f\_] := \frac{1 + f}{f}\ hprm;$$

Isentropic compression

sh0 = shinitial

0

ph0 = phinitial pic

2

$$eq1h = \frac{x}{Thinitial} == \left(\frac{ph0}{phinitial}\right)^{\frac{\gamma-1}{\gamma}}$$

x == 1.18229

Th0 = Solve[eq1h, x][[1]][[1, 2]]

1.18229

$$eq2v = \frac{ph0}{phinitial} == \left(\frac{vhinitial}{x}\right)^{\gamma}$$

$$2 == \left(\frac{1}{x}\right)^{1.31854}$$

vh0 = Solve[eq2v, x][[1]][[1, 2]]

0.591146

vh1 = vh0

0.591146

$$Th1 = Th0\left(1 + \alpha 2\ \frac{(\gamma - 1)}{\gamma}\right)$$

9.08942

$$ph1 = \frac{Th1}{Th0}\ \frac{ph0\ vh0}{vh1}$$

15.3759

$$sh1 = \frac{\gamma}{\gamma - 1}\ Log\left[\frac{Th1}{Th0}\right] - Log\left[\frac{ph1}{ph0}\right]$$

6.40312

ph2 = phinitial

1

$$vh2 = Solve\left[\frac{ph2}{ph1} == \left(\frac{vh1}{x}\right)^{\gamma}, x\right][[1]][[1, 2]]$$

4.69691

$$Th2 = Solve\left[\frac{\gamma}{\gamma - 1} Log\left[\frac{TTh2}{Th1}\right] - Log\left[\frac{ph2}{ph1}\right] == 0, TTh2\right][[1]][[1, 2]]$$

4.69691

```
sh2 = sh1
```

6.40312

```
vppointsh = ListPlot[{{vhinitial, phinitial}, {vh0, ph0}, {vh1, ph1}, {vh2, ph2}},
    PlotStyle -> {Black}, PlotMarkers -> {"o", 12}]

stpointsh = ListPlot[{{shinitial, Thinitial}, {sh0, Th0}, {sh1, Th1}, {sh2, Th2}},
    PlotStyle -> {Black}, PlotStyle -> {Black}, PlotMarkers -> {"o", 12}]
```

Isentropic relations

$$\frac{p}{p0} = \left(\frac{v0}{v}\right)^{\gamma}$$

$$pline[vv\_] := Solve\left[\left(\frac{ppx}{ph0} + \mu^2\right)\left(\frac{vv}{vh0} - \mu^2\right) == 1 - \mu^4 + 2\,\mu^2\,\alpha 1, ppx\right][[1]][[1, 2]]$$

```
line1 = Plot[pline[vv], {vv, vhinitial, vh0}, PlotStyle -> {Dashed, Black}]

pvplot2h = Table[{vh0, p}, {p, ph0, ph1, 0.001}];
```

ph1

15.3759

```
line2 = ListLinePlot[pvplot2h, PlotStyle -> {Dashed, Black}]
```

$$line3 = Plot\left[ph1\left(\frac{vh1}{x}\right)^{\gamma}, \{x, vh1, vh2\}, PlotStyle \to \{Dashed, Black\}, PlotRange \to \{\{0, 7\}, \{0, 16\}\}\right]$$

```
pvplot24h = Table[{vvh, phinitial}, {vvh, vhinitial, vh2, 0.001}];

line4 = ListLinePlot[pvplot24h, PlotStyle -> {Dashed, Black}]

pvhumphrey = Show[vppointsh, line1, line2, line3, line4, AxesLabel -> {"v/v0", "p/p0"},
    AxesStyle -> {"Times", 12}, LabelStyle -> {"Times", 12}, PlotRange -> {{0, 6}, {0, 15}}]
```

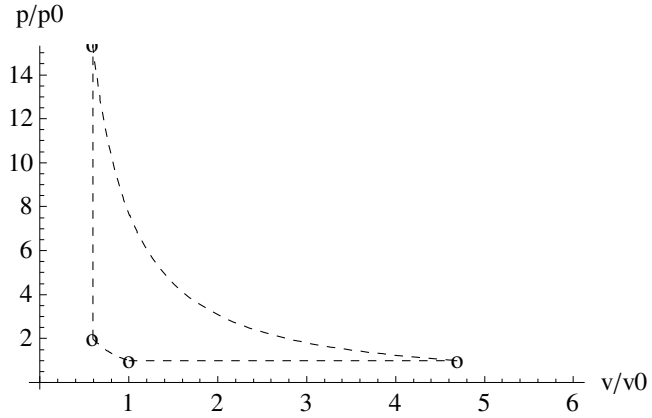


```
st = Table[{shinitial, tt}, {tt, Thinitial, Th0, 0.00001}];

line1h = ListLinePlot[st, PlotStyle -> {Dashed, Black}]

TTplot[ssh_] := Solve[1/(γ - 1) Log[TTh2/Th0] + Log[vh1/vh0] == ssh - sh0, TTh2][[1]][[1, 2]]

line2h = Plot[TTplot[ssh], {ssh, sh0, sh1}, PlotStyle -> {Dashed, Black}]

stploth = Table[{sh1, ttt}, {ttt, Th1, Th2, -0.0001}];

line3h = ListLinePlot[stploth, PlotStyle -> {Dashed, Black}]

TTplot2[ssh_] := Solve[γ/(γ - 1) Log[TTh2/Thinitial] - Log[ph2/phinitial] == ssh - shinitial, TTh2][[1]][[1, 2]]

line4h = Plot[TTplot2[ssh], {ssh, shinitial, sh2}, PlotStyle -> {Dashed, Black}]

tshumphrey =
  Show[stpointsh, line1h, line2h, line3h, line4h, AxesLabel -> {"Δs/R", "T/T0"}, AxesStyle -> {"Times", 12},
    LabelStyle -> {"Times", 12}, PlotRange -> {{0, 10}, {0, 10}}, Axes -> {True, True}]
```

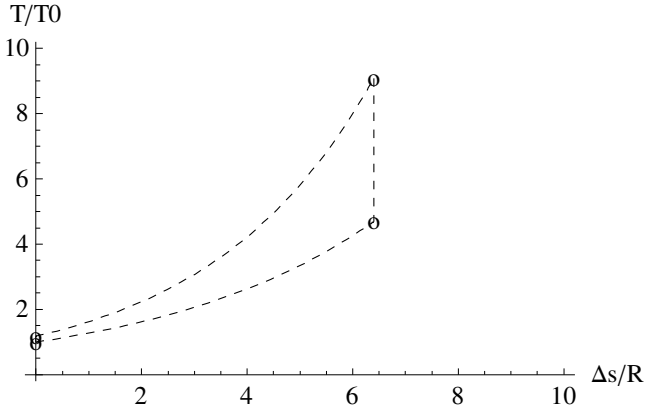

finalpv = Show[pv1, pvhumphrey, pvbrayton, PlotRange −> {{0, 6}, {0, 75}}]

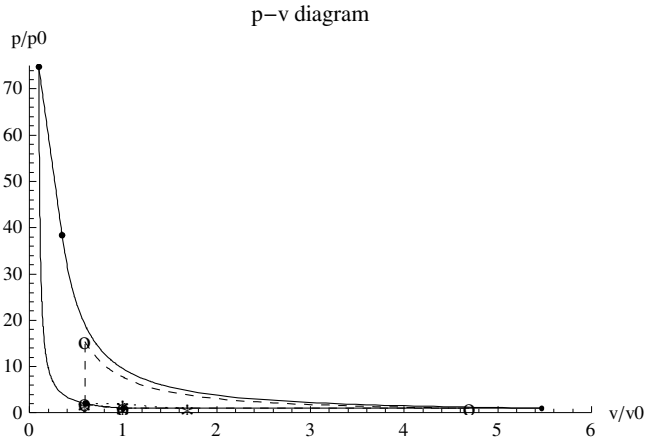

finalts = Show[ts1, tshumphrey, tsbrayton]

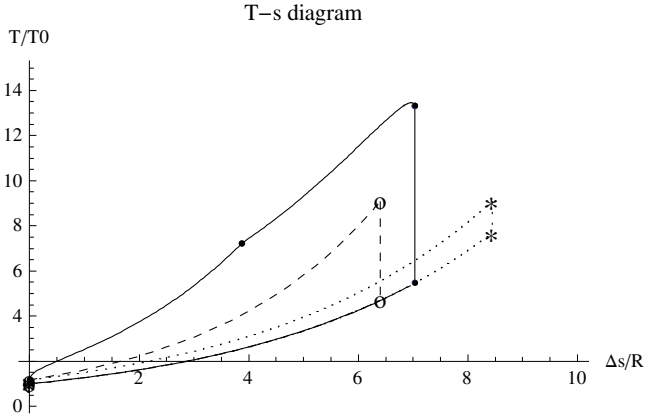

```
Needs["PlotLegends`"]

leg2 = Graphics[
    Legend[{{Graphics[{Line[{{0, 0}, {1, 0}}]}], Style["ZND cycle", FontFamily -> "Times", FontSize -> 14]},
        {Graphics[{Dotted, Line[{{0, 0}, {1, 0}}]}], Style["Brayton cycle",
            FontFamily -> "Times", FontSize -> 14]}, {Graphics[{Dashed, Line[{{0, 0}, {1, 0}}]}],
          Style["Humphrey cycle", FontFamily -> "Times", FontSize -> 14]}},
      LegendShadow -> None, LegendBorder -> None], ImageSize -> 180]

GraphicsRow[
  {Show[finalts, ImageSize -> 400, AxesStyle -> {"Times", 14}, LabelStyle -> {"Times", 14}], leg2},
  Spacings -> -120]
```

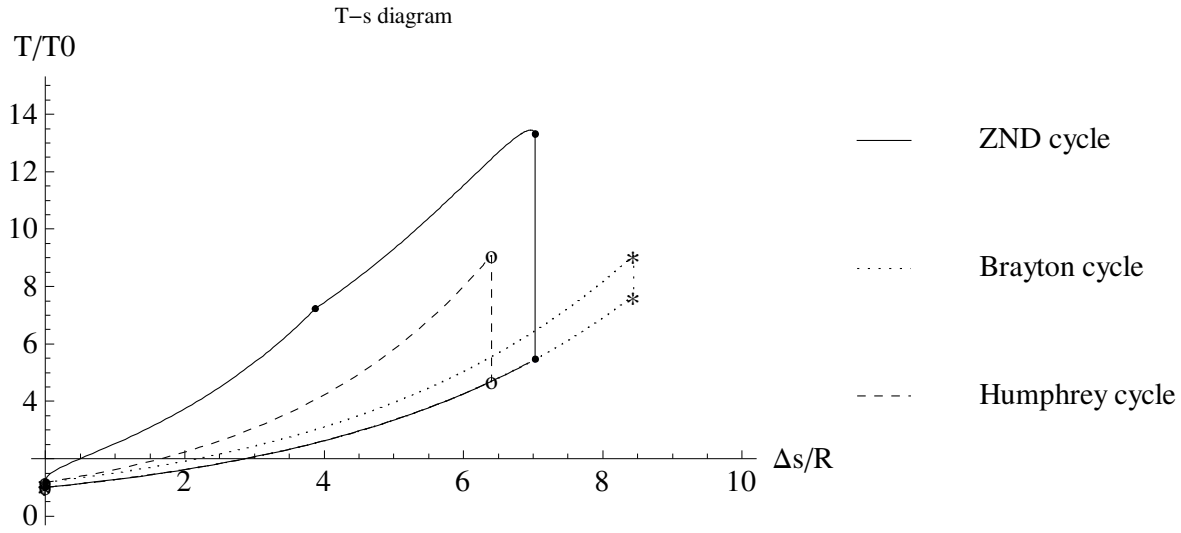


```
GraphicsRow[
  {Show[finalpv, ImageSize -> 400, AxesStyle -> {"Times", 14}, LabelStyle -> {"Times", 14}], leg2},
  Spacings -> -120]
```

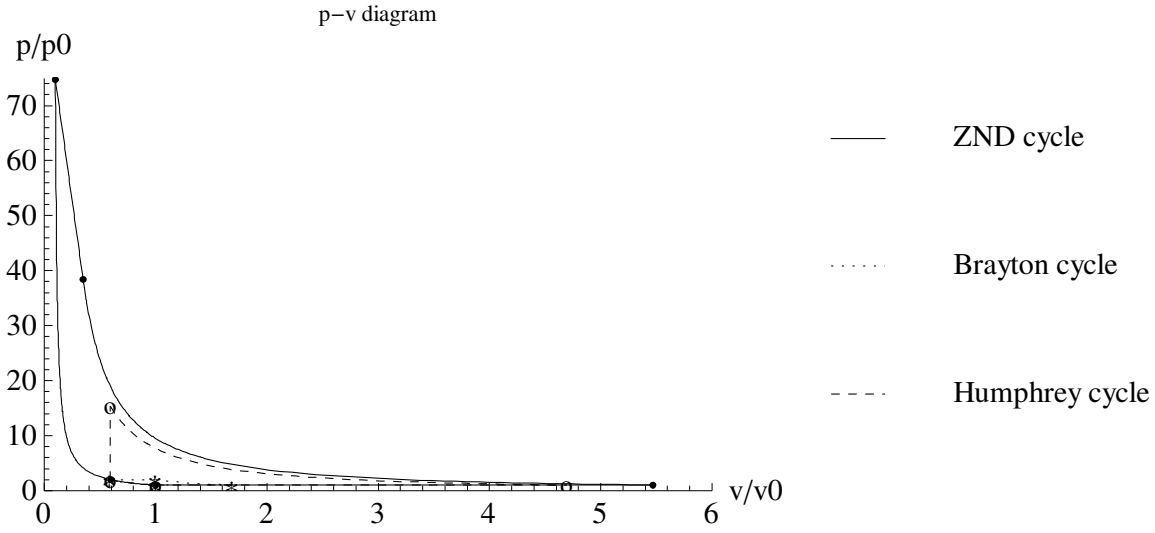
p−v diagram
p/p0
70
60
50
40
30
20
10
0
0
1
2
3
4
5
6
v/v0
ZND cycle
Brayton cycle
Humphrey cycle

REFERENCES

[1] P. K. Panicker, "The development and testing of pulsed detonation engine ground demonstrators," Ph.D. dissertation, The University of Texas at Arlington, 2008.

[2] K. K. Kuo, *Principles of combustion.* New York, N.Y.: Wiley, 1986.

[3] W. Fickett and W. C. Davis, *Detonation: Theory and Experiment.* New York: Dover Publications, Inc, 1979.

[4] M. A. Nettleton, *Gaseous detonations: Their Nature, Effects and Control.* New York: Chapman and Hall, 1987.

[5] M. Berthelot and P. Vieille, "On the velocity of propagation of explosive processes in gases," *C. R. Hebd. Sceances Acad. Sci.*, vol. 93, no. 2, pp. 18–21, 1881.

[6] ——, "On explosive waves," *C. R. Hebd. Sceances Acad. Sci.*, vol. 94, no. 2, pp. 149–152,882, 1882.

[7] E. Mallard and H. L. Chatelier, "Sur la vitesse de propagation de l'inflammation dans les mélanges gazeux explosifs," *Comptes Rendus Académie des Sciences*, vol. 93, pp. 145–148, 1881.

[8] ——, "Recherches de paul vieille à la connaissance des détonations et des ondes de choc," in *Annales des Mines*, ser. 8th, vol. 4, 1883, pp. 274–568, 10 Plates/VIII-XVII.

[9] G. D. Roy, S. M. Frolov, A. A. Borisov, and D. W. Netzer, "Pulse detonation propulsion: challenges, current status, and future perspective," *Progress in Energy and Combustion Science*, vol. 30, pp. 545–672, 2004.

[10] D. L. Chapman, "On the rate of explosion in gases," in *Philos. Magazine*, vol. 47, 1899, pp. 90–104.

[11] W. J. M. Rankine, "On the thermodynamic theory of finite longitudinal disturbance," *Philos. Trans. R. Soc. London*, vol. 160, pp. 277–288, 1870.

[12] H. Hugoniot, "Propagation des mouvements dans les corps et spécialment dans les gaz parfaits (propagations of movements in bodies and specially in ideal gases)," *J. De l'Ecole Polytechn.*, vol. 57, pp. 1–97, 1887.

[13] E. Jouguet, "Sur la propagation des réactions chemiques dans les gaz," in *Journal de Mathématiques Pures et Appliquées*, vol. 1/2, 1905/1906, pp. 347–425/5–86.

[14] C. Campbell and D. W. Woodhead, "The ignition of gases by an explosion wave. part i. carbon monoxide and hydrogen mixtures," *J. Chem. Soc.*, vol. 4, pp. 1572–1578, 1927.

[15] J. B. Zeldovich, "K teori rasprostranenia detonazi v gasoobrasnikh systemakh (On the theory of the propagation of detonation in gaseous systems)," *Zhurnal Experimentalnoi i Teoritiskeskoi Fiziki*, vol. 10, pp. 543–568, 1940, English translation: NACA TM 1261, 1960.

[16] ——, "Teoria gorenia i detonazii gasov (Theory of combustion and detonation of gases)," *Academy of Sciences*, 1944, English translation: TR GDAM, Ag-T-45, Air Material Command.

[17] J. von Neumann, "Progress report on the theory of detonation wave," *O.S.R.D. Rept.*, vol. 549, 1942.

[18] W. Döring, "Uber den detonationsvorgang in gasen (On the detonation process in gases)," *Annalen der Physik, 5e Folge*, vol. 43, pp. 421–436, 1943.

[19] Y. B. Zel'dovich, "On the use of detonative combustion in power engineering," *Journal of Technical Physics*, vol. 10, no. 17, pp. 1453–1461, 1940.

[20] M. Roy, "Propulsion par statoréacteur à detonation (Detonation ramjet propulsion)," in *Comptes Rendus de l'Acad. de Sciences*, vol. 222, 1946, pp. 31–32.

[21] S. Eidelmann and W. Grossmann, "Pulsed detonation engine experimental and theoretical review," *AIAA Paper*, no. 92-3168, 1992.

[22] T. Bussing and G. Pappas, *An Introduction to Pulse Detonation Engines.* AIAA Paper 94–0263, 1994.

[23] T. E. Bratkovich and T. R. A. Bussing, "A pulse detonation engine performance model," *AIAA Paper*, no. 95-3155, 1995.

[24] T. Bussing and G. Pappas, "Pulse detonation engine theory and concepts," in *Developments in High-Speed-Vehicle Propulsion Systems*, ser. Progress in Astronautics and Aeronautics, vol. 165. Washington, DC: AIAA, 1996.

[25] E. D. Lynch, R. Edelman, and S. Palaniswamy, "Computational fluid dynamic analysis of the pulse detonation engine concept," *AIAA Paper*, no. 94-0264, 1994.

[26] D. G. Talley and E. B. Coy, "Constant volume limit of pulsed propulsion for a constant gamma ideal gas," *Journal of Propulsion and Power*, vol. 18, no. 2, pp. 400–406, 2002.

[27] E. Wintenberger and J. E. Shepherd, "Thermodynamic analysis of combustion processes for propulsion systems," *AIAA Paper*, no. 2004-1033, 2004.

[28] T. E. Bratkovich, M. J. Aarnio, J. T. Williams, and T. R. A. Bussing, "An introduction to pulse detonation rocket engines (PDREs)," *AIAA Paper*, no. 97-2742, 1997.

[29] S. Eidelman, "Pulse detonation engine: A status review and technology development road map," *AIAA Paper*, no. 97-2740, 1997.

[30] D. Bouchard, B. Forrat, D. Piton, and P. Yvart, "AEROSPATIALE and CELERG investigations on pulse detonation propulsion," *AIAA Paper*, no. 99-2658, 1999.

[31] K. Kailasanath, "Recent developments in the research on pulse detonation engines," *AIAA Journal*, vol. 41, no. 2, pp. 145–159, 2003.

[32] K. Kailasanath and G. Patnaik, "Performance estimates of pulsed detonation engines," in *Proceedings of the Combustion Institute*, vol. 28, Pittsburgh, PA, 2000, pp. 595–601.

[33] M. A. Mawid, T. W. Park, B. Sekar, and C. Arana, "Numerical analysis of pulse detonation engines using global and reduced hydrocarbon kinetics," *AIAA Paper*, no. 99-4901, 1999.

[34] M. A. Mawid and T. W. Park, "Towards replacement of turbofan engines afterburners with pulse detonation devices," *AIAA Paper*, no. 2001-3470, 2001.

[35] M. A. Mawid, T. W. Park, B. Sekar, and C. Arana, "Application of pulse detonation combustion to turbofan engines," *ASME Transactions. Journal of Engineering for Gas Turbines and Power*, vol. 125, no. 1, pp. 270–283, 2003.

[36] B. Frankey, F. Schauer, R. Bradley, and J. Hoke, "Evaluation of a hybrid-piston pulsed detonation engine," *AIAA Paper*, no. 2002–0474, 2002.

[37] J. Hoke, R. Bradley, and F. Shauer, "Heat transfer and thermal management in a pulse detonation engine," *AIAA Paper*, no. 2003-0852, 2003.

[38] S. Germain, *B., and Olds, J., "Evaluation of Two Alternate Propulsion Concepts for Bantam-Argus: Deeply-Cooled Turbojet Rocket and Pulsed Detonation Rocket Ramjet," AIAA Paper 99–2354*, 1999.

[39] F. Falempin, D. Bouchaud, and E. Daniau, "Pulse detonation engine towards a tactical missile application," *AIAA Paper*, no. 2000-3473, 2000.

[40] F. Falempin, D. Bouchaud, B. Forrat, D. Desbordes, and E. Daniau, "Pulsed detonation engine–possible application to low cost tactical missile and to space launcher," *AIAA Paper*, no. 2001-3815, 2000.

[41] L. A. Povinelli and S. Yungster, "Thermodynamic cycle and CFD analyses for hydrogen fueled air-breathing pulse detonation engines," *AIAA Paper*, no. 2002-3629, 2002.

[42] W. Woodrow, B. Jr., R. A., and I. M. Blankson, *Airbreathing Concepts for Access to Space*. NASA/TM–2001-210564, 2001.

[43] R. Munipalli, V. Shankar, D. R. Wilson, H. Kim, F. K. Lu, and P. E. Hagseth, "A pulsed detonation based multimode engine concept," *AIAA Paper*, no. 2001-1786, 2001.

[44] P. A. Czysz and C. P. Rahaim, "Comparison of SSTO launchers powered by an RBCC propulsion system and a pulse detonation wave propulsion system," *Proceedings of 6th International Symposium on Propulsion for Space Transportation of the 21st Century*, pp. 14–16, 2002.

[45] L. A. Povinelli and S. Yungster, *Airbreathing Pulse Detonation Engine Performance*. NASA/TM–2002-211575, 2002.

[46] T. Kaemming, "Integrated vehicle comparison of turbo-ramjet engine and pulsed detonation engine," *ASME Journal of Engineering for Gas Turbines and Power*, vol. 125, no. 1, pp. 257–262, 2003.

[47] F. K. Lu, H. Fan, and D. R. Wilson, "Propulsion utilizing detonation waves induced by a confined wedge," *Proceedings 17th International Symposium on Air Breathing Engines*, pp. 4–9, 2005.

[48] V. E. Tangirala, A. J. Dean, D. M. Chapin, P. F. Pinard, and B. Varatharajan, "Pulsed detonation engine processes: Experiments and simulations," *Combustion Science and Technology*, vol. 176, no. 10, pp. 1779–1808, 2004.

[49] T. V. Bazhenova and V. Golub, "Use of gas detonation in a controlled frequency mode (review)," *Combustion, Explosion, and Shock Waves*, vol. 39, no. 4, pp. 365–381, 2003.

[50] Y. A. Nikolaev, A. A. Vasil'ev, and U. B. Y., "Gas detonation and its application in engineering and technologies (review)," *Combustion, Explosion, and Shock Waves*, vol. 39, no. 4, pp. 382–410, 2003.

[51] K. Hanjalic and I. Smajevic, "Detonation-wave technique for on-load deposit removal from surfaces exposed to fouling: Part i - experimental investigation and development of the method," *Journal of Engineering for Gas Turbines and Power*, vol. 116, no. 1, pp. 223–230, 1994.

[52] R. J. Litchford, B. R. Thompson, and J. T. Lineberry, "Pulse detonation magnetohydrodynamic power," *Journal of Propulsion and Power*, vol. 16, no. 2, pp. 251–262, 2000.

[53] J.-L. Cambier and D. Lofftus, "MHD power extraction from a pulse detonation rocket engine," *AIAA Paper*, no. 2002-2115, 2002.

[54] J.-L. Cambier and J. K. Tegnér, "Strategies for pulsed detonation engine performance optimization," *Journal of Propulsion and Power*, vol. 14, no. 4, pp. 489–498, 1998.

[55] S. Eidelman and X. Yang, "Analysis of the pulse detonation engine efficiency," *AIAA Paper*, vol. 1998, no. 98-3877.

[56] D. E. Paxson, "Optimal area profiles for ideal single nozzle air-breathing pulse detonation engines," *AIAA Paper*, no. 2003-4512, 2003.

[57] H. B. Ebrahimi, R. Mohanraj, and C. L. Merkle, "Multi-level analysis of pulsed detonation engines," *AIAA Paper*, no. 2000-3589, 2000.

[58] J.-L. Cambier, "Preliminary modeling of pulse detonation rocket engines," *AIAA Paper*, no. 99-2659, 1999.

[59] C. I. Morris, "Quasi-one-dimensional modeling of pulse detonation rocket engines," *AIAA Paper*, no. 2003-5204, 2003.

[60] T. Endo and T. Fujiwara, "A simplified analysis on a pulse detonation engine model," *Transactions of the Japan Society for Aeronautical and Space Sciences*, vol. 44, no. 146, pp. 217–222, 2002.

[61] W. Heiser and D. Pratt, "Thermodynamic cycle analysis of pulse detonation engines," *Journal of Propulsion and Power*, vol. 18, no. 1, pp. 68–76, 2002.

[62] J. A. C. Kentfield, "Fundamentals of idealized airbreathing pulse-detonation engines," *Journal of Propulsion and Power*, vol. 18, no. 1, pp. 77–83, 2002.

[63] Y. Wu, V. Yang, and S.-C. Chang, "Numerical simulation of detonation with detailed chemical kinetics using the space-time method," *AIAA Paper*, no. 2000-0317, 2000.

[64] T. Sakurai, N. Yamane, T. Obara, S. Ohyagi, and M. Murayama, "A study on thermodynamic cycle analysis of pulse detonation gas turbine engine," *Proceedings of the 17th International Symposium on Air Breathing Engines*, pp. 4–9, 2005.

[65] V. Tangirala, B. Varantharajan, and A. J. Dean, "Numerical investigations of detonation initiation," *AIAA Paper*, no. 2003-0716, 2003.

[66] E. Wintenberger and J. E. Shepherd, "Model for the performance of airbreathing pulse-detonation engines," *Journal of Propulsion and Power*, vol. 22, no. 3, pp. 593–603, 2006.

[67] T. E. Hutchins and M. Metghalchi, "Energy and exergy analyses of the pulse detonation engine," *Journal of Engineering for Gas Turbines and Power*, vol. 125, pp. 1075–1080, 2003.

[68] A. Bejan, *Advanced Engineering Thermodynamics*. New York, N.Y.: J. Wiley & Sons, 1997.

[69] E. Wintenberger and J. E. Shepherd, "Thermodynamic cycle analysis for propagating detonations," *Journal of Propulsion and Power*, vol. 22, no. 3, pp. 694–697, 2006.

[70] S. Gordon and B. J. McBride, *Computer Program for Calculation of Complex Chemical Equilibrium Compositions, Rocket Performance, Incident and Reflected Shocks, and Chapman–Jouguet Detonations*. NASA SP-273, 1976.

[71] G. Ciccarelli, T. Ginsburg, J. Boccio, C. Economos, C. Finfrock, L. Gerlach, K. Sato, and M. Kinoshita, "High-temperature hydrogen–air - steam detonation experiments in the BNL small-scale development apparatus," U.S. Nuclear Regulatory Commission, Washington, DC 20555-0001, Tech. Rep., 1994.

[72] M. J. Moran, *Fundamentals of engineering thermodynamics*. New York: J. Wiley and Sons, 2000.

[73] N. A. Cumpsty, *Jet propulsion: a simple guide to the aerodynamics and thermodynamic design and performance of jet engines*, 2nd ed. Cambridge University Press, 2003.

[74] Y. A. Çengel and M. Boles, *Thermodynamics: An Engineering Approach*. McGraw Hill, 1998.

[75] I. Wolfram Research, *Mathematica Edition: Version 7.0*. Champaign, Illinois: Wolfram Research, Inc., 2008.

[76] T. R. A. Bussing and G. Pappas, "An introduction to pulse detonation engines," *AIAA Paper*, no. 94-0263, January 1994.

[77] P. Lynwander, *Gear Drive Systems*. CRC Press, 1983.

[78] W. Fan, C. Yana, X. Huanga, Q. Zhanga, and L. Zhenga, "Experimental investigation on two-phase pulse detonation engine," *Combustion and Flame*, vol. 133, no. 4, pp. 441–450, 2003.

[79] R. J. Pegg, B. D. Couch, and L. G. Hunter, "Pulse detonation engine air induction system analysis," *AIAA Paper*, no. 96-2918, 1996.

[80] R. Bellini and F. K. Lu, "Exergy analysis of a ppulse detonation power device," in *10th Brazilian Congress of Thermal Engineering and Sciences*, Rio de Janeiro, Brazil, November 2004.

[81] ——, "Exergy analysis of a ppulse detonation power device," *Journal of Propulsion and Power*, vol. 26, no. 4, pp. 875–877, 2010.

BIOGRAPHICAL STATEMENT

Rafaela was born in the city of Rio de Janeiro, Brazil, where she obtained her bachelor's and master's degrees in mechanical engineering from the Federal University of Rio de Janeiro in Rio de Janeiro. She also worked, during the senior year of her bachelor's courses through to the completion of her master's level courses, in a project for the Brazilian Nuclear Agency (Eletrobrs Termonuclear S.A.), following in the footsteps of her father who worked as a nuclear engineer at the Nuclear Engineering Institute (IEN) in Brazil for most of his working career. Rafaela enrolled at the University of Texas at Arlington for her PhD in mechanical engineering at the behest of a former professor in the Mechanical and Aerospace Engineering Department. At UT Arlington, she met her future husband, Philip K. Panicker, as classmates. They were married in April 2009. Rafaela has certifications in personal training, group exercise and kickboxing instruction. She taught a number of exercise classes at the UT Arlington's Maverick Activities Center, including aerobics, water aerobics, Pilates, kickboxing and stationary cycle. Rafaela also has a black belt in Aikido.